IDENTIFICATION OF AMINO ACID RESIDUES ESSENTIAL FOR GDP INHIBITION OF UCP-MEDIATED FATTY ACID ANION UNIPORT

Martin Modriansky
B.S., Palacky University (Czech Republic), 1992

A dissertation submitted to the faculty of the
Oregon Graduate Institute of Science and Technology
in partial fulfillment of the
requirements for the degree
Doctor of Philosophy
in
Biochemistry

July 1997

The thesis "Identification of Amino Acid Residues Essential for GDP Inhibition of UCP-Mediated Fatty Acid Anion Uniport" by Martin Modriansky has been examined and approved by the following Examination Committee:

Keith D. Garlid
Professor, Thesis Advisor

James M. Crega
Professor

Jack H. Kaplan
Professor, Oregon Health Sciences University

Gebre Woldegiorgis
Associate Professor

DEDICATION

This work is dedicated to my mother Ludmila.

ACKNOWLEDGMENTS

I would like to thank Dr. Keith Garlid for his support, encouragement and thoughtful advice throughout the last five years. It was fun to work on an exciting project with one of the great "mitochondriacs." I would like to thank Drs. Gebre Woldegiorgis, James Cregg, and especially Jack Kaplan for serving on my thesis committee.

Big thank yous go to: David Orosz who taught me the secrets of uncoupling protein and darts, not necessarily in that order; Petr Jezek for working the late night experiments for me; Debbie Inglis for making me a yeast fan; Hansa Patel for her motherly patience while teaching me about "bugs" and things; and Dr. Karl Freeman for having me over to learn about molecular biology.

Many thanks to Martin Jaburek, Bohdana Korcakova, Baoyu Lin, Petr Paucek, Jianying Shi, Peter Schindler, Stefano Vassanelli, Vladimir Yarov-Yarovoy, and Hongfa Zhu for sharing laboratory space and time with me.

I would like to thank Craig Semrad for letting me fiddle around with equipment, computers in particular, and for sharing with me the secrets of American culture and the occasional game of tennis.

I would like to thank Terrie Hadfield and Nancy Christie for patiently fixing my typographical and copy machine blunders (there were quite a few).

Last, but not least, to receive my appreciation is my wife Pavla who kept showing her love and affection during the ups and downs of my struggle with science.

TABLE OF CONTENTS

LIST OF TABLES

LIST OF FIGURES

ABBREVIATIONS

2-azido-ATP	2-azidoadenosine 5′-triphosphate
8-azido-ATP	8-azidoadenosine 5′-triphosphate
ADIFAB	acrylodated intestinal fatty acid binding protein
ADP	adenosine 5′-diphosphate
ATP	adenosine 5′-triphosphate
BAT	brown adipose tissue
BSA	bovine serum albumin
CCCP	carbonyl cyanide m-chlorophenylhydrazone
CNBr	cyanogen bromide
DABS	diazobenzenesulfonic acid
DNP	2,6-diiodo-4-nitrophenol
DOXYL	4,4-dimethyl-3-oxazolinyloxyl-
DTT	dithiothreitol
EGTA	[ethylene-bis(oxyethylenenitrilo)]tetraacetic acid
FA	fatty acid
FCCP	carbonyl cyanide p-(trifluoromethoxy)phenylhydrazone
FDNP-ATP	3′-O-(5-fluoro-2,4-dinitrophenyl)adenosine 5′-triphosphate
GDP	guanosine 5′-diphosphate
GTP	guanosine 5′-triphosphate
McN-3802	2-tetradecylglycidic acid
MES	2-(N-morpholino)ethanesulfonic acid
NEM	n-ethylmaleimide
Nbs_2	5,5′-dithio-bis(2-nitrobenzoic acid)
Octyl-POE	n-octylpentaoxyethylene ether
PBFI	potassium-binding benzofuran isophthalate

SPQ	6-methoxy-*N*-(3-sulfopropyl)quinolinium
TEA	tetraethylammonium cation
TES	*N*-tris(hydroxymethyl)methylaminoethenesulfonic acid
TNBS	2,4,6 trinitrobenzenesulfonic acid
TNP	trinitrophenyl-
TRIS	tris(hydroxymethyl)aminomethane
UCP	uncoupling protein

ABSTRACT

Identification of Amino Acid Residues Essential for GDP Inhibition of UCP-Mediated Fatty Acid Anion Uniport

Martin Modriansky

Supervising Professor: Keith D. Garlid, M.D., dr. techn.

Uncoupling protein (UCP) is a transport protein found exclusively in the inner membrane of brown adipose tissue mitochondria. Its primary function is non-shivering thermogenesis. UCP does so by catalyzing passive back-flux of H^+ ions into the matrix in the presence of free fatty acids. UCP transports electrophoretically monovalent anions, such as halides, nitrate, and alkylsulfonates. Both proton and anion transports are allosterically inhibited by purine nucleoside di- and triphosphates. Proton transport induced by fatty acids is competitive with anion transport.

The goal of this project was to establish a model for the mechanism of UCP-mediated transport and use it in subsequent structure–function studies. The differential effects of laurate and its analogue, undecanesulfonate, on transport mediated by UCP were the basis for the proposed model. The kinetic experiments on purified, reconstituted UCP suggested that the ability of laurate to induce UCP-mediated proton transport is the result of nonionic flip-flop of the protonated laurate. Undecanesulfonate, an anionic substrate of UCP, cannot induce the proton transport due to its inability to flip-flop in the bilayer. Subsequent experiments with several fatty acid analogues showed the flip-flop ability is indeed crucial for induction of UCP-mediated proton transport.

We have previously expressed UCP in the yeast *S. cerevisiae* and have used this system to carry out structure–function studies by site-directed mutagenesis to

determine the residues essential for transport and nucleotide inhibition. Seven single Cys → Ser mutants showed no effect on both proton transport and GDP inhibition, while multiple Cys → Ser mutations showed a decrease in proton transport and GDP sensitivity of transport. Mutations of Arg276 → Leu or Gln, Arg83 → Gln, and Arg182 → Thr abolished GDP sensitivity of proton transport but had no effect on transport function. The data indicated that arginines 83, 182, and 276 are essential for nucleotide regulation of UCP-mediated transport. Our studies identify residues critical for nucleotide inhibition and suggest a cluster of residues are involved in proton transport mediated by UCP.

Chapter 1
INTRODUCTION

The primary function of brown adipose tissue is the production of heat, called non-shivering thermogenesis, that is designed to maintain or raise body temperature under the circumstance of low ambient temperature. Thermogenesis also occurs with over-eating (called diet-induced thermogenesis) to waste excess food energy (1). The heat is enthalpic in nature and results from the action of a 32-kDa inner mitochondrial membrane protein known as uncoupling protein (UCP) or thermogenin.

1.1 Oxidative Phosphorylation

The basis for understanding the coupling of substrate oxidation and phosphorylation processes is Peter Mitchell's chemiosmotic hypothesis (2). His four postulates—(i) ATP synthase is a chemiosmotic membrane-located reversible ATPase; (ii) respiratory chains are chemiosmotic membrane-located systems; (iii) proton-linked solute porter systems support osmotic stabilization and metabolite transport; and (iv) systems 1–3 are plugged through a topologically closed insulating membrane that has a nonaqueous osmotic barrier phase of low permeability to solutes in general, and to hydrogen and hydroxyl ions in particular—have achieved vast experimental support.

Mitochondrial respiration, the transfer of electrons from a substrate to oxygen via the respiratory chain, is the energy source for pumping protons from the mitochondrial matrix across the inner membrane into the intermembrane space. The resulting proton gradient is intended for ATP production. Indeed, the majority of protons re-enter the mitochondrial matrix through the ATP synthase, driving the conversion of ADP into ATP. A small portion of protons participates in ion gradient

rectification (3), volume homeostasis (4), metabolite transport (5), and energy dissipation via leak (6).

Two terms are important for further discussion. The first, the *coupling*, or *coupled state* of mitochondria, refers to the condition in which proton extrusion through the respiratory chain is balanced by proton re-entry through ATP synthase. This means that the mitochondria are under respiratory control, regulated by substrate availability and demand for ATP. The second term, the *uncoupling*, or the *uncoupled state* of mitochondria, refers to the condition in which the protons ejected by the respiratory chain re-enter the matrix by alternate pathways, thus bypassing the ATP synthase. In the *uncoupled* state, ADP is not phosphorylated and mitochondria are not under respiratory control, although substrate oxidation proceeds at a high rate.

Any mitochondrion can be uncoupled by a foreign substance, an uncoupler or protonophore. Well-known uncouplers are DNP, FCCP, and CCCP. The brown adipose tissue (BAT) mitochondrion is different because it possesses an intrinsic uncoupler in the form of UCP (Fig. 1.1), a protein that spans the inner mitochondrial membrane and allows for proton re-entry in the presence of free fatty acids (FA). The action of this protein causes release of the protonmotive energy in the form of heat, hence its alternative name: thermogenin.

Fleury et al. (7) recently identified a gene sequence that highly resembles UCP, but, in contrast to UCP, it is expressed in all tissues. Over-expression of this protein encoded by the clone, named UCP2, caused a dramatic drop in membrane potential in yeast cells. The substrate specificity, regulation, and mechanism of UCP2 are as yet unknown (see Section 8.3.5). The protein was suggested to cause a *natural* leak of protons across the mitochondrial membrane. Location of the gene within human chromosome 11 and mouse chromosome 7, both linked to hyperinsulinemia and obesity, opens a whole new area of research.

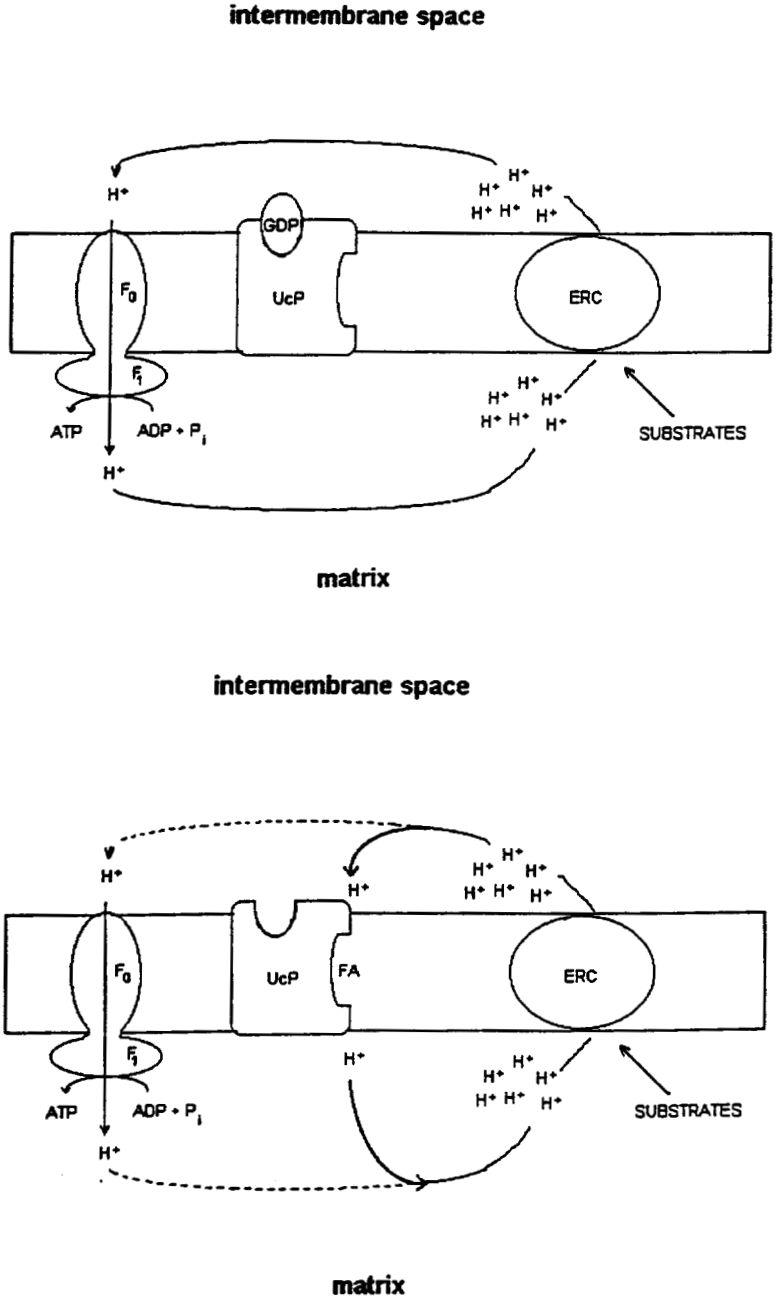

Figure 1.1 Respiration coupling in BAT mitochondria. The electron respiratory chain (ERC) transfers electrons from the substrate to oxygen. Resulting energy is used for pumping protons from the mitochondrial matrix into the intermembrane space. *Top:* Protons re-enter the matrix via ATP synthase (F_0 and F_1), thus allowing production of ATP. The uncoupling protein (UCP) is inhibited by GDP. This is the coupled state. *Bottom:* Protons re-enter the matrix mainly through UCP and only sparsely through ATP synthase. The energy not captured in the form of ATP is released as heat. This is the uncoupled state.

1.2 Non-shivering Thermogenesis

The physiological reason for the presence of UCP in BAT mitochondria is to enable the organism to respond to changes in ambient temperature. Non-shivering thermogenesis, observed in rodents, hibernators, and mammalian newborns, is activated by exposure to cold (1, 8). In addition to the acute thermogenic response, prolonged cold exposure triggers physical growth of brown adipose tissue that is characterized by increased UCP mRNA in the cell (9, 10) and increased UCP expression.

Small mammals and mammalian newborn, including human infants, depend on UCP-mediated non-shivering thermogenesis. Brown fat accounts for at least 70% of the increased oxygen consumption after norepinephrine infusion into newborn rabbits. Hibernating animals undergo extraordinary heat demands upon arousal, to the extent that a sizable fraction of cardiac output is directed to brown fat (11). UCP gene expression stimulated by exposure to cold appears to be mediated by norepinephrine acting on both α_1- and β-receptors (10).

UCP provides a crucial heat source for human newborns. In a recent study of the inhibition of thermogenesis by volatile anesthetic agents (12), slow recovery times indicated that hypothermia in infants is largely due to ineffective non-shivering thermogenesis. There is evidence that decreased levels of UCP in infant brown fat deposits may play a role in the etiology of Sudden Infant Death Syndrome (13). It is generally recognized that obesity may reflect failure of normal energy-wasting mechanisms. It has been suggested that premature atrophy of brown adipose tissue may lead to obesity and, conversely, that regeneration of brown adipose tissue in adults may help to reverse obesity. Direct evidence for these hypotheses, which is difficult to obtain, is lacking. Lowell et al. (14) created transgenic mice defective in UCP1 and found that these mice exhibited two phenotypes simultaneously: they were grossly obese and were also hyperphagic. These experiments established that the energy-wasting role of UCP1 is essential for health in the animal model. Conversely, thermogenically active brown fat is often found in alcoholics (15). A brown fat lipoma exists, known as hibernoma (16).

1.3 Regulation of UCP-mediated Proton Transport

There are two means of regulating UCP-mediated transport on the molecular level: nucleotide inhibition and free fatty acid activation. Hormonal signals trigger a cascade of events that lead to both relief from nucleotide inhibition and release of free fatty acids.

1.3.1 Hormonal signals

A vast collection of data identifies norepinephrine as the hormone responsible for stimulating thermogenesis; triggered by cold, noradrenaline release is directed to BAT, where the hormone can interact with a number of adipocytic receptors. The β_3-type appears the one mainly responsible for acute thermogenic response (17). Recent mutagenic experiments by Susulic et al. (18), who used targeted disruption of the β_3-AR gene coding for the β_3-type receptor to create mice lacking the receptor type, showed that β_1 receptors can substitute for the missing β_3. Noradrenaline interaction with β-receptors increases adenylate cyclase activity resulting in increased cAMP levels inside the cell, a starting point for the cascade of cAMP-dependent events. A protein kinase is activated, which in turn activates a lipase that releases free fatty acids from the triglyceride stores. Free fatty acids are destined for oxidation mainly in mitochondria, are exported out of the cell, or activate the UCP-dependent H^+ transport. This transport dissipates the energy from substrate oxidation as heat by allowing proton entry into the matrix compartment. The respiratory chain responds to such energy dissipation by accelerating its rate, which increases demand for substrates. The result is very fast β-oxidation of fatty acids and increasing rates of all dehydrogenases of the citric acid cycle that feed into the respiratory chain. It is not clear if a hormonal signal exists that would initiate the termination of thermogenesis after it is no longer needed. According to Nicholls and Locke (11), the termination of lipolysis reverses the order of events and ends with shutdown of thermogenesis and steady-state oxidation.

There are four environmental changes (reviewed in ref. 1) that can trigger thermogenic response: (i) cold, (ii) over-eating, (iii) fasting, and (iv) photoperiod. In

all four cases, sympathetic nervous activity, i.e., norepinephrine stimulation, is indicated as the starting signal.

The idea of excess external fatty acids activating thermogenesis, as in the state of overeating, prompted *in vitro* tests on isolated brown adipocytes (19, 20). Indeed, addition of external free fatty acids mimics 80% of the norepinephrine effect (20).

1.3.2 Free fatty acid activation

Initially it was proposed that fatty acids uncouple oxidative phosphorylation allowing thermogenesis to occur (21, 22). Inclusion of BSA did recouple mitochondria (22, 23), but purine nucleotides at millimolar concentrations were capable of complete recoupling, hinting at the existence of a specific pathway in the inner membrane (24, 25). The effect of fatty acids was deemed non-specific, because they were already known for protonophoric effects on isolated mitochondria and direct interactions with UCP were not observed (26).

Extensive experiments on BAT mitochondria of cold- versus warm-adapted guinea pigs demonstrated that the uncoupling effect of fatty acids is specific to BAT mitochondria from cold-adapted guinea pigs (27, 28). Only BAT mitochondria from cold-adapted guinea pigs contained sufficient 32-kDa UCP, as shown by SDS–PAGE, to allow fatty acids to stimulate high proton flux into the mitochondrial matrix. Cunningham et al. (29) confirmed that levels of UCP present in BAT mitochondria from warm-adapted animals required a much higher concentration of fatty acids for uncoupling to occur at rates comparable to BAT mitochondria from cold-adapted animals.

Reconstitution of isolated, purified UCP into lipid vesicles gave the strongest evidence of direct involvement of fatty acids in UCP-mediated proton transport (30–34). Jezek et al. (35) demonstrated binding of azido-labeled fatty acids to UCP. The azido-labeled fatty acid derivative activated UCP-mediated proton transport in the absence of UV illumination, but inhibited both anion and proton transports through UCP after photoactivation. EPR experiments with spin-labeled 5-DOXYL-stearic acid (5-SASL) demonstrated direct interaction of the fatty acid with the isolated UCP (36).

Moreover, increasing ATP concentration converted the 5-SASL signal from bound to free, an effect reversed by raising the pH from 7.2 to 8.5 (37).

The evidence is sufficient to support direct interaction between UCP and fatty acids, but the mechanism of fatty acid action is still disputed. The evolution of UCP transport mechanism hypotheses is summarized below:

1. UCP is a putative OH^- carrier which can transport other monovalent anions, namely Cl^-, Br^-, and NO_3^-, as accidental substrates (38–40).
2. UCP is a simple proton carrier (41).
3. UCP contains two independent pathways, one for protons and the other for anions (42). Garlid (43) further proposed that a fatty acid-binding site is the cause of anion transport.
4. UCP binds one or more fatty acids that serve with their unesterified carboxy groups as a local buffer for protons, allowing their transport (34).
5. UCP is a pure anion transporter which transports fatty acid anions across the inner membrane. This is a protonophoretic cycle, because protonated fatty acids can diffuse rapidly across the membrane and cause acidification (33, 44). The proposed role of the fatty acid-binding site in anion transport is still true (43).

The last two are the most current models and are being actively investigated. Data in Chapters 4 and 5 provide evidence for the fatty acid cycling hypothesis. Although the buffer hypothesis cannot be ruled out completely, it seems less likely, especially in view of the existence of *active* and *inactive* fatty acids (see Chapter 5).

1.3.3 Nucleotide inhibition

The fatty acid activation of uncoupling led initially to a generalized hypothesis of fatty acid permeabilization (21) in which norepinephrine stimulation of lipolysis, and consequently availability of free fatty acids in the cell, would modulate the uncoupling. However, depletion of fatty acids failed to recouple oxidative phosphorylation completely (23, 24, 45, 46).

The inclusion of purine nucleotides does recouple BAT mitochondria completely (23, 24, 45, 46) with respiratory control values close to those obtained for

mitochondria from other tissues. Respiration is coupled completely by millimolar concentrations of ATP or GTP (24, 47). Purine nucleotides stimulate Ca^{2+} uptake in a system where respiratory control is followed as respiration-driven uptake (48). Two effects depend on ADP concentration: micromolar ADP stimulates and millimolar ADP recouples respiration (25). This evidence suggests that a specific site within the inner membrane is responsible for uncoupling of respiration. The site is later identified as UCP.

The affinity of UCP for different ligands was estimated by several methods and the results are summarized (49–51). UCP has high specificity for purine nucleoside di- and triphosphates, whereas purine nucleoside monophosphates or pyrimidine nucleotides do not recouple BAT mitochondria (23, 50). The interaction is non-covalent, reversible binding typical for ligand–receptor interactions (50). The nucleotide binding site is located on the cytosolic side of UCP, and binding is not accompanied by hydrolysis (50). The inhibition of UCP transport by purine nucleotides is non-competitive (allosteric) in nature (34, Chapter 3). Nucleotide binding is modulated by pH and Mg^{2+} (23, 51, 52). Short-chain alkylsulfonates, which are anionic substrates of UCP (53), are competitive inhibitors of GDP binding (54).

1.4 Anion Transport by UCP

Nicholls and Lindberg (59) were the first to demonstrate nucleotide-sensitive anion conductances in BAT mitochondria. Addition of valinomycin to the mitochondria caused swelling in the presence of potassium salts of Cl^-, Br^-, NO_3^-, and SCN^-. With all but KSCN, swelling was inhibited by purine nucleotides at concentrations equal to those required for mitochondrial recoupling, suggesting an electrophoretic pathway for anions. The lack of nucleotide inhibition of KSCN-induced swelling is due to high permeability of biological membranes to SCN^-.

Cl^- transport was not affected by pH (59), thus ruling out a known phenomenon of pH-dependent, but nucleotide-independent, Cl^- flux in rat liver mitochondria due to the inner membrane anion channel (IMAC) (60, 61). Jezek et al.

(62) provided evidence for IMAC presence in addition to the nucleotide-sensitive anion pathway in BAT mitochondria.

A more sensitive, quantitative assay of mitochondrial swelling revealed a much broader range of anionic substrates of UCP (32, 53), including alkylsulfonates and their derivatives, monovalent phosphate analogs, oxohalogenides, and various monovalent organic anions. The assays were performed under conditions of low pH to prevent IMAC opening. All the substrates showed nucleotide-sensitive transport, with the extent of inhibition dependent on the size of the anion. Experiments of Nedergaard and Cannon (54) established that hexanesulfonate, benzenesulfonate, and sulfanilate are weak ligands for the GDP-binding site on UCP, implying this competitive interaction can partially account for the old observation of a discrepancy between the binding and inhibition constants for GDP (63).

Regarding substrate specificity, the anion pathway has several requirements for transport: the anion must be monovalent and unipolar with the polar moiety attached to an alkyl and aryl group. Data in Table 1.1 demonstrate clear preference for hydrophobic anions as indicated by the apparent K_m. Structural features of fatty acids in relation to UCP-mediated proton transport are discussed in Chapter 5. The two apparently contrasting features of UCP, transport of anions and protons, led to the fatty acid cycling hypothesis (33, 44). Although no direct demonstration of fatty acid cycling exists, the data presented in Chapters 4 and 5 offer strong support for the hypothesis.

1.5 Exploring Structure/Function Relationships in UCP

Functions of a protein are always associated with specific structural features that need to be examined to establish or improve a model for protein mechanism and its regulation. The initial tests consist of reacting the protein with specific amino acid modifiers, for example NEM, or digestion of the protein with proteases and assaying for alterations in protein function. In the case of UCP, the functional assays are (i) UCP-mediated proton transport; (ii) UCP-mediated anion transport; (iii) nucleotide inhibition of transport; and finally (iv) changes in nucleotide binding to UCP.

Table 1.1

Affinity of UCP Increases with Substrate Hydrophobicity

The table contains selected anion substrates of UCP and their apparent K_m. The number of plus signs in the hydrophobicity column designates the respective anions' hydrophobic behavior, which is based on the water solubility of the sodium salt of each anion listed.

Anion	K_m (M)	Hydrophobicity
Cl^-	1.4×10^{-1}	±
Hexanesulfonate	1.2×10^{-2}	++
Undecanesulfonate	1.2×10^{-5}	+++
Laurate	8.0×10^{-6}	+++
Oleate	5.0×10^{-6}	++++

Knowledge of the UCP gene coding sequence, the deduced amino acid sequence, and membrane topology enables comparisons with other known proteins. This approach, in combination with site-directed mutagenesis, led us to uncovering the role of essential amino acids (see Chapters 7 and 8).

1.5.1 Chemical and protease modifications of UCP

Chemical modification of UCP by sulfhydryl reagents offered the first insight into the protein's structure/function relationships. Rial and Nicholls (64) showed modification of GDP binding by both NEM and tetranitromethane. NEM increased both H^+ and Cl^- transport by up to 80%, while it decreased GDP inhibition of Cl^- transport but not GDP inhibition of H^+ transport. A single cysteine residue was shown to be water-accessible by reacting undenatured UCP with Nbs_2, while up to three residues were accessible to more hydrophobic reagents (64). Jezek (65) described one essential -SH group that is water-accessible on the cytosolic surface of UCP and proposed two separate pathways for H^+ and Cl^- transports based on the effects of mersalyl, which inhibits H^+, but not Cl^-, transport.

Further tests led to more elaborate models. Rial et al. (66) proposed a two-step modification of UCP to explain a time-dependent exponential increase in both H^+ and Cl^- transport caused by three sulfhydryl reagents. Jezek and Drahota (67) developed a model for distinct cysteine residues based on the accessibility to reagents and effects of these reagents on both H^+ and Cl^- transports and on GDP inhibition.

Lin and Klingenberg (49) concluded that neither cysteine nor methionine residues were involved in binding, because DTT treatment had no effect on GDP binding. However, treatment with TNBS, a lysine-specific reagent, did inhibit GDP binding (49) as did two arginine-specific reagents, phenylglyoxal and 2,3-butanedione (31). The proton conductance through UCP treated by the latter two reagents was not affected, implying two distinct sites: one for GDP binding and the other for fatty acid interaction (56). DABS, a chemical that reacts with ionizable groups, decreased UCP sensitivity to GDP (68). These results were confirmed and extended by experiments with site-directed mutants of UCP (Chapters 7 and 8).

Azido derivatives of ATP allow covalent binding to UCP upon illumination with near-UV light (69). Subsequent cleavage of the labeled polypeptide with CNBr followed by peptide sequencing help to localize residues involved in ATP binding. 8-azido-ATP was shown to bind the stretch of residues 173–280 (69), while 2-azido-ATP associated with residues 258–283 and FDNP–ATP with residues 238–255 (70). The combined stretch of residues 170–283 is located within the third domain of the tripartite UCP structure, namely α-helices 5 and 6. Mayinger and Klingenberg (70) proposed that Thr263 and Cys253 are the residues directly involved in ATP binding.

Chymotrypsin caused proteolytic fragmentation of UCP and parallel decrease of both H^+ and Cl^- transport with the polypeptide pattern affected by GDP (71). A crosslink formed between the C-terminal residues by Cu^{2+}-phenantroline oxidation did not interfere with GTP binding or proton transport. The crosslink can be removed by trypsin digestion; trypsin cleaves UCP at Lys292 (72) without affecting proton transport or nucleotide binding (73). Thus, the 13 C-terminal amino acid residues, including Cys304, are not essential for transport or nucleotide binding. Several different Cys304 mutants prepared and tested by Gonzalez-Barroso et al. (74) suggested that the Cys304 modulates the K_m for fatty acids.

The findings of these chemical modification studies are useful in narrowing the search for an essential residue, even though a specific single residue cannot be pinpointed. The more powerful technique of site-directed mutagenesis is better suited to finding the essential amino acid residues in proteins.

1.5.2 UCP is a member of the mitochondrial anion carrier gene family

The relative impermeability of the inner mitochondrial membrane requires a host of transport proteins to facilitate metabolite or ion flux into and out of the matrix. The anion carrier family, of which UCP is a member, encompasses most of the essential transporters: ADP/ATP carrier (AAC), phosphate carrier (PiC), oxoglutarate carrier, citrate carrier, dicarboxylate carrier, carnitine carrier, aspartate/glutamate carrier, and ornithine carrier (5, 75). In addition to their specificity for anionic substrates, these proteins share general structural features that can serve as clues in elucidating their respective mechanisms.

The molecular masses of anion transport proteins range from 28 through 34 kDa as estimated by SDS–PAGE. They span the inner membrane six times with the N and C polypeptide termini facing the cytosol. All the proteins contain three similar parts, each of about 100 amino acid residues. This feature is called the tripartite structure. No common functional role of any of these parts is known, but homologous residues exist among the anion carriers.

The most extensively studied member of this gene family, the AAC, also appears to be the closest relative of UCP among the anion carriers. Thus, experiments aimed at studying the AAC became the basis for experiments developed to study UCP. The observation of AAC-mediated free fatty acid-induced uncoupling in mitochondria (76, 77), together with a wide range of anion substrates of UCP (53), led Skulachev to propose the fatty acid cycling mechanism of UCP (44). Now data are available in support of the cycling hypothesis (33, Chapters 4 and 5). Site-directed mutagenesis experiments identified essential arginine and lysine residues within the AAC protein (78). These data were then used to design single mutants of UCP, which led to identification of three arginines essential for GDP binding and inhibition (79, Chapters 7 and 8).

The tricarboxylate carrier (80) is another example. Multiple Cys → Ser mutants of this protein resulted in the gradual loss of activity as compared to wild type, but sensitivity to benzenetricarboxylic acid inhibition was unaffected. The loss of activity appeared to depend on the number of cysteine residues mutated (81). Similar effects of multiple Cys → Ser mutations are observed in UCP (Chapter 6). Activity of the tricarboxylate carrier lacking all four cysteine residues was restored to about 60% of wild type when valine or alanine were used for substitutions instead of serine (81). It is very likely that similar combinations of Cys → Ser and Cys → Val substitutions in UCP will allow construction of a cysteine-less mutant that retains a high percentage of wild-type activity. The cysteine-less mutant can then be used in EPR experiments to elucidate the three-dimensional structure of the UCP and its conformation in the membrane.

1.5.3 The UCP yeast expression system

Availability of a cDNA sequence for UCP (82–87) made possible structure/function studies that would use over-expressed protein. A system yielding high amounts of reconstitutively active UCP was the necessary next step, because UCP is a low activity protein. The bacterial system proved successful for over-expression of reconstitutively active oxoglutarate (88) and tricarboxylate (89) carriers, but it failed with the phosphate carrier for suspected translational incompatibilities (90). Fusion proteins consisting of MalE and UCP fragments were used to achieve expression of UCP in *Escherichia coli* (91). These fusion proteins, however, could not be used for kinetic experiments or ligand binding studies. Klingenberg (pers. comm.) is re-exploring *E. coli* expression of UCP, without success so far. Attempts were also made to over-express UCP in *Xenopus* oocytes (92) and Chinese hamster ovary cells (93). The latter was successful, but was not practical because of low yield.

Yeast cells are widely used for expression of foreign proteins (reviewed in ref. 94). The reasons are: (i) yeasts are food organisms known to mankind for millennia; (ii) they can be manipulated almost as easily as *E. coli*; (iii) they are single-cell eukaryotes with genetics more advanced than any other eukaryotes; and (iv) they grow rapidly on simple media to high cell densities. Yeast cells do contain mitochondria that allow incorporation of foreign mitochondrial proteins and subsequent respiratory control experiments or application of purification methods developed for the original source mitochondria.

A yeast expression system using *Saccharomyces cerevisiae* has proven to yield large amounts of reconstitutively active protein indistinguishable from native UCP (95) and was successfully used for over-expression of mutagenized UCP (74, 79, 96, 97). The over-expressed UCP is tested in a whole cell environment by using flow cytometry (74) in isolated mitochondria (95, 97) or purified and reconstituted into liposomes (79, 96, Chapters 6, 7, and 8).

The system developed in Dr. Freeman's laboratory (McMaster University) uses a 2-micron-circle-based *E. coli/S. cerevisiae* shuttle vector that contains a rat UCP cDNA insert (95). The UCP cDNA fragment is under control of the inducible

GAL1 promoter. Initial low yield of expressed UCP was increased by changing the region around the 5′ translation start codon into a sequence resembling that of a highly expressed yeast protein and also resembling commonly used yeast codons (95). The yeast-expressed UCP is present in the mitochondrial and postmitochondrial fractions as demonstrated by immunoblotting of the cell fractions of the transformant yeast cells grown in the presence of 0.2% galactose for ten hours. Mitochondria isolated from the yeast transformants contained UCP in amounts (about 10% of mitochondrial protein) similar to amounts in BAT mitochondria. Therefore, isolation and reconstitution protocols can be readily applied to yeast mitochondria.

Chapter 2

TRANSPORT OF ANIONS AND PROTONS BY THE MITOCHONDRIAL UNCOUPLING PROTEIN AND ITS REGULATION BY NUCLEOTIDES AND FATTY ACIDS[1]

The physiological function of uncoupling protein (UCP) is to catalyze passive electrophoretic back flux of protons across the inner membrane of brown adipose tissue mitochondria, thereby uncoupling oxidative phosphorylation and producing heat. UCP mediates proton flux, and this transport is also inhibited by purine nucleotides. These basic properties have been demonstrated in intact brown adipose tissue mitochondria and with purified reconstituted UCP (8, 30, 32, 39, 40, 53, 98).

Several specific hypotheses relating to nucleotide regulation of UCP were introduced by Nicholls and co-workers (38, 63, 99, 100). These hypotheses have been influential, but they have remained largely untested, clouding our understanding of these mechanisms. Taking advantage of our ability to measure transport kinetics in proteoliposomes reconstituted with purified UCP (32, 53), we have been able to refute these hypotheses, thereby clarifying the role of nucleotides as strictly allosteric inhibitors of UCP. Thus, GDP inhibition of Cl^- transport is strictly noncompetitive with Cl^-, is not voltage-gated, and is not affected by the concentration of fatty acids.

The relationship between anion transport and proton transport has similarly been obscured by untested hypotheses. There is now broad agreement that fatty acids are required for activation of UCP-mediated proton transport. Nicholls (39) further proposed that Cl^- is an accidental substrate of a carrier specialized to transort OH^-, a suggestion that was supported by Klingenberg (40). Furthermore, the consensus in the field has been that there is no interaction between fatty acids and anion transport (30, 99, 100). These hypotheses predict strong interaction between Cl^- and H^+/OH^- ions and no interaction between Cl^- and fatty acids. Our results show the opposite to

be true; Cl^- transport kinetics were unaffected by pH. On the other hand, Cl^- transport in both mitochondria and UCP-containing proteoliposomes was strongly inhibited by fatty acids, and this inhibition was reversed by fatty acid removal.

Clearing away these old hypotheses sharply narrows the search for biophysical mechanisms of UCP transport and regulation and focuses attention on the relationships between anion transport and fatty acid activation of proton transport (*cf.* Ref. 34). Thus, our findings support the hypothesis (43) that anions are transported through the fatty acid binding domain of UCP and that this domain is separate from the nucleotide binding domain.

2.1 Materials and Methods

2.1.1 Mitochondrial preparations

Brown adipose tissue mitochondria were isolated from Syrian hamsters in a medium containing 250 mM sucrose, 5 mM TES, and 1 mM EGTA, adjusted with KOH to pH 6.7 (62). The isolation medium contained 2 mg BSA/ml to reduce carryover of endogenous fatty acids. The final stock suspension, at 50 mg of protein/ml, was used for purification of UCP.

2.1.2 Light-scattering assays of Cl^- and H^+ fluxes on brown adipose tissue mitochondria

In intact mitochondria, the effects of fatty acids on ion transport assayed by light scattering were obscured by a significant partial lysis that occured within the dose range of fatty acids that we wanted to study. The following pretreatment protocol avoided this problem. Stock mitochondria were mixed in a 1:1 ratio with 250 mM sucrose containing 100 mg/ml BSA. 100-μl aliquots of this suspension were supplemented with palmitic acid at a final concentration between 0.24 and 16 μM. After 2.5 min of incubation on ice, 15 μl of this mixture was transferred into 3 ml of medium at 25°C for light-scattering assay. The final concentrations in the assay medium were 0.1 mg of mitochondrial protein/ml and 0.25 mg of BSA/ml (3.8 μM). Final total [palmitate] ranged between 1.2 and 81.1 μM. Assay media contained 50

mM KCl or potassium acetate and K-TES buffer, pH 7.2, and flux was induced by 0.25 μM valinomycin. In KCl, valinomycin-induced K^+ influx must be balanced by Cl^- influx. In potassium acetate, neutral acetic acid penetrates the membrane, and valinomycin-induced K^+ influx must be balanced by H^+ efflux. Uptake of salts and water causes mitochondria to swell and absorbance (A) to decrease, and the rate of change of the light-scattering signal ($A^{-1} \cdot mg\ protein^{-1} \cdot min^{-1}$) is quantitatively related to salt uptake (4, 101, 102).

2.1.3 Purification and reconstitution of uncoupling protein

Following protocols previously described (32, 53), mitochondria were solubilized in 13% octylpentaoxyethylene in the presence of phosphatidylcholine, cardiolipin, and phosphatidic acid, and this mixture was applied to a hydroxyapatite column. Internal medium was adjusted to the desired composition, and the fluorescent probe SPQ was added at 2 mM. Vesicle formation and external probe removal were accomplished by sequential treatment with Bio-Beads SM-2 and Sephadex G-25.

2.1.4 Obtaining fluxes from quenching of SPQ fluorescence

Aliquots of the proteoliposome suspension containing 40 mg of lipid/ml were added to 2 ml of assay medium at a final concentration of 0.5 mg of lipid/ml. Fluorescence assays with SPQ-loaded proteoliposomes were carried out using an SLM 8000 fluorometer (SLM-AMINCO, Urbana, IL). Internal liposomal volume (V_i), determined from the volume of distribution of SPQ, was 1.1–1.6 μl/mg of lipid. Protein content (P), estimated by the amidoblack method (103), was 1–3 μg of protein/mg of lipid. Transports of Cl^- and H^+ were quantitated from quenching of SPQ fluorescence by Cl^- and the anion of TES buffer, respectively. The relationship between net fluorescence (F) and the concentration of analyte anion ($[A]_i$) is as follows (104):

$$1/F = 1/F_A + m_A[A]_i \qquad \text{(Eq. 1.1)}$$

where F_A and m_A are constants determined by calibration. If no other quenchers are present in the solution, m_A is equal to the Stern–Vollmer constant. Where used, normalized flux, J (nmol/mg protein • min), was obtained by multiplying $d[A]_i/dt$ by V_i/P.

Equation 1.1 is fully valid in the presence of other quenching solutes which reduce sensitivity but do not otherwise pose a problem if they remain constant. The small contribution from GDP fluorescence was removed by subtraction (104).

2.1.5 Media compositions

Media compositions were designed to minimize quenching of SPQ fluorescence by interfering solutes, to balance internal and external osmotic strengths, and to achieve the gradients required to drive transport. Within these limits, composition of internal and external media could be varied over a wide range without adverse effects on UCP transport. For example, when we wanted to study Cl^- kinetics up to 240 mM Cl^-, we raised the osmotic strenght of both media from the customary 270 to 450 mosM. Media were buffered to the desired pH. When measuring H^+ transport, the internal buffer was TES. The anion of TES buffer quenches SPQ fluorescence, whereas the zwitteriion does not. Therefore, changes in SPQ fluorescence monitor changes in intraliposomal acid content due to H^+ transport across the membrane (104). When measuring Cl^- transport, the internal buffer was Tris and/or phosphate, neither of which quenches SPQ fluorescence (104). Sulfate was used as the indifferent anion in both types of experiment. Media typically contained 0.6 mM EGTA. Electrophoretic fluxes were typically driven by a K^+ gradient and initiated by addition of 0.1 μM valinomycin. TEA^+ was used as the indifferent cation.

2.1.6 GDP titrations

The GDP-binding site on UCP is only accessible from the cytosolic side of brown adipose tissue mitochondria (39), but the orientation of reconstituted UCP is random (32). Therefore, when titrating with external GDP, it is necessary to subtract the flux that is not inhibitable by external GDP. This was done by subtracting flux observed at saturating doses of external GDP, which were determined by experiment

to be [GDP] 0.2 mM at pH 7.2, consistent with observed K_i values of 10–20 μM. This procedure corrects for flux through outwardly oriented UCP and for residual transport due to ion leak. We have carefully compared residual transport in GDP-inhibited proteoliposomes with liposome leak. For both Cl^- (32) and H^+, the transport rate in the presence of 500 M GDP on both sides of the proteoliposomal membrane was nearly identical with the rate in liposomes.

2.1.7 Materials

SPQ was purchased from Calbiochem, fatty acid-free BSA was purchased from Sigma, and the sources of other materials for reconstitution were the same as previously described (32, 53).

2.2 Results

2.2.1 GDP inhibition of Cl^- transport through UCP is strictly noncompetitive

To examine the hypothesis that GDP is a competitive inhibitor of Cl^- transport (63), we measured Cl^- uptake kinetics at varying levels of GDP using protocols previously described (32). The data are contained in Fig. 2.1 as Eadie–Hofstee plots. The kinetic curves at different [GDP] are parallel, showing that the K_m for Cl^- was independent of [GDP] and that a reduction in V_{max} completely accounted for the effects of GDP inhibition. Thus, GDP inhibition of Cl^- transport through UCP is strictly noncompetitive with Cl^-. K_i values for GDP were derived from the intercepts, assuming 50% outward orientation of nucleotide binding sites (32). The mean K_i value for GDP inhibition of Cl^- transport in this series of five experiments was 9.6 $\pm$ 1.8 μM at pH 7.2.

2.2.2 pH does not affect the K_m for Cl^- transport through UCP

The hypothesis that Cl^- competes with OH^- for a common carrier site (63) was examined by studying the kinetics of Cl^- transport over a wide range of pH. We observed no effect of pH on the K_m or V_{max} for Cl^- transport. Fig. 2.2 contains Hanes

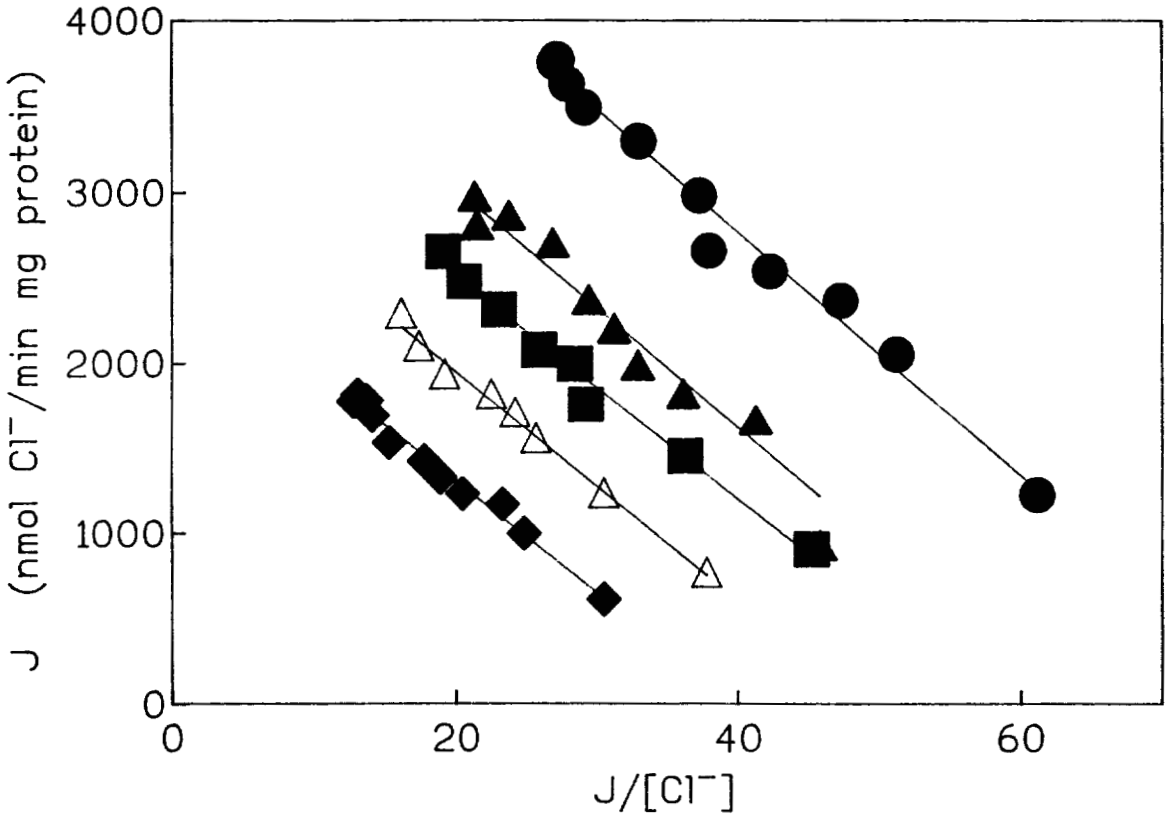

Figure 2.1 GDP inhibits Cl^- uptake with noncompetitive kinetics in proteoliposomes containing reconstituted UCP. Eadie–Hofstee plots were constructed from values of Cl^- influx, and J, calculated per milligram of total protein, was measured at varying medium [Cl^-] (mM). The *lines* connect sets of data obtained in different GDP concentrations. Linear regressions of the data yielded K_m values for Cl^- of 69 $\pm$ 4 mM in the absence of GDP (●), 70 $\pm$ 6 mM in 5 mM GDP (▲), 65 $\pm$ 3 mM in 20 mM GDP (■), 68 $\pm$ 3 mM at 40 mM GDP (△), and 65 $\pm$ 4 mM at 60 mM GDP (◆). For these experiments, external medium contained 25 mM TEA-TES, pH 7.2, and 150 mM K^+ salts of Cl^- or MES to achieve the desired $[Cl^-]_{out}$.

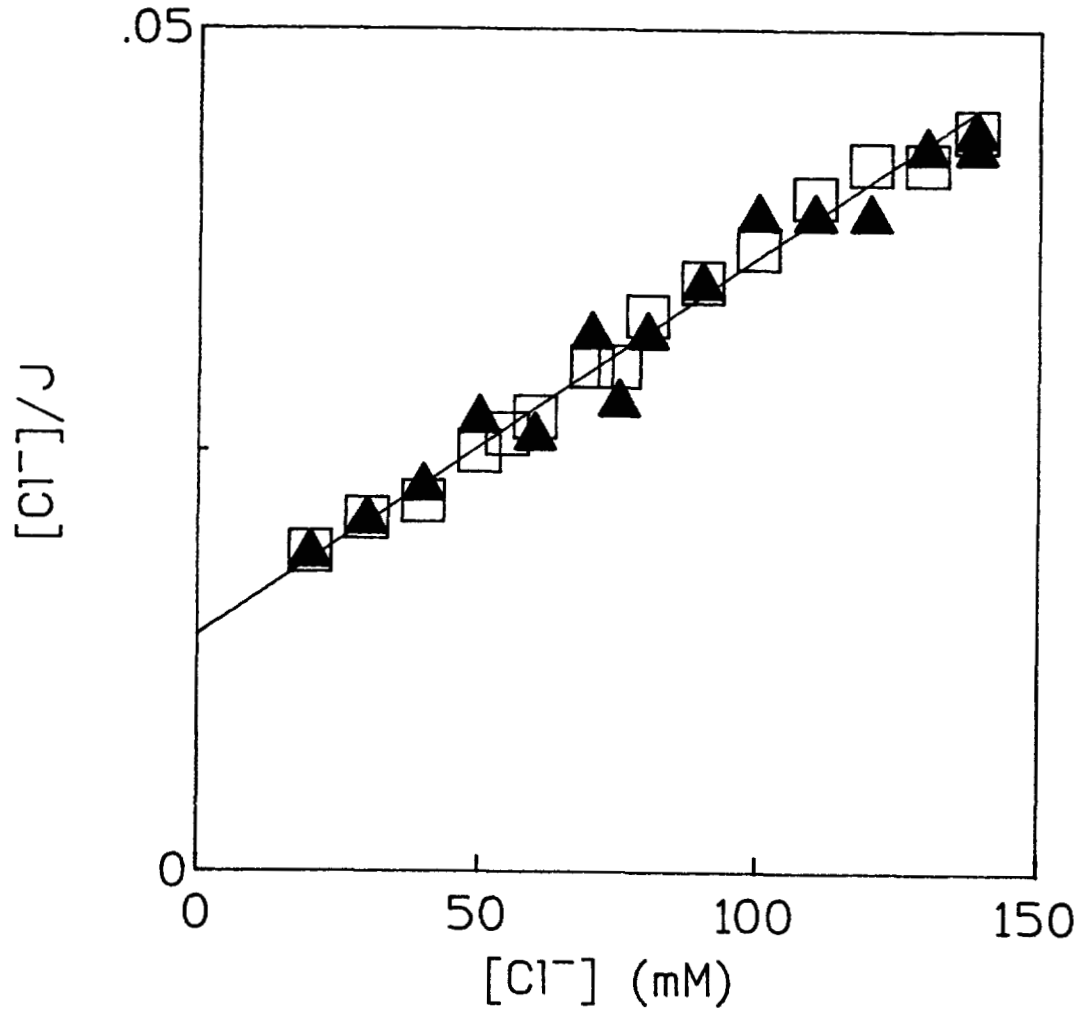

Figure 2.2 The kinetics of Cl^- uptake through reconstituted UCP are unaffected by pH. Hanes plots were constructed from values of Cl^- influx, and J was measured at varying medium [Cl^-]. The *line* connects two different sets of data obtained at pH 6.8 (▲) and pH 7.8 (□). Internal pH equaled media pH in both cases. Linear regressions of the data yielded $K_m = 61 \pm 7$ mM at pH 6.8 and $K_m = 62 \pm 4$ mM at pH 7.8. External medium contained 150 mM K^+ salts of Cl^- or MES to achieve the desired $[Cl^-]_{out}$. 25 mM Tris-MES were used for measurements at pH 6.8 and 7.8, respectively.

plots at the extreme values studied, pH 6.8 and 7.8. The K_m values for Cl^- for the two measurements were 61 $\pm$ 6 mM and 62 $\pm$ 4 mM, respectively, similar to values previously obtained at pH 7.2 (32).

2.2.3 $\Delta\psi$ does not affect GDP inhibition of UCP-mediated Cl^- or H^+ transport

We examined the hypothesis that GDP inhibition of Cl^- and H^+ transport is voltage-gated (38, 99, 100, 105). In no case did we observe any effect of $\Delta\psi$ on the K_i for GDP dose–response curves for inhibition of either Cl^- or H^+ transport in the reconstituted system. $\Delta\psi$ was clamped at the K^+ equilibrium potential by valinomycin. Fig. 2.3A contains representative GDP dose–response curves for inhibition of Cl^- efflux in two experiments carried out at 176 and 60 mV. Fig. 2.3B contains GDP dose–response curves for inhibition of H^+ efflux, induced by 30 μM laurate, in two experiments carried out at 185 and 140 mV. The dose–response curves for GDP inhibition are practically identical, and least squares fit of the data yielded K_i values of 8.7 $\pm$ 0.5 μM at 176 mV and 9.6 $\pm$ 0.6 μM at 60 mV for inhibition of Cl^- efflux and 16 $\pm$ 1 μM at 185 and 140 mV for inhibition of H^+ efflux.

2.2.4 Fatty acids do not affect the K_i for GDP inhibition of H^+ or Cl^- transport

Summarizing the results of an extensive series of experiments in both proteoliposomes and mitochondria, we observed no effects of fatty acid concentration on the K_i for GDP inhibition of H^+ or Cl^- transport. Fig. 2.4 contains GDP dose–response curves in proteolipoxomes containing different levels of fatty acids. These titrations were collected in pairs from experiments prepared on different days. The mean K_i values for GDP inhibition were 17 μM in one experiment and 13 μM in the other. As can be seen in the normalized plots of Fig. 2.4B, this variation did not arise from effects of fatty acids. Similarly, the K_i for GDP inibition of Cl^- transport in proteoliposomes was unaffected by the amount of palmitate or laurate present (data

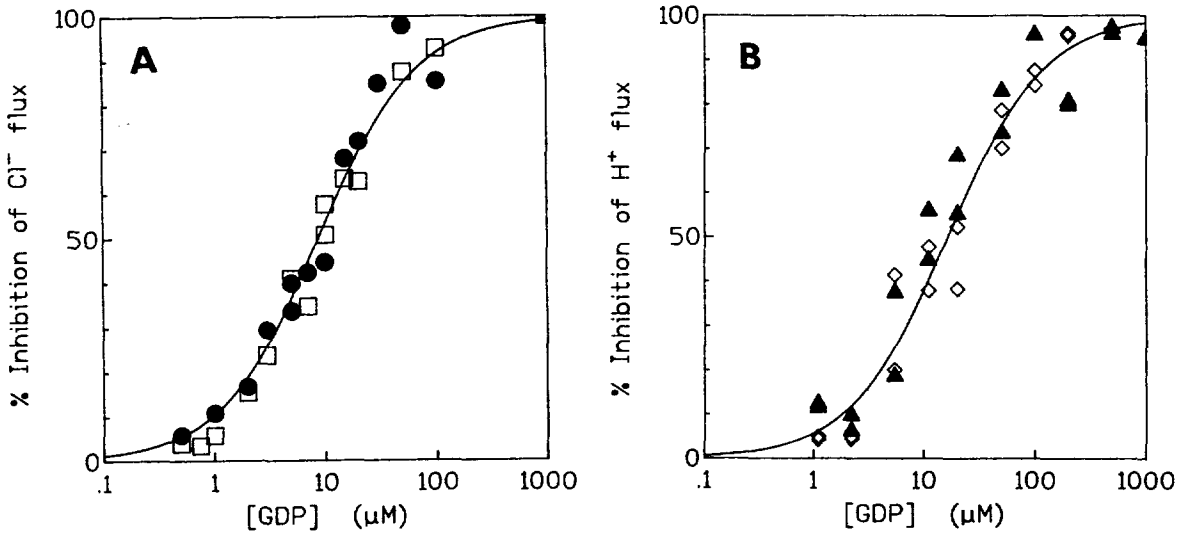

Figure 2.3 The K_i for GDP inhibition of UCP-mediated Cl^- uptake and H^+ efflux in proteoliposomes is unaffected by $\Delta\psi$. *Panel A*, percent inhibition of Cl^- influx *versus* external [GDP]. GDP dose-response curves were obtained at 176 (●) and 60 mV (□), and the resulting K_i values for GDP inhibition were 8.7 ± 0.5 μM and 9.6 ± 0.6 μM, respectively. Hill plots (not shown) were linear, and the Hill coefficient was 1 within experimental error, as previously observed (32). The *solid curve* was drawn with the Hill coefficient = 1 and K_i = 9 μM. These data are from two separate reconstitutions whose internal [K^+] was 0.14 and 13.4 mM. External [KCl] was 138 mM, and $\Delta\psi$ was calculated from the K^+ distribution. 100% inhibition was defined by the flux at external [GDP] = 1 mM, as described in Section 2.1.6. *Panel B*, percent inhibition of H^+ efflux versus [GDP]. GDP dose-response curves were obtained at 185 (◇) and 140 mV (▲). The *solid curve* was drawn with the Hill coefficient = 1 and K_i = 16.3 μM. These data are from two separate reconstitutions. Internal [K^+] was 0.14 mM. External [K^+] was 169 (185 mV) or 11.9 mM (140 mV), and was calculated from the K^+ distribution. 100% inhibition was defined by the flux at external [GDP] = 1 mM, as described in Section 2.1.6.

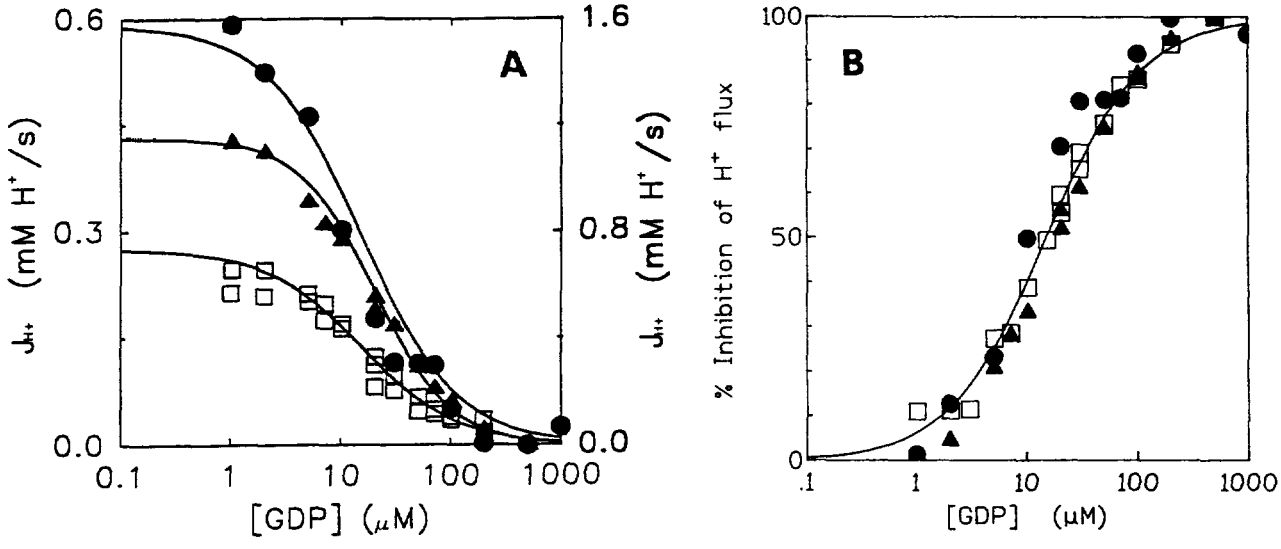

Figure 2.4 The K_i for GDP inhibition of H^+ transport in proteoliposomes is independent of fatty acid concentration. *Panel A*, net proton influx into proteoliposomes containing UCP, JH^+, is plotted *versus* external [GDP]. The rates in the presence of laurate (●) were faster than the other rates and therefore were plotted on a different scale. JH^+ is defined as total H^+ flux minus the flux observed in the presence of 1 mM GDP, as described in Section 2.1.6. The data are pairs of titrations from two experiments carried out on separate days. One pair compares preparations containing endogenous fatty acids (▲) with BSA-treated brown adipose tissue mitochondria (□). The K_i values observed on this pair were 16.9 and 16.8 μM, respectively. The second pair compares preparations containing 25 μM laurate in the assay medium (●) with BSA-treated brown adipose tissue mitochondria (□). The K_i values observed in this pair were 13.0 and 12.6 μM, respectively. K_i values were obtained from nonlinear regression of all data in each set, with 100% inhibition defined as flux at 1 mM GDP as described in Section 2.1.6. Derived Hill slopes ranged between 0.9 and 1.05. The curves in the figure are plotted with Hill coefficient = 1. *Panel B*, the data sets contained in Panel A were each normalized to rates in the absence of GDP. Percent inhibition of these rates is plotted *versus* [GDP]. The *solid curve* was plotted by fitting all data to the Hill equation with Hill coefficient = 1. H^+ uptake rates were determined by quenching of SPQ, as described in Section 2.1.6. Internal medium contained 50 mM K_2SO_4, 29 mM Na_2SO_4, 0.5 mM Na-EGTA, and 29.7 mM Na-TES, pH 8.0. External medium contained 0.625 mM K_2SO_4, 79 mM Na_2SO_4, 0.5 Na-EGTA, and 46.7 mM Na-TES, pH 7.0. Transport was initiated by 0.1 μM valinomycin.

not shown). The absence of a fatty acid-induced shift in the K_i for GDP inhibition of H^+ and Cl^- transport in proteoliposomes has been observed in 10 and 5 experiments, respectively.

Entirely consistent results were obtained in brown adipose tissue mitochondria (data not shown). The results with mitochondria, pretreated as described in Section 2.1.2, were particularly straightforward; fatty acids had no effect on the K_i for GDP inhibition of either H^+ or Cl^- transport. Because this result was not in agreement with a reported fatty acid-induced shift in the K_i for ATP inhibition of Cl^--dependent swelling (100), we also examined non-pretreated brown adipose tissue mitochondria, as used by Rial et al. (100). In this preparation, increasing fatty acids did appear to cause a shift of the K_i for GDP inhibition of Cl^- transport toward higher values; however, the light-scattering base line also increased. The K_i shift disappeared when the rates were normalized to ionophore-dependent (and UCP-independent) transport rates measured at each fatty acid concentration. Thus, the shift is presumably an artifact caused by a shift on the light-scattering base line that in turn may have been due to fatty acid-dependent lysis of some fraction of mitochondria.

2.2.5 BSA activates and fatty acids inhibit Cl^- transport through UCP in brown adipose tissue mitochondria

It was concluded from qualitative light-scattering experiments on brown adipose tissue mitochondria that BSA and fatty acids have no effect on Cl^- transport through UCP (63, 99, 100). The pretreatment protocol described in Section 2.1.2 was used to study the effects of added fatty acids on Cl^- and H^+ transport in intact brown adipose tissue mitochondria. Transport rates were estimated using quantitative light-scattering analysis (43). KCl transport and potassium acetate transport were induced by valinomycin and inhibited by GDP, demonstrating electrophoretic UCP-mediated Cl^- and H^+ transport, respectively.

The data in Fig. 2.5 show that palmitate inhibited Cl^- transport (circles) and stimulated H^+ transport (triangles) and that the dose ranges of these effects were nearly coincident. Similar results were observed with decanoate, laurate, myristate, and oleate (data not shown). The apparent inhibition of H^+ transport at high doses of

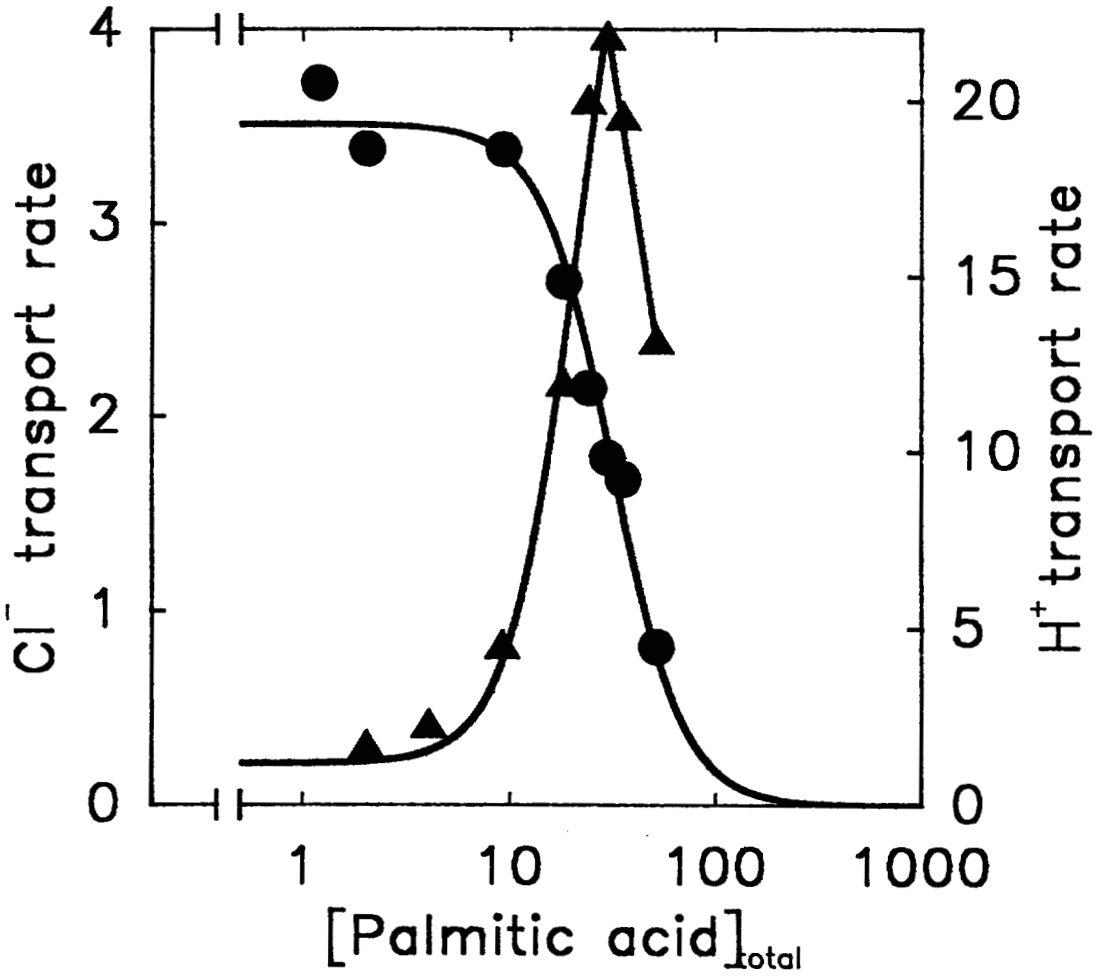

Figure 2.5 Palmitate activates H^+ transport and inhibits Cl^- transport in brown adipose tissue mitochondria. Rates of Cl^- influx (●) and H^+ efflux (▲), in light-scattering units of $A^{-1} \cdot mg\ protein^{-1} \cdot min^{-1}$, are plotted versus total [palmitate] in the assay medium. Cl^- and H^+ transport in brown adipose tissue mitochondria were initiated by 0.25 μM valinomycin in KCl and potassium acetate assay medium, respectively. Media compositions and protocols for palmitate treatment and light scattering assay are described in Section 2.1.2.

palmitate (Fig. 2.5) was observed with high doses of all amphiphiles. We attribute this phenomenon to surface-active effects.

Cl^- transport in the absence of added palmitate, plotted on the *ordinate* of Fig. 2.5, was the maximum attainable rate of Cl^- transport and is due to removal of fatty acids during the pretreatment protocol. Thus, we routinely observed that Cl^- transport in brown adipose tissue mitochondria containing endogenous fatty acids was stimulated 20–30% by BSA (data not shown). This further demonstrates that Cl^- transport through UCP is inhibited by fatty acids.

Conversely, apparent H^+ transport in the absence of added palmitate, plotted on the *ordinate* of Fig. 2.5, was the minimum attainable rate of potassium acetate transport and is also due to removal of fatty acids during the pretreatment protocol. This minimum rate was reproducibly different from zero and was inhibited by GDP (not shown). We have evidence to indicate that this is not due to fatty acid-independent H^+ transport but rather to acetate anion uniport through UCP.

2.2.6 BSA activates Cl^- transport through UCP in proteoliposomes

We routinely observed that Cl^- transport in proteoliposomes was activated by BSA and inhibited by fatty acids. The traces in Fig. 2.6 show that Cl^- efflux from liposomes reconstituted with UCP and supplemented with laurate was strongly activated by BSA, which presumably acts by removing laurate from UCP.

2.2.7 Laurate competitively inhibits Cl^- transport through UCP

The laurate dose-response curve in Fig. 2.7 demonstrates laurate inhibition of Cl^- efflux from proteoliposomes with a K_i value of approximately 30 μM. Proteoliposomes contained 0.5 mM internal GDP, and Cl^- efflux was inhibited by nearly 100% when external GDP was added (not shown). We always observed fatty acid inhibition of Cl^- transport in the reconstituted system, but the extent of maximal inhibition ranged between 50–90% under the conditions of Fig. 2.7. This degree of variability is atypical of measurements with reconstituted UCP and may reflect nonspecific effects of laurate at the high doses required for complete inhibition of Cl^-

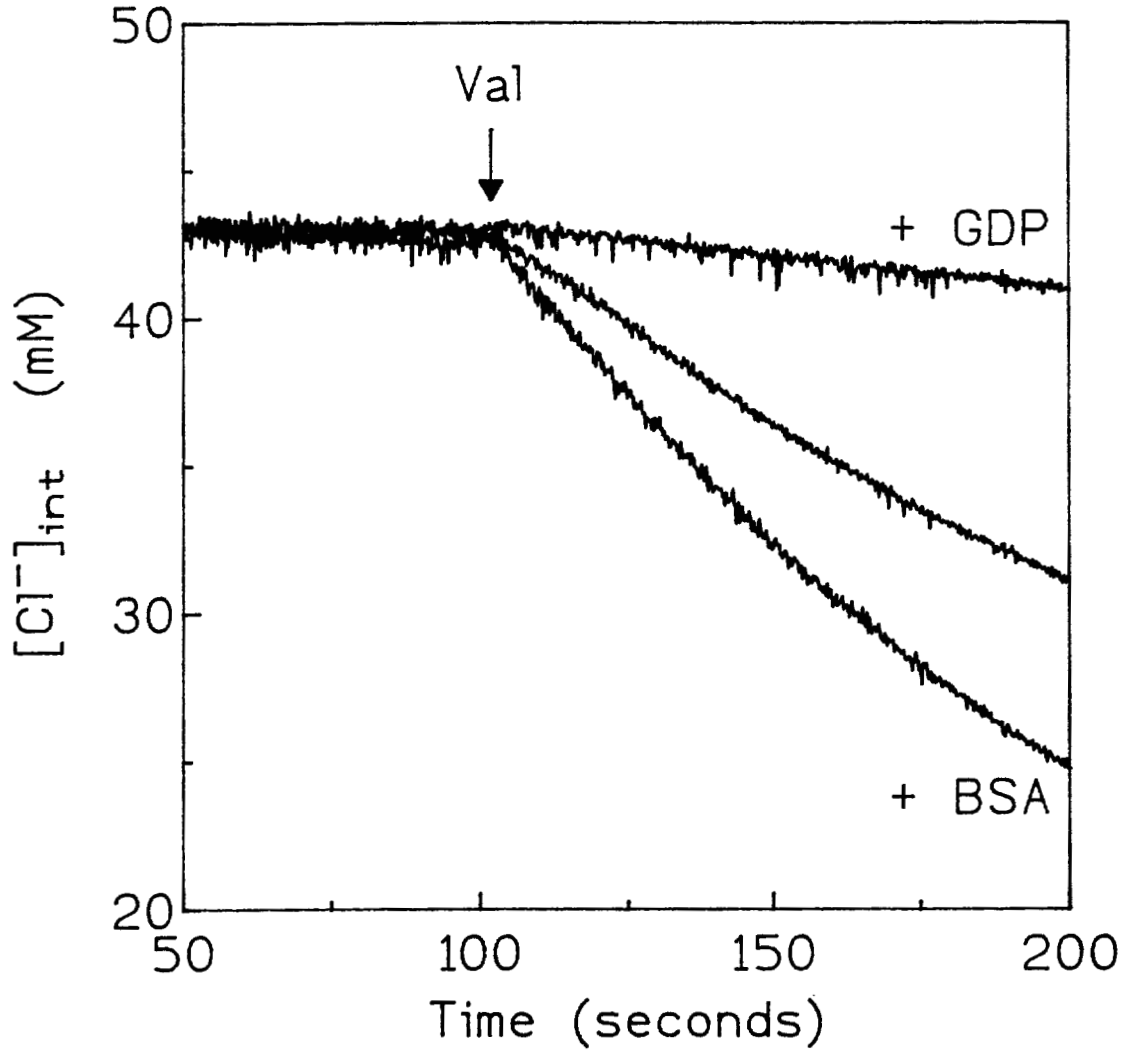

Figure 2.6 Bovine serum albumin activates Cl^- transport through reconstituted UCP. The three traces follow intraliposomal $[Cl^-]$ ($[Cl^-]_{int}$) after initiation of efflux by 0.1 μM valinomycin (*Val*). 16.5 mg of laurate/mg of lipid were added to the lipid/detergent/protein mixture prior to reconstitution. Initial rates (nmol Cl^-/min/mg protein) were 1300 in the absence of BSA or GDP (*middle trace*), 2240 in the presence of 5 mg of BSA/ml (+BSA), and 210 in the presence of 0.5 mM GDP (+GDP). Liposomes contained 45 mM KCl and 0.5 mM GDP. Internal medium contained 17.4 mM phosphate ($Tris^+$, pH 7.2), 25.7 mM Tris (sulfate), 45 mM KCl, 34.4 mM TEA_2SO_4, 0.6 mM TEA–EGTA, 0.5 mM GDP, and 2 mM SPQ. External medium contained 17.4 mM phosphate ($Tris^+$, pH 7.2), 25.7 mM Tris (sulfate), 0.56 mM KCl, 64.4 mM TEA_2SO_4, and 0.6 mM TEA–EGTA.

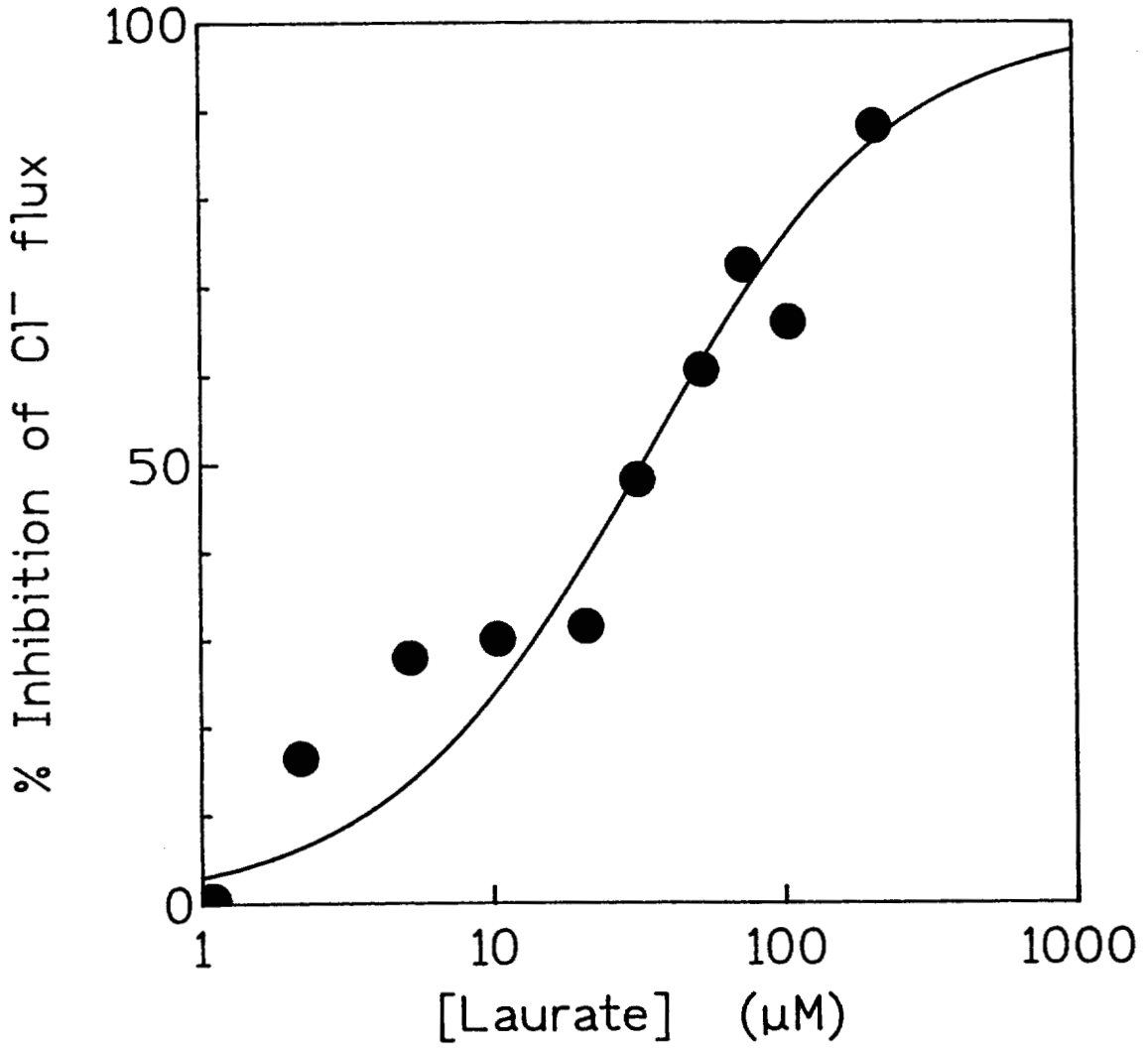

Figure 2.7 Laurate inhibits Cl^- transport through reconstituted UCP. Dose-response curve for inhibition of Cl^- efflux from proteoliposomes by laurate is shown. Proteoliposomes contained 45 mM KCl and 0.5 mM GDP. 100% inhibition for each point was set at the proton leak rate observed with 1 mM external GDP (see Section 2.1.6). The curve was fit with Hill coefficients of 1, yielding an IC_{50} value of 32 μM laurate.

through UCP. The 90% inhibition demonstrated in this experiment suggests that laurate can completely inhibit Cl^- transport.

We measured Cl^- kinetics in the presence of a low dose of laurate, and results of a typical experiment are contained in Fig. 2.8. The converging lines demonstrate competitive inhibition. The K_i for laurate was calculated as 31 μM.

2.2.8 Nitrate and hexanesulfonate competitively inhibit laurate-induced H^+ transport mediated by UCP

Our fluorescence assay does not enable us to study inhibition of laurate-induced H^+ transport by Cl^-, because SPQ is quenched by both buffer anion and Cl^- (104). Nitrate and hexanesulfonate are two well-established anionic substrates of UCP that do not quench SPQ fluorescence. The Lineweaver–Burke plots in Fig. 2.9 show that these anionic substrates are competitive with laurate as an inducer of H^+ transport.

2.3 Discussion

Mitochondrial UCP, which is expressed uniquely in brown adipose tissue, is a member of a gene family that includes the ADP/ATP translocase and the phosphate–H^+ symporter, which are expressed in all cells (40). UCP has been cloned (98), and a method for its heterologous overexpression has been developed that permits purification, reconstitution, and quantitative assays of function (95). These techniques have been coupled with site-directed mutagenesis, and new results reveal aspects of structure that affect nucleotide inhibition of H^+ transport (79).

The challenge is to bring understanding of UCP function to the level required for interpretation of structure–function studies. It is agreed that UCP mediates transport of anions and protons and that purine nucleotides inhibit these transport activities (8, 30, 32, 41, 53, 95, 106). It is now agreed that fatty acids are required to activate UCP-mediated proton transport, as proposed by Locke et al. (107) and first demonstrated with reconstituted UCP by Strieleman et al. (30). The essential role of fatty acids in activating proton transport was disputed by Klingenberg and Winkler

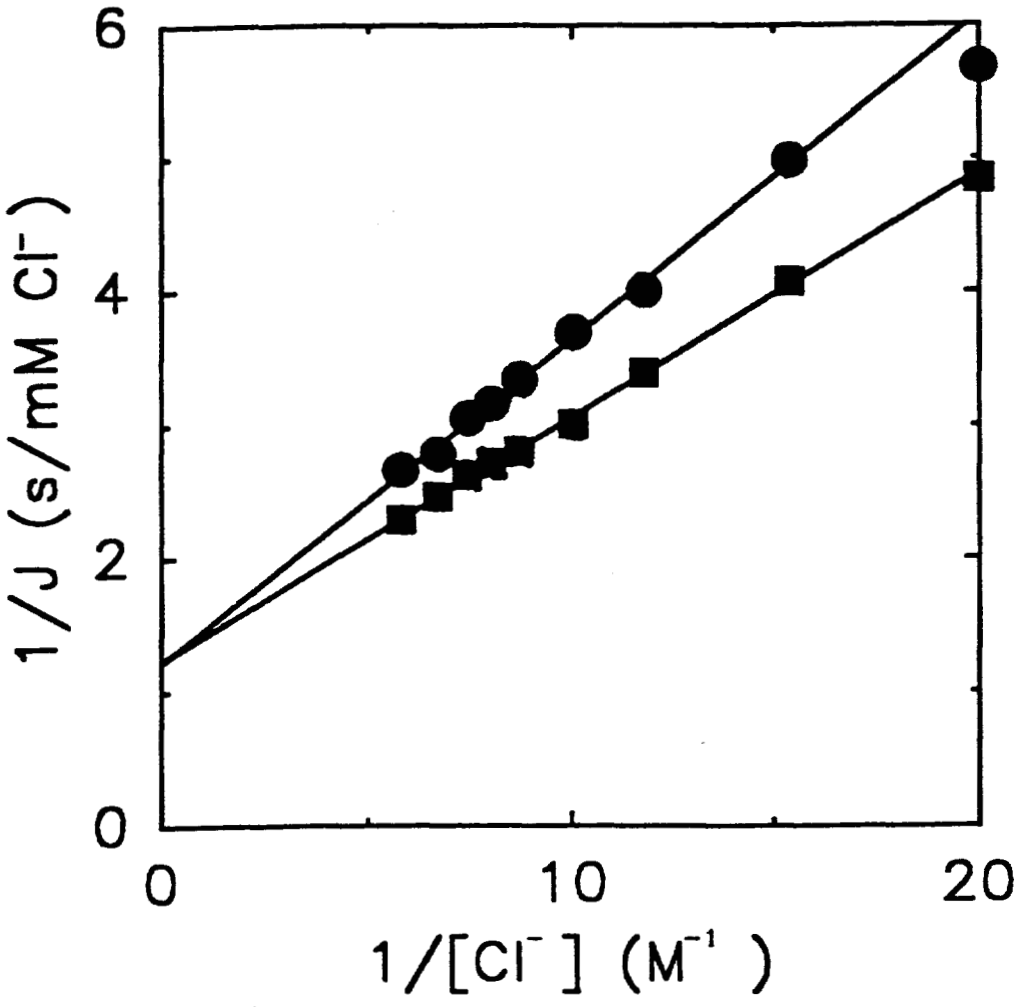

Figure 2.8 Competitive inhibition of UCP-mediated Cl^- transport by laurate. Double reciprocal plots constructed from values of Cl^- influx measured at different values of external [Cl^-] are shown. The *lines* connect sets of data obtained in the absence (●) and in the presence of 10 μM laurate (■). Assay Cl^- concentrations were obtained by mixing two isosmolal media, one containing 175.5 mM KCl and the other 175.5 mM potassium glucuronate. The sodium salt of 10 μM laurate was added to the proteoliposomes in the desired medium, followed by addition of 0.1 μM valinomycin to initiate Cl^- uptake. Linear regression of the initial rates yielded a K_m of 149 mM and V_{max} of 0.81 mM/s for control and a $K_{m(app)}$ of 199 mM in the presence of 10 μM laurate.

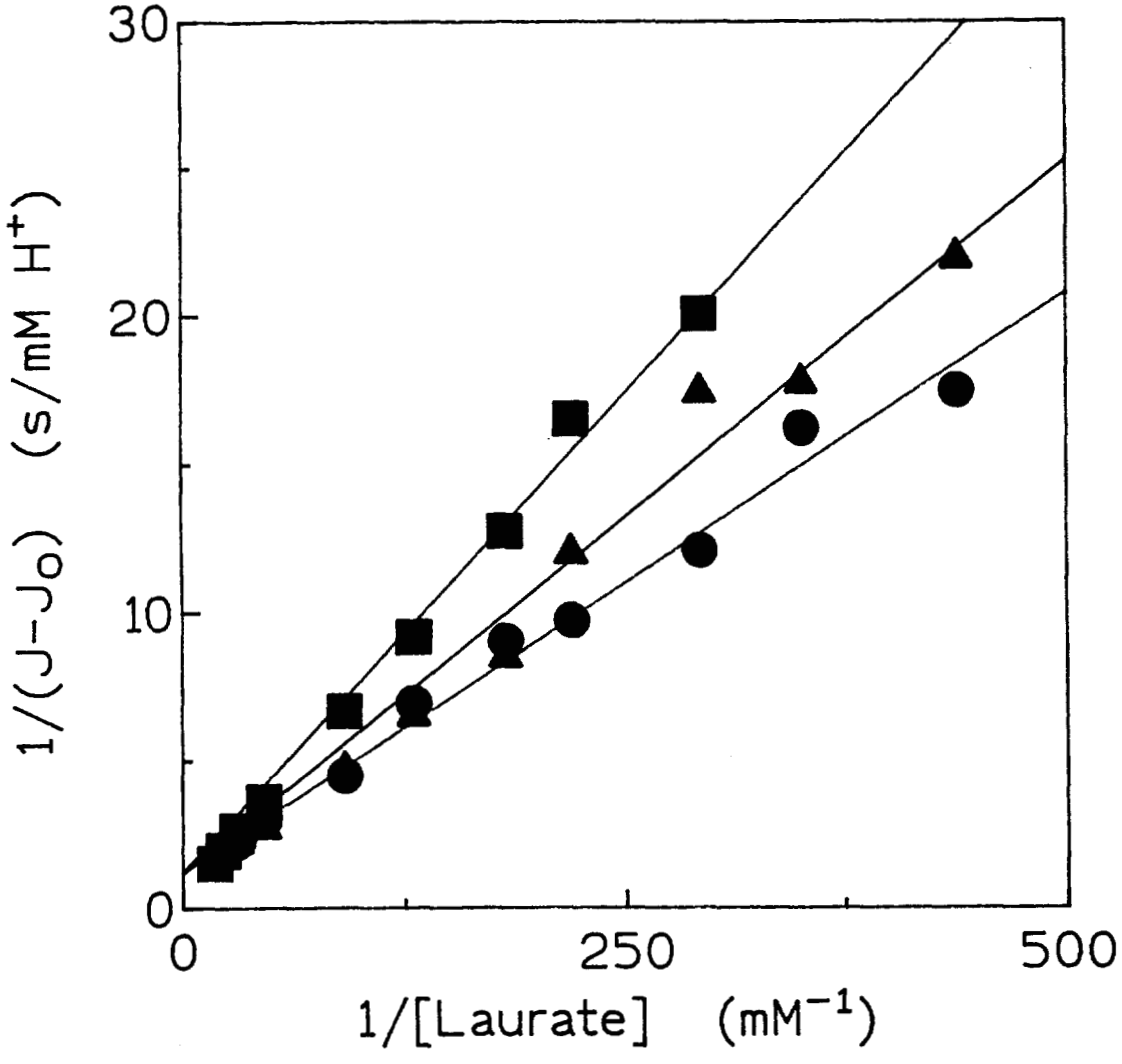

Figure 2.9 Competitive inhibition of laurate-induced, UCP-mediated H^+ transport by nitrate and hexanesulfonate. Double reciprocal plots constructed from values of laurate-induced H^+ efflux measured at different values of external [laurate] are shown. The *lines* connect sets of data obtained in the presence of 99 mM nitrate (■), in the presence of 10 mM hexanesulfonate (▲), and in the absence of both nitrate and hexanesulfonate (●). The rates are J–J_0, where J_0 is the rate in the absence of laurate. Linear regressions of the data yielded a K_m of 33 mM and V_{max} of 0.83 mM H^+/s, and a $K_{m(app)}$ of 54 mM in the presence of 99 mM nitrate and 55 mM in the presence of 10 mM hexanesulfonate. Based on competitive-type inhibition, K_i values of 152 mM for nitrate and 44 mM for hexanesulfonate were calculated.

(41, 69); however, they have recently reversed their position (34). Beyond these simple descriptive facts, nothing is established about the mechanisms of transport or regulation or about the interrelationships among anions, protons, fatty acids, and nucleotides.

In this regard, the published hypotheses examined in this chapter are particularly important. They postulate specific mechanisms of UCP transport and gating, but they have not been previously subjected to critical evaluation. Our data indicate that these hypotheses are false, and we have analyzed their original experimental support to determine why this is so.

2.3.1 Hypothesis: Cl^-, OH^-, and GDP compete for a common site on the UCP anion carrier

Because Cl^- ions cannot cycle across the mitochondrial membrane, Cl^- flux through UCP under normal physiological conditions will merely cause Cl^- to come to electrochemical equilibrium. Nicholls (39, 38) raised the following question: Why is Cl^- ion transported by UCP if it plays no physiological role? Rial and Nicholls (63) postulated that UCP is an anion carrier designed to transport OH^- anions, that Cl^- is an accidental substrate of UCP because it fits with the OH^- binding site on the carrier, and that nucleotides compete for the anion transport site. A test of these hypotheses requires kinetic studies; however, as shown by Jezek et al. (32), the high K_m for Cl^- ion prevents its determination in intact brown adipose tissue mitochondria. Accordingly, these suggestions were without experimental support. The fluorescent probe technique makes this kinetic analysis accessible.

Our results show that the K_m for Cl^- was unaffected by GDP (Fig. 2.1), and purine nucleotide inhibition of Cl^- transport is therefore strictly allosteric. Secondly, the K_m for Cl^- is independent of pH (Fig. 2.2), strongly weighing against the hypothesis that Cl^- and OH^- compete for a common site. It might be contended that competition is obscured by the 10^{-4}–10^{-5} difference in concentrations of Cl^- and OH^-, but this is not a persuasive argument. For UCP to carry out its physiological function, particularly in the presence of 10–30 mM cytosolic [Cl^-], its affinity for OH^- must be on the order of 10^{-7} M or less. If the affinity for OH^- were in this

range, an effect on the K_m for Cl^- should have been detected by the experiments shown in Fig. 2.2.

2.3.2 Hypothesis: GDP inhibition of Cl^- transport is voltage-gated

This hypothesis arose from the results of complicated light-scattering experiments in intact mitochondria (38, 99). The K_i for GDP inhibition was first determined during valinomycin-induced KCl uptake in nonrespiring brown adipose tissue mitochondria and again during Cl^- release caused by initiating respiration. The K_i for GDP inhibition of Cl^- efflux was higher than that for passive Cl^- influx. Since $\Delta\psi$ was about zero during Cl^- influx and tended toward negative values during respiration-driven Cl^- efflux, Nicholls (38) attributed the change in K_i values to voltage regulation of GDP inhibition. Our data using purified UCP (Fig. 2.3A) show that $\Delta\psi$ is without effect on the K_i for GDP inhibition.

It is relatively straightforward to account for this apparent discrepancy. Brown adipose tissue mitochondria contain the inner membrane anion channel, a parallel pathway for Cl^- uniport (43, 60). This pathway is latent under the conditions used to study Cl^- influx and activated under the conditions used to study Cl^- efflux. Participation of this GDP-insensitive pathway for Cl^- transport would manifest itself as a loss of GDP sensitivity during respiration-driven Cl^- efflux, as observed. Thus, Nicholls and co-workers (38, 99) came to the wrong conclusion because they failed to recognize the coexistence of a parallel pathway for Cl^- uniport in mitochondria.

We also considered another possibility for Nicholls' observation (38). Because GDP binds only to the external side of UCP (50), its effect may differ for influx and efflux of Cl^-. We found no significant difference in the K_i for GDP inhibition between Cl^- flux measured in one direction *versus* the other (data not shown).

2.3.3 Hypothesis: GDP inhibition of H^+ transport is voltage-gated

Nicholls and co-workers (38, 99, 100, 105) showed that GDP inhibition of H^+ flux is incomplete at high $\Delta\psi$ and attributed this to voltage-dependent loss of UCP nucleotide sensitivity. This interpretation is incorrect. H^+ flux in the presence of GDP is nothing more than normal diffusive leak. Decreased sensitivity to GDP at

high voltages is therefore to be expected because H^+ leak exponentially increases with $\Delta\psi$ above 100 mV (108). Our data show that is without effect on the K_i for GDP inhibition of H^+ flux (Fig. 2.3B).

2.3.4 Hypothesis: fatty acids shift the K_i for nucleotide inhibition of UCP-mediated transport

The interrelationships between fatty acids and nucleotides have remained a mystery for many years, despite extensive study (29, 30, 34, 38, 39, 63, 99, 100, 105–107). Rial et al. (100) suggested that there was interaction between the nucleotide and fatty acid sites on the protein, based on studies of Cl^--dependent swelling in brown adipose tissue mitochondria. All of our studies in brown adipose tissue and in proteoliposomes showed to the contrary that fatty acids have no effect on the K_i for GDP inhibition of Cl^- or H^+ transport. We also identified the probable cause of the discrepancy with the findings of Rial et al. (100) (see Section 2.2.4).

It must be emphasized that some anionic substrates of UCP do affect the K_i for GDP inhibition. This is particularly noteworthy in the series of hydrophilic short chain alkylsulfonates studied by Jezek and Garlid (53). The K_i for GDP inhibition of alkylsulfonate (50 μM) transport strikingly increased with increasing chain length, ranging from 1.6 μM for methylsulfonate to 175 μM for hexanesulfonate. This phenomenon is most simply explained by competition with GDP for the nucleotide binding site and implies that the sulfonates have a higher affinity for this site than fatty acids or Cl^-. Such competition by alkylsulfonates has recently been reported by Nedergaard and Cannon (54).

2.3.5 Hypothesis: fatty acids do not affect anion transport through UCP

Despite the fact that it has achieved the status of dogma in the field (39, 40, 63, 99), our results (Figs. 2.5–2.8) render this hypothesis untenable. The following statement summarizes the results of hundreds of experiments carried out in our laboratory over three years in both mitochondria and proteoliposomes. If endogenous fatty acids were not completely removed, we *invariably* observed activation of Cl^- transport by BSA, and we *invariably* observed inhibition of Cl^- transport by added

fatty acids from C10 to C18. On close examination, the experimental evidence for the consensus hypothesis is slim. The most likely explanation for the divergence is that we have used more sensitive and more quantitative assays in both mitochondria and proteoliposomes.

2.3.6 Mechanism of purine nucleotide inhibition of UCP-mediated transport

Our data show that the UCP sites responsible for transport of anions and fatty acid-activated H^+ transport are kinetically independent of the sites involved in purine nucleotide inhibition. This finding clarifies the role of purine nucleotides as purely allosteric inhibitors of UCP. It reinforces the concern of earlier workers who asked this question: How is UCP activated to induce uncoupling in the presence of high cytosolic ATP? Readers are referred to excellent studies from the laboratories of Nicholls (29, 38, 39, 99, 100, 105, 107), Cannon (8, 55), Houstek (52), La Noue (109), Shrago (110), and Girardier (111) and their co-workers for their assessments of this unresolved question.

2.3.7 Mechanism of anion and proton transport mediated by UCP

Our data show that fatty acids competitively inhibit anion transport (Fig. 2.8) and that transported anions competitively inhibit H^+ transport with laurate (Fig. 2.9). These findings support the hypothesis, developed from other evidence, that anions are transported through the fatty acid docking site of UCP. This hydrophobic intramembrane domain serves as an energy well (weak binding site) for fatty acids within the membrane (43, 53). In the absence of fatty acids, the docking site constitutes a defect in the permeability barrier to anions, and anion flux will consequently increase. In this sense, Cl^- and other transported anions are accidental substrates of UCP.

The foregoing establishes new limits to UCP behavior and clears the way to address the two principal unresolved questions surrounding its transport mechanism. How does anion transport fit into UCP function, and how do fatty acids activate proton transport? Broadly speaking, two hypotheses are consistent with the new data.

Fatty acids may be allosteric activators of H^+ transport through a separate pathway on the protein (53). Winkler and Klingenberg (34) have proposed a mechanism of this type in which fatty acid head groups align within a proton channel to facilitate H^+ transport. A second concept is that the fatty acids weakly bound to their docking site in the anion channel may be transported from one side to the other, i.e., that UCP is an anion channel designed to conduct fatty acid anions and does not transport protons at all. A similar mechanism was proposed by Skulachev (44). According to this mechanism, the function of UCP is to permit fatty acids, whose anions are normally unable to cross biomembranes, to act as cycling protonophores.

---

[1] This material has been published in this or similar form in *The Journal of Biological Chemistry* and is used here by permission of The American Society for Biochemistry and Molecular Biology:

Jezek, P., Orosz, D. E., Modriansky, M., and Garlid, K. D. (1994) Transport of anions and protons by the mitochondrial uncoupling protein and its regulation by nucleotides and fatty acids. *J. Biol. Chem.* **269,** 26184–26190.

Chapter 3

REGULATION OF MITOCHONDRIAL UNCOUPLING PROTEIN BY PALMITOYL-CoA AND PURINE NUCLEOTIDES

The uncoupling protein (UCP) is a unique mitochondrial membrane protein designed to facilitate proton entry from the cytosol back into the mitochondrial matrix, thus effectively dissipating the proton gradient and thereby generating heat (1). The UCP is exclusively expressed in brown adipose tissue (BAT), a tissue found in most newborn mammals including humans, cold-acclimated rodents, and hibernators (112). UCP requires the presence of free fatty acids to facilitate H^+ transport (33, 34). This transport activity is readily and tightly inhibited by purine di/trinucleotides (40, 100). The binding constants for ATP, ADP, GTP, and GDP were found to be in the low micromolar range (49, 51). The finding of high affinity of UCP to ATP raises the question of how the UCP can ever be active if the ATP concentration in the cytosol is estimated to be in the millimolar range. Does a physiological antagonist or partial agonist exist?

The relative abundance of palmitoyl-CoA offers an easy solution, and palmitoyl-CoA was suggested to act as the partial agonist in a study performed on brown fat mitochondria (55). The reconstitution studies, on the other hand, brought highly opposing results: no effect of palmitoyl-CoA on GDP-inhibited UCP (34, 113) or complete reversal of GDP inhibition by palmitoyl-CoA (56).

Nedergaard and Cannon (8) re-introduced the idea of palmitoyl-CoA being a partial agonist based on isolated BAT mitochondria experiments. Palmitoyl-CoA was able to inhibit UCP activity in the absence of GDP, but maintained some UCP-dependent transport in the presence of GDP (8).

We have used a sensitive fluorescence assay to measure changes in the liposomal internal medium acidity to study the effects of palmitoyl-CoA on UCP-

mediated H^+ transport into liposomes containing purified, reconstituted UCP. Presented here are kinetic data that support the findings of binding experiments (57, 58), ruling out palmitoyl-CoA as a positive regulator of UCP activity *in vivo*. We also present kinetic data that for the first time clearly demonstrate the non-competitive inhibition by GDP and ATP of the fatty acid-induced H^+ transport through UCP. In agreement with previous binding studies (49, 51) and a study on isolated mitochondria (52), pH is identified as a modulator of nucleotide inhibition. The non-competitive-type inhibition by ATP gives further support to the direct regulation of non-shivering thermogenesis by fluctuations in cytosolic ATP concentration.

3.1 Materials and Methods

3.1.1 Purification and reconstitution of UCP

Brown adipose tissue mitochondria were isolated from Golden Syrian hamsters. UCP was purified and reconstituted into proteoliposomes by following protocols previously described in detail (32).

3.1.2 H^+ flux quantitation in proteoliposomes

All data presented in this chapter are based solely on H^+ flux measurements. The measurements were obtained from changes in SPQ fluorescence due to TES buffer anion quenching (104). External medium contained K^+ salt of 84.4 mM SO_4^{-2}; internal medium contained TEA^+ salt of 84.4 mM SO_4^{-2}, to set up an electrochemical gradient to drive the H^+ transport upon addition of valinomycin to the assay. External medium also contained 29 mM TES, 0.6 mM EGTA, pH 7.2 or 7.6, to match the respective values of internal medium. It must be noted that Mg^{2+}-free nucleotides were used in all experiments.

The SPQ fluorescence (347-nm excitation, 442-nm emission) was quenched by TES anion but not by TES zwitterion (104), thus offering sensitive measurement of changes in medium acidity while maintaining sufficient buffering of the whole system. The system can be easily calibrated when liposomes suspended in internal medium are subjected to stepwise additions of 1 N KOH in the presence of 1 μM nigericin. The

slope of the resulting calibration curve is equal to the quenching constant of the TES anion in a given system and is subsequently used in the rate calculations.

The fluorescence changes were monitored using an SLM-8000 (SLM AMINCO, Urbana, IL) spectrofluorometer. The assay cuvettes contained 0.5 mg lipid/ml and reconstituted UCP at 1–3 μg protein/mg lipid. Intraliposomal volume was estimated from the volume of distribution of the probe and typically was 1.1–1.6 μl/mg lipid. The protein content of proteoliposomes was estimated by the Amido-Black method (103).

3.1.3 Materials

SPQ was purchased from Calbiochem. Palmitoyl-CoA was purchased from Pharmacia LKB. Essentially fatty acid-free BSA (Factor IV), fatty acids, and ionophores were purchased from Sigma. Materials for protein purification and liposome formation were obtained from sources described in Jezek et al. (32).

3.2 Results

It is clear that a compound capable of reversing the ATP inhibition of UCP should possess two properties: (i) the ability to bind at the nucleotide-binding site and compete out GDP, and (ii) the ability to restore the transport activity to full (antagonist) or significant (partial agonist) extent by posing as a H^+ transport mediator itself or by not interfering with physiological substrates, i.e., free fatty acids.

Two binding studies—one utilizing ^{125}I-labeled palmitoyl-CoA (58) and the other azido-labeled palmitoyl-CoA (57)—showed competition between GDP and palmitoyl-CoA for the UCP nucleotide-binding site. These results make feasible the role of palmitoyl-CoA as a partial agonist.

3.2.1 Palmitoyl-CoA is not an activator of UCP-mediated H^+transport

The inability of palmitoyl-CoA to induce UCP-mediated H^+ transport is demonstrated in Fig. 3.1. The comparison of UCP activity at 10 μM laurate (●) and palmitoyl-CoA (▲) gave an estimated difference of 3.5 μmol H^+/min/mg protein.

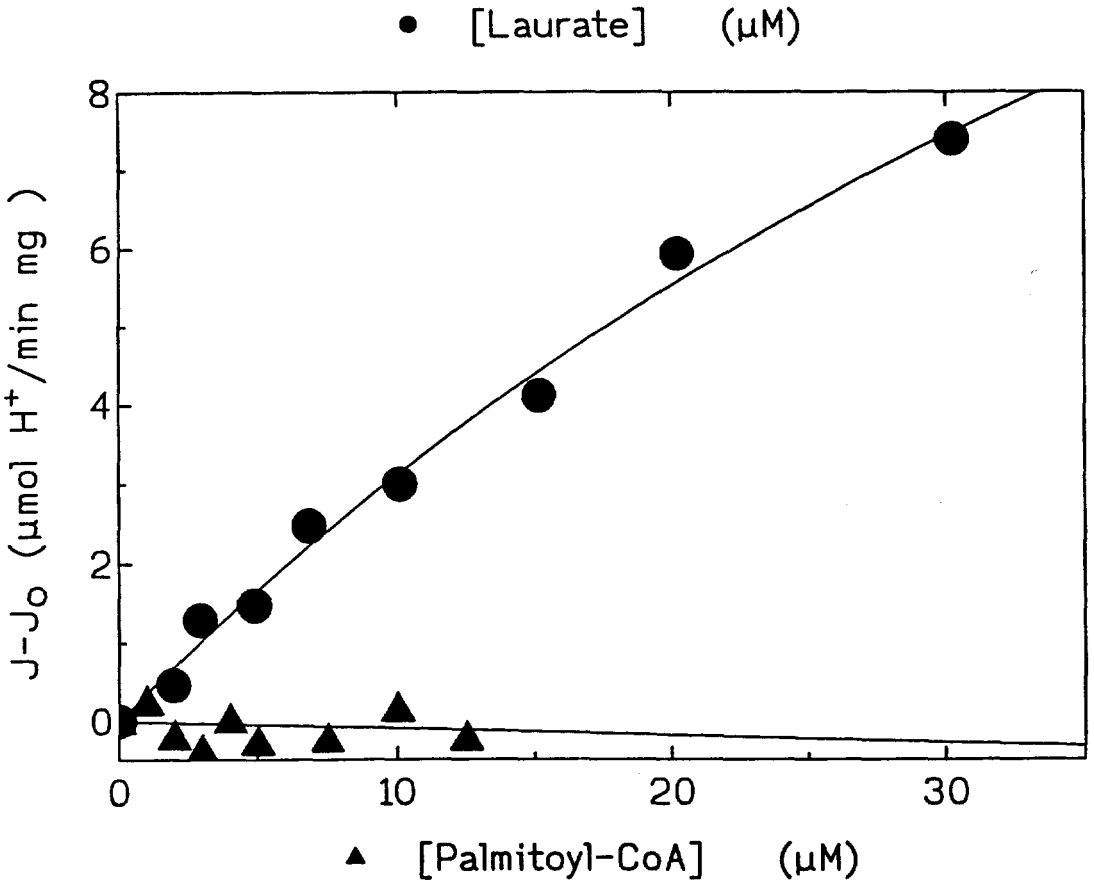

Figure 3.1 Palmitoyl-CoA does not induce UCP-mediated H^+ transport. The figure contains initial rates of UCP-mediated H^+ transport plotted versus [laurate] (●) and [palmitoyl-CoA] (▲). The rates are $J - J_0$, where J_0 is the rate in the absence of laurate and palmitoyl-CoA. The laurate titration data were fit with a binding isotherm and yielded K_m = 23 μM and V_{max} = 14 μmol/min/mg protein. The solid line through the palmitoyl-CoA titration data merely simulates the tendency of the initial rate to decrease with increasing [palmitoyl-CoA].

More importantly, the rate in the presence of palmitoyl-CoA was on the level of natural H^+ leak. Neither palmitoyl-CoA nor laurate concentrations used in all experiments caused leak into liposomes lacking or containing reconstituted UCP (data not shown). The tendency to decrease J_0, the rate in the absence of free fatty acids, is simulated by the solid line. Very similar behavior was observed with undecanesulfonate, a competitive inhibitor of laurate-induced UCP-mediated H^+ flux (33).

3.2.2 Palmitoyl-CoA inhibits laurate-induced H^+ transport

Both agonist and antagonist must interact with a protein in order to affect that protein's activity. The interaction of palmitoyl-CoA with UCP we observed was inhibition of UCP-mediated H^+ transport by palmitoyl-CoA with an IC_{50} of 2.7 μM in the absence of GDP (Fig. 3.2). When titrated in the presence of a constant dose of GDP, which gave $\sim$50% inhibition at pH 7.2, the GDP present in the assay shifted the IC_{50} for palmitoyl-CoA by two-fold. However, the rate in the presence of 8.5 μM palmitoyl-CoA was essentially the same regardless of GDP presence. Thus, GDP does not alter the overall inhibition by palmitoyl-CoA, opposing the observation made by Nedergaard and Cannon in mitochondria (8).

Essentially the same result was obtained when GDP was titrated against a constant dose of palmitoyl-CoA (not shown). It is then very likely that both compounds interact with the same binding site on the UCP.

3.2.3 Palmitoyl-CoA exhibits non-competitive-type inhibition of laurate-induced H^+ transport

Laurate kinetics performed in the absence and presence of palmitoyl-CoA revealed a change in the V_{max}, but no change in the K_m for laurate (Fig. 3.3A) as demonstrated by the parallel linear regressions (*solid lines*) of the data, which are typical for non-competitive-type inhibition. Linear regressions of the data yielded a K_m = 25.3 μM and V_{max} of 17.6 (●), 13.2 (■), and 7.9 (▲) μmol/min/mg protein. The K_i calculated from available kinetic parameters was 3 μM, which is very close to the observed IC_{50} for palmitoyl-CoA (Fig. 3.2).

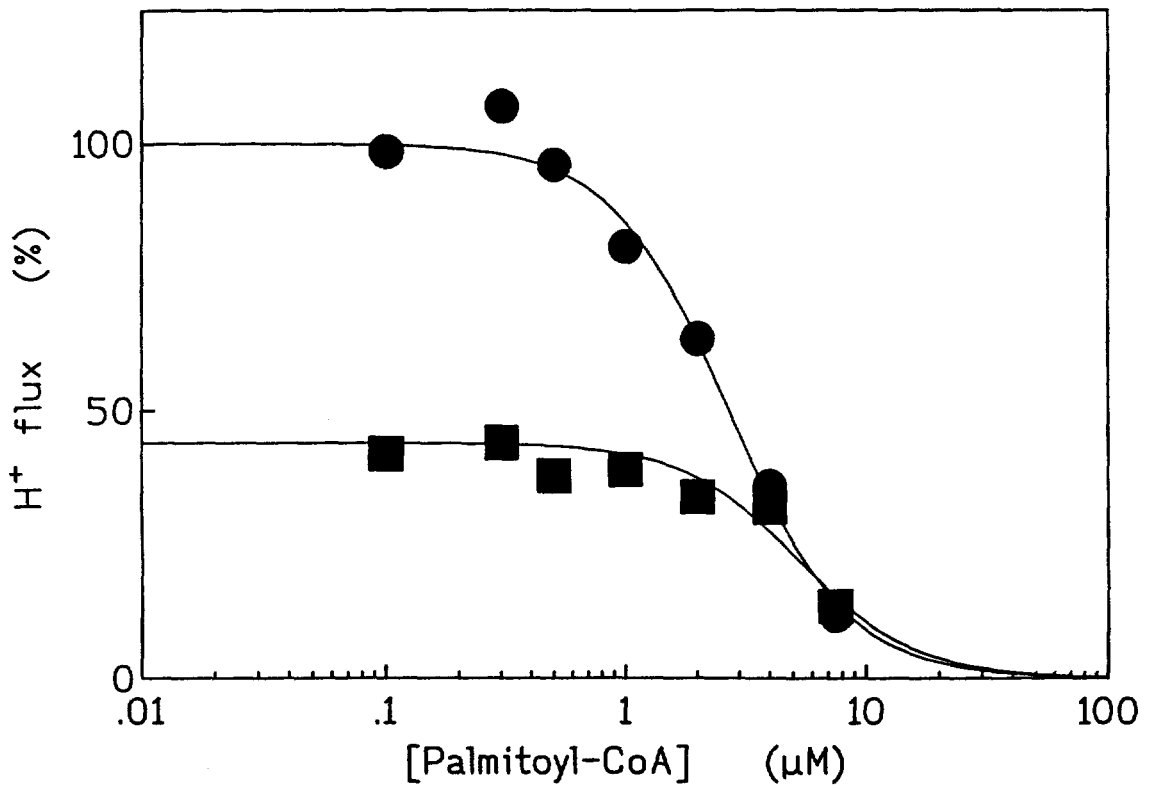

Figure 3.2 Palmitoyl-CoA inhibits UCP-mediated H^+ transport in the presence and absence of GDP. Dose-response curves of 30 μM laurate-induced H^+transport through UCP were obtained by titrating palmitoyl-CoA in the presence (■) or absence (●) of 20 μM GDP. No inhibition (100% H^+ flux) was observed in the absence of both palmitoyl-CoA and GDP; complete inhibition (0% H^+ flux) was observed in the presence of 0.5 mM GDP_{out} and no palmitoyl-CoA. Data fit yielded an IC_{50} of 2.7 μM and 5.4 μM in the absence and presence of GDP_{out}, respectively.

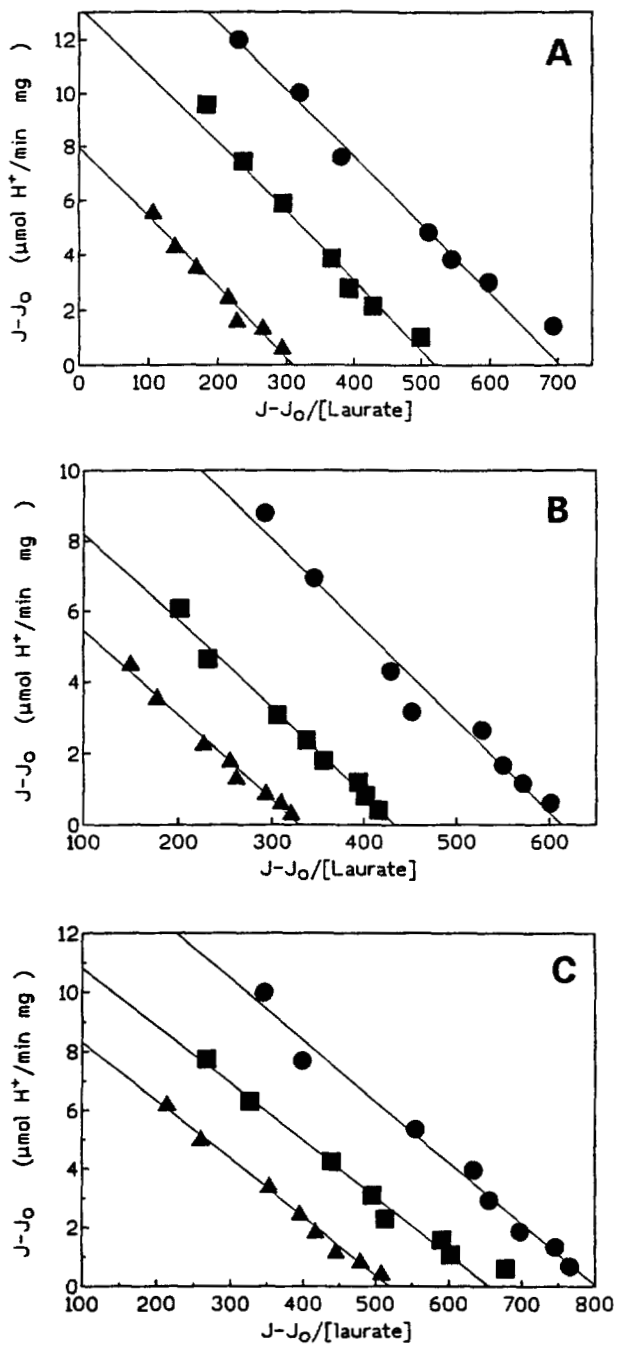

Figure 3.3 Non-competitive inhibitors of laurate-induced UCP-mediated H^+ transport. (**A**) *Palmitoyl-CoA:* Eadie–Hofstee plots of laurate kinetics in the presence of 0 μM (●), 2 μM (■), and 4 μM (▲) palmitoyl-CoA. The rates are J – J_0, where J_0 is the rate in the absence of laurate. (**B**) *GDP:* Eadie–Hofstee plots of laurate kinetics in the presence of 0 μM (●), 10 μM (■), and 30 μM (▲) GDP. The rates are defined as in panel A. (**C**) *ATP:* Eadie–Hofstee plots of laurate kinetics in the presence of 0 μM (●), 50 μM (■), and 200 μM (▲) GDP. The rates are defined as in panel A.

To compare the palmitoyl-CoA data with known inhibitors, we performed laurate kinetics studies in the absence and presence of GDP (Fig. 3.3B) and ATP (Fig. 3.3C). Both exhibited non-competitive-type inhibition as demonstrated by the parallel linear regressions of the data (*solid lines* in Figs. 3.3B and 3.3C). Linear regressions of the data yielded a K_m = 24.6 μM and V_{max} = 15.7 (●), 10.6 (■), and 7.8 (▲) μmol/min/mg protein for varied GDP, and a K_m = 20.4 μM and V_{max} = 16.7 (●), 12.2 (■), and 10.3 (▲) μmol/min/mg protein for varied ATP. The calculated K_is were 21 μM for GDP and 134 μM for ATP. Both values are close to the respective IC_{50}s.

3.2.4 pH is a modulator of nucleotide inhibition

Two studies of nucleotide binding indicated that an increase in pH causes a shift in K_d to higher values (49, 51). The same pH-dependent shift has been reported for nucleotide inhibition in isolated mitochondria (52). We evaluated the pH-induced shift in simple dose–response experiments performed in liposomes containing purified UCP.

The dose–response curves shown in Fig. 3.4 demonstrate a two-fold increase in IC_{50} for GDP when the pH is raised from 7.2 to 7.6. A more dramatic change was observed for ATP inhibition. Here not only was the IC_{50} shifted by ten-fold, but only 85% inhibition was observed for 5 mM ATP at pH 7.6, compared to 1 mM GDP (0% H^+ flux) at pH 7.6.

Further kinetic experiments in the presence of varying ATP concentration at pH 7.6 confirmed the pH-induced shift while the non-competitive-type inhibition remained unchanged (not shown).

3.3 Discussion

3.3.1 The role of palmitoyl-CoA

Physiological studies indicate that non-shivering thermogenesis takes place upon norepinephrine stimulation (1, 11), to a very large extent via β_3-receptors (17). There is no direct connection between the cell receptors and UCP, but rather a

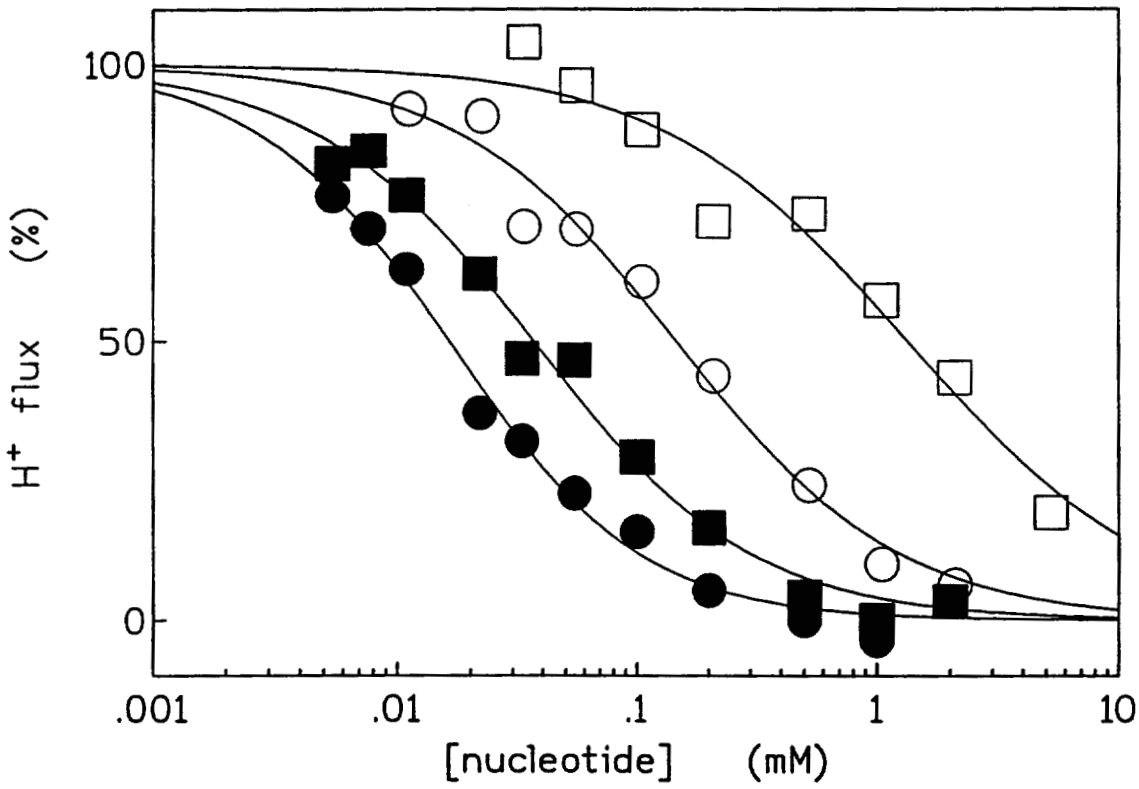

Figure 3.4 pH-induced shift in IC_{50} for GDP and ATP. Dose-response curves of 30 μM laurate-induced H^+ transport through UCP were obtained by titrating GDP at pH 7.2 (●) and pH 7.6 (■), and ATP at pH 7.2 (○) and pH 7.6 (□). No inhibition (100% H^+ flux) was observed in the absence of nucleotides. Complete inhibition (0% H^+ flux) was set equal to the rate in the presence of 1 mM GDP at the indicated pH. Data fit of the curves yielded an IC_{50} of 16 μM (pH 7.2) and 33 μM (pH 7.6) for GDP, and 124 μM (pH 7.2) and 1.34 mM (pH 7.6) for ATP.

cascade of events that precedes the actual UCP activity (20). The minimum hypothesis describes the hormonally induced release of free fatty acids that become substrates for β-oxidation and for thermogenesis (11). The necessary step before β-oxidation is activation of the fatty acid to acyl-CoA. The required step for UCP activity is relief from nucleotide inhibition in the presence of 5 mM ATP, some 45-fold higher than the estimated IC_{50} for ATP. Since free fatty acids are unable to overcome purine nucleotide binding (34) or inhibition (33, 114, 115), can fatty acyl-CoAs do the job?

We present data that agree with previous reports from other laboratories (34, 113), effectively excluding palmitoyl-CoA as a partial agonist of UCP-mediated H^+ transport. Palmitoyl-CoA does not induce UCP-mediated H^+ transport, but it does inhibit such a transport induced by laurate, regardless of GDP presence. Moreover, palmitoyl-CoA inhibits the laurate-induced transport in the exact same fashion as GDP and ATP. Thus, palmitoyl-CoA is a purely allosteric inhibitor of UCP.

Demonstrating the allosteric inhibition by palmitoyl-CoA, however, does not answer the main question: What activates UCP if nucleotides remain high?

3.3.2 The minimal hypothesis

The observations of allosteric inhibition by GDP and ATP conflict with the minimal hypothesis of acute thermogenic response as postulated by Nicholls and Locke (11). The minimal hypothesis states that free fatty acids released in response to norepinephrine stimulation can overcome the ATP inhibition of UCP and become subtrates for both β-oxidation and uncoupling. Bukowiecki et al. (20) demonstrated in isolated brown adipocytes that the action of 100 nM norepinephrine can be 80% mimicked by externally added 1 mM palmitic acid. The presence of free fatty acids is undoubtedly crucial, but mainly due to inactive UCP in their absence.

Bieber et al. (116) estimated the cell-associated free fatty acid concentration to be 20 mM. But if free fatty acids could overcome nucleotide inhibition of UCP, why is uncoupling of mitochondrial respiration observed only after hormonal stimulation or extracellular free fatty acid addition, i.e., overall increase of free fatty acid concentration in the cell?

3.3.3 Intracellular pH modulates nucleotide inhibition

The dose-response curves in Fig. 3.4 show a shift in IC_{50} for ATP when the pH is increased. Indeed, the alkalinization of the cytosol occurs after brown adipocyte exposure to norepinephrine (117). The shift is relatively small, only 0.05–0.1 pH unit. Based on data published by Lin and Klingenberg (49), Rafael et al. (51), and data presented herein, the observed shift represents roughly a two-fold shift in K_i for ATP, putting it at $\sim 300\ \mu M$.

An important feature is the observed discrepancy between the binding and inhibition constants of nucleotides, originally pointed out by Rial and Nicholls (63). Indeed, 124 μM ATP gives half-maximal inhibition of isolated UCP (this paper), whereas in mitochondria it is observed at 1 mM ATP (118). The experiments on pH modulation of nucleotide inhibition performed by Jezek et al. (52) indicate a three-fold shift when pH is increased from 7.1 to 7.5. We can then estimate the K_i for ATP at about 1.5 mM under the pH shift observed *in vivo*. The estimate takes into account the pH reached after addition of norepinephrine, about 7.2 according to Lee et al. (117).

3.3.4 The ATP hypothesis

A candidate for direct regulation of UCP activity is ATP itself. ATP fluctuations due to free fatty acid increase would be a plausible explanation for the allosteric inhibition in the presence of apparently millimolar concentrations of nucleotides in the cell. Further, it is likely that the concentration of ATP *in vivo* fluctuates significantly enough to allow this kind of regulation. Prusiner et al. (119) observed a 60% decrease in cellular ATP upon norepinephrine stimulation. LaNoue et al. (118) estimated the decrease to be only 20%, but concluded that this may partially activate UCP allowing a further drop in [ATP] and amplifying the initial decrease. The same conclusion about direct regulation of thermogenesis by changes in cytosolic ATP was reached in a later study based on membrane potential measurements in brown fat mitochondria (109).

The missing piece of information is whether the concentration of ATP in the cytosol drops upon addition of extracellular free fatty acids. The drop is feasible in

view of two facts: fatty acyl-CoA synthetase activity and the cytosol volume. Acyl-CoA synthetase alone requires conversion of one ATP into AMP and PP_i in order to activate a single molecule of fatty acid to acyl-CoA (120). The AMP, which is considered a very weak inhibitor of UCP because of its K_d = 165 μM (49), is not readily recycled into ATP. Once UCP becomes active and respiration is loosely coupled, there is apparently still enough net ATP generated (26) to maintain essential functions of the cell.

Numerous metabolic events follow interaction with norepinephrine (1) which leads us to propose two other events crucial for thermogenesis that must be triggered along with or by increase in free fatty acid content: (i) Matrix volume is increased to activate β-oxidation. Volume activation of electron transport was identified in isolated brown adipose tissue mitochondria by Nicholls et al. (121) and a 50% increase in mitochondrial volume was observed in electron micrographs of tissue 30 minutes after norepinephrine injection into newborn rats (122). Halestrap (123), who has studied the matrix volume phenomenon in detail, identifies the site of activation as the point where electrons feed into ubiquinone. The mechanism by which mitochondrial swelling affects the respiratory chain is unclear. However, volume must be increased by K^+ uptake, and preliminary data obtained in our laboratory suggest involvement of a mitochondrial K_{ATP} channel (124). (ii) Cytosolic pH is increased. It is well established that pH shift from 6.8 to 7.5 rapidly reduces the affinity of UCP for ATP (49). It has been shown that norepinephrine stimulation causes cell alkalinization of approximately 0.05–0.1 pH units (117). This most likely occurs by concerted activation of a plasma membrane protein, possibly the ubiquitous Na^+/H^+ exchanger (125) or Na^+/K^+ ATPase (111).

3.3.5 Summary

The signal for non-shivering thermogenesis is norepinephrine stimulation that triggers primarily lipolysis. The increase in free fatty acids, also mimicked by extracellular fatty acids as in overeating, is accompanied by alkalinization and mitochondrial swelling. Free fatty acids become substrates for β-oxidation, closely followed by uncoupling. The uncoupling is directly regulated by changes in cytosolic ATP concentration and indirectly by cytosolic pH.

Chapter 4

ON THE MECHANISM OF FATTY ACID-INDUCED PROTON TRANSPORT BY MITOCHONDRIAL UNCOUPLING PROTEIN[2]

The mitochondrial uncoupling protein (UCP) is a remarkable chemiosmotic device engineered to dissipate the protonmotive energy of brown adipose tissue mitochondria and provide heat to the animal. It is known that UCP-mediated uncoupling is activated by fatty acids (FA), and the consensus has been that UCP is a H^+ (or OH^-) transporter (8, 39, 40). It is also known that UCP, like other members of its gene family, is an anion transporter (30, 32, 39, 40, 53). Both H^+ and anion transport are inhibited by purine nucleotides.

The mechanism by which FAs activate proton transport via UCP is unknown. We have long considered UCP-mediated anion transport to hold the key to this mystery, because this property has been difficult to integrate with the physiological function of UCP. We have recently shown that FAs inhibit Cl^- transport through UCP with competitive kinetics (115), supporting our hypothesis that anions are transported through the FA-binding domain of UCP (43). The close relationship between FA interaction and anion transport permits at least two possibilities for the mechanism of H^+ transport. Either FAs activate proton transport while being anchored within the UCP (34) or FA anions are directly transported by UCP (44, 126). FA anion transport by UCP would not be unexpected, in view of the fact that UCP transports monovalent anions generally, and transport rates increase with anion hydrophobicity (32, 53).

To distinguish between these possibilities, we compared the properties of laurate and its close analogue, undecanesulfonate. We measured fluxes of H^+, Cl^-, and K^+ in proteoliposomes reconstituted with purified UCP (32). K^+ flux, in the presence of valinomycin, was used as a measure of anionic or protonic charge flux.

Both undecanesulfonate and laurate are competitive inhibitors of UCP-mediated Cl^- transport, and undecanesulfonate is a competitive inhibitor of laurate-induced H^+ transport. Both anions catalyzed charge movement across the proteoliposomal membrane, and they did so with hyperbolic kinetics and with similar K_m and V_{max} values. In the case of laurate, the charge movement was due to H^+ flux. Undecanesulfonate did not catalyze H^+ flux, from which it follows that it is transported as the anion by UCP, as are other alkylsulfonates (53). This difference in behavior of the two analogues in proteoliposomes could be fully explained by their behavior in protein-free liposomes: laurate supported rapid electroneutral H^+ transport across the bilayer due to nonionic flip-flop of the FA. Undecanesulfonate, a strong acid, was unable to catalyze electroneutral H^+ transport. We conclude that FAs cause electrophoretic H^+ transport in the presence of UCP, because UCP is an anion channel designed for electrophoretic transport of FA anions. According to this mechanism, UCP-mediated uncoupling is due to futile cycling of FAs across the inner membrane of brown adipose tissue mitochondria. Seen in this light, UCP-transported monovalent anions are accidental substrates of the FA anion pathway in UCP.

4.1 Materials and Methods

4.1.1 Purification and reconstitution of UCP

Brown adipose tissue mitochondria were isolated from Syrian hamsters, and UCP was purified and reconstituted into proteoliposomes using protocols previously described (127). Where used, protein-free liposomes were prepared by the same protocol. When fresh mitochondria were used, H^+ flux in proteoliposomes was nearly identical to the background rates observed in liposomes, indicating that Bio-Beads SM-2 removed virtually all endogenous FAs (34). When frozen mitochondria were used, a higher GDP-inhibited H^+ flux was observed in the absence of added FAs. Accordingly, frozen mitochondria were first washed with 5 mg BSA/ml, which eliminated this effect.

4.1.2 Quantitation of ion fluxes in liposomes and proteoliposomes

Media compositions were designed to set up an electrochemical K^+ gradient to drive transport of anions or H^+ in the appropriate direction when valinomycin was added. Fluorescence was assayed in cuvettes containing 0.5 mg lipid/ml and UCP at 1–3 μg protein/mg lipid. Intraliposomal volume, estimated from the volume of distribution of probe, was 1.1–1.6 μl/mg lipid.

The data presented here are based on flux measurements of three ions. Measurement of UCP-mediated *H^+ flux* was obtained from changes in SPQ fluorescence due to quenching by the anion of TES buffer (104, 127). Internal medium contained 84.4 mM TEA_2SO_4, 0.6 mM TEA–EGTA, and 28.8 mM TEA–TES, pH 7.2. External medium contained 60 mM K_2SO_4, 24.4 mM TEA_2SO_4, 0.6 mM TEA–EGTA, and 28.8 mM TEA–TES, pH 7.2. Measurement of UCP-dependent *K^+ flux*, reflecting the movement of ionic charge across the membrane (128), was obtained from changes in PBFI fluorescence (3, 127). Except for different probes, internal and external media were identical to those used for H^+ flux. Measurement of UCP-mediated *Cl^- flux* was determined from changes in SPQ fluorescence due to Cl^- quenching (32, 127). Internal medium contained 79.5 mM TEA_2SO_4, 0.6 mM TEA–EGTA, and 20 mM TRIS–PO_4, pH 7.2. External medium contained 119.25 mM KCl, 0.6 mM TEA–EGTA, and 20 mM TRIS–PO_4, pH 7.2.

4.1.3 Evaluation of lytic effects of laurate and undecanesulfonate in liposomes and proteoliposomes

We investigated non-specific effects of FAs and long-chain sulfonates and obtained the following results (data not shown): (i) Laurate and undecanesulfonate were poor lytic agents, in that neither induced liposomal lysis, even at levels up to 1 mM. Lysis, detected when internal probe was exposed to external medium, was apparent with high doses of longer-chain FAs or alkylsulfonates. (ii) The K_i for GDP-inhibition of H^+ or Cl^- transport in proteoliposomes was unaffected by the amount of FA present during the assay (115). (iii) Laurate caused increases in the rates of valinomycin-induced H^+ or Cl^- transport in liposomes. This effect was amplified by increasing valinomycin concentration, suggesting ion pair transport of

laurate with the valinomycin–K^+ complex (129). At 100 nM (the amount of valinomycin used in these experiments), this effect was small, linear with [laurate], and scarcely detectable below 50 μM laurate. In general this effect was observed with all amphiphiles. In our experience, the non-specific transport could be distinguished by its insensitivity to GDP.

4.1.4 Materials

SPQ and PBFI were purchased from Calbiochem and Molecular Probes, respectively. Essentially FA-free BSA (Factor IV), FAs, and ionophores were purchased from Sigma. Alkylsulfonates were purchased from Research Plus, Inc. (New Jersey). Materials for protein purification and liposome formation were obtained from sources described in Jezek et al. (32).

4.2 Results

4.2.1 Undecanesulfonate and laurate induce GDP-sensitive electrophoretic fluxes in liposomes reconstituted with UCP

The traces in Fig. 4.1A follow valinomycin-induced H^+-efflux from proteoliposomes containing UCP and treated with 10 μM laurate. H^+ transport was measured directly from quenching of SPQ fluorescence by TES anion. The traces in Fig. 4.1B were obtained under identical conditions except that H^+ transport was measured indirectly as K^+ uptake, determined from PBFI fluorescence. The traces in Fig. 4.1C also follow K^+ uptake determined from PBFI fluorescence; however, undecanesulfonate was used instead of laurate to induce UCP-dependent ion movement.

An acidification jump can be seen following addition of laurate when H^+ flux was measured (20–24 s; Fig. 4.1A). This reflects rapid equilibration of lauric acid across the membrane. A capacitative K^+ jump can be seen following addition of valinomycin when K^+ flux was measured (Figs. 4.1B and 4.1C).

These experiments establish several key aspects of UCP behavior. (i) The observed fluxes were electrophoretic, because they required valinomycin and a K^+

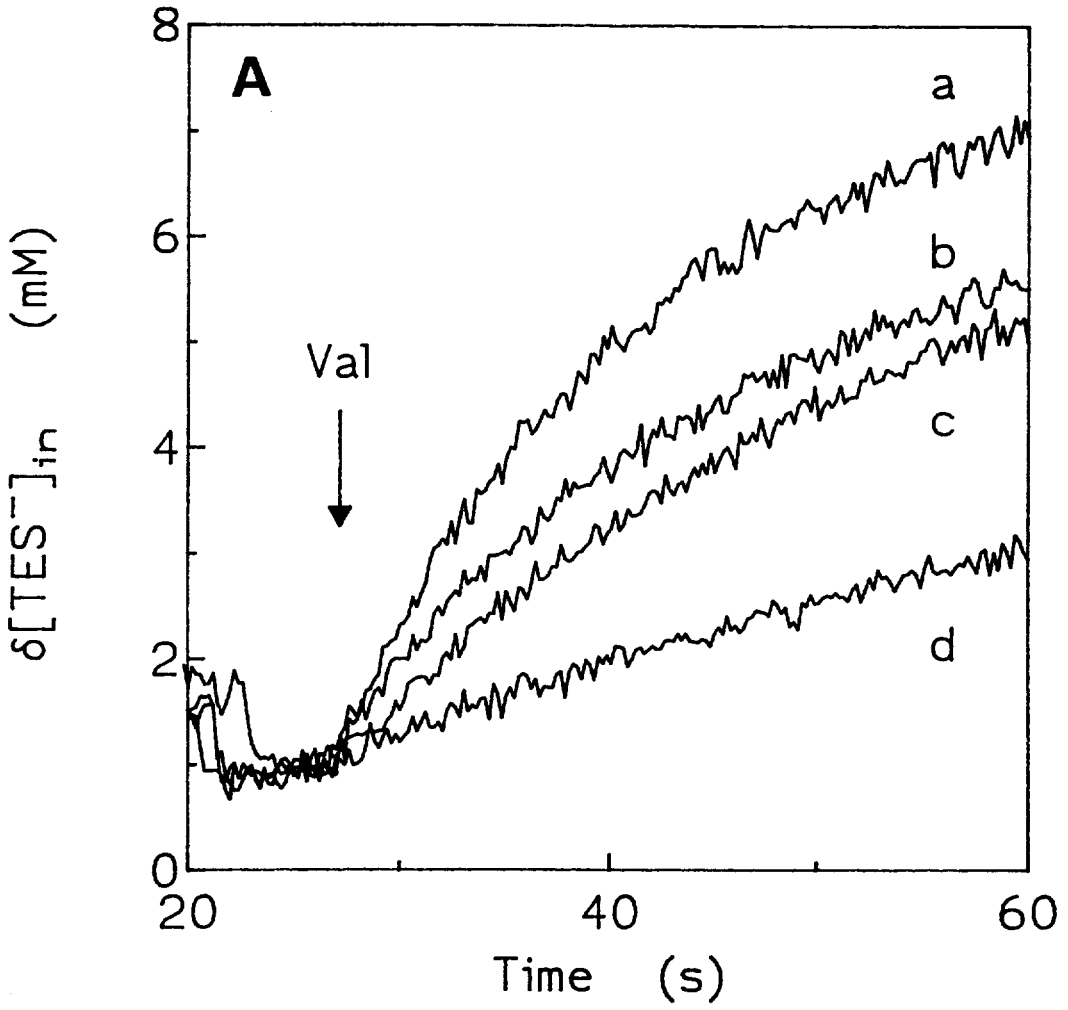

Figure 4.1 GDP-sensitive H^+ and K^+ fluxes in the presence of undecanesulfonate and laurate in liposomes reconstituted with UCP.

Panel A: H^+ efflux in the presence of laurate. The traces obtained from SPQ fluorescence were converted to increases in intraliposomal [TES^-] ($[TES^-]_{in}$) and plotted versus time. H^+ flux was induced by addition of 0.1 μM valinomycin (indicated by arrow) in the presence of 10 μM laurate. The experiment was carried out on two separate preparations: one containing no internal GDP, the other 0.5 mM internal GDP. Traces were obtained in the absence of GDP (*trace a*), with 0.5 mM external GDP only (*trace b*), with 0.5 mM internal GDP only (*trace c*), and with 0.5 mM GDP on both sides of the membrane (*trace d*).

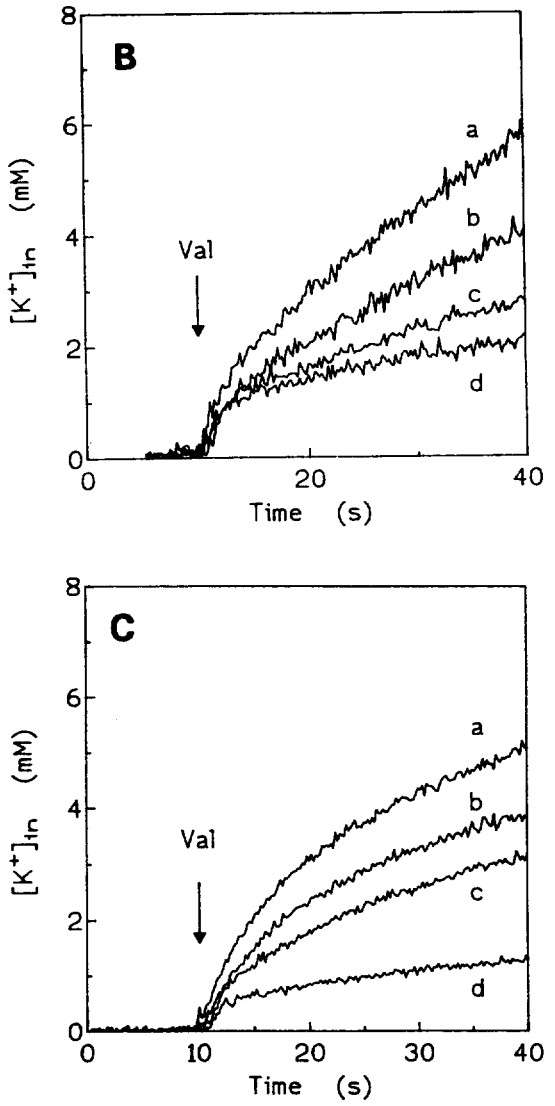

Figure 4.1 GDP-sensitive H^+ and K^+ fluxes in the presence of undecanesulfonate and laurate in liposomes reconstituted with UCP.

Panel B: K^+ flux in the presence of laurate. The traces obtained from PBFI fluorescence were converted to intraliposomal $[K^+]$ ($[K^+]_{in}$) and plotted versus time. K^+flux was induced by addition of 0.1 μM valinomycin (arrow) in the presence of 20 μM laurate. In this experiment, valinomycin-mediated K^+ flux reflects the limiting flux of H^+, as measured in Panel A. The presence or absence of internal and/or external GDP is designated exactly as for Panel A.

Panel C: K^+ flux in the presence of undecanesulfonate. The experiment was carried out exactly as described for Panel B, except that 20 μM undecanesulfonate was present in the assay medium. The presence or absence of internal and/or external GDP is designated exactly as for Panel A. Media compositions for all three panels are given in Section 4.1.2.

gradient. (ii) The observed fluxes required addition of 10–100 μM of a long-chain FA or alkylsulfonate. In their absence, observed fluxes were nearly identical with *trace d* in each figure (see below). (iii) The observed fluxes required UCP and were not observed in liposomes lacking UCP (not shown). (iv) Fluxes were completely inhibited when GDP was present on both sides of the membrane. Thus, traces from identical experiments in liposomes lacking UCP were superimposable on the lowest traces of each panel in Fig. 4.1. (v) The pattern of GDP-sensitivity of fluxes induced by 10^{-5} M laurate and 10^{-5} M undecanesulfonate (Fig. 4.1) is entirely similar to that previously observed for flux induced by 10^{-1} M Cl^- (40). Thus, these fluxes were partially inhibited when GDP was present on one side of the membrane and fully inhibited when GDP was present on both sides. This reflects the facts that the GDP binding site is accessible only from one side of the protein (70) and UCP is more or less randomly inserted into the liposomal membrane (32). (vi) K^+ flux in the presence of valinomycin is a reliable measure of charge movement through UCP.

4.2.2 The laurate analogue, undecanesulfonate, is transported by UCP but does not catalyze UCP-mediated H^+ flux

We measured proton flux in proteoliposomes reconstituted with UCP as a function of [laurate] and [undecanesulfonate], and the results are plotted in Fig. 4.2. Undecanesulfonate (▲, Fig. 4.2) was incapable of catalyzing UCP-dependent H^+ flux and even inhibited the small endogenous H^+ flux. Laurate, in contrast, induced profound activation of H^+ efflux (●, Fig. 4.2) in proteoliposomes reconstituted with UCP with an apparent K_m in the micromolar range.

As shown in Figs. 4.1B and 4.1C, both laurate and undecanesulfonate catalyzed net charge movement via UCP at comparable rates. These differential effects on H^+ transport were confirmed in swelling experiments on intact brown adipose tissue mitochondria (not shown). The results of these experiments support two important conclusions: the behavior of undecanesulfonate differs from that of its close analogue, laurate, and measurements of K^+ flux under the conditions of Fig. 4.1C show influx of the undecanesulfonate anion and not efflux of H^+.

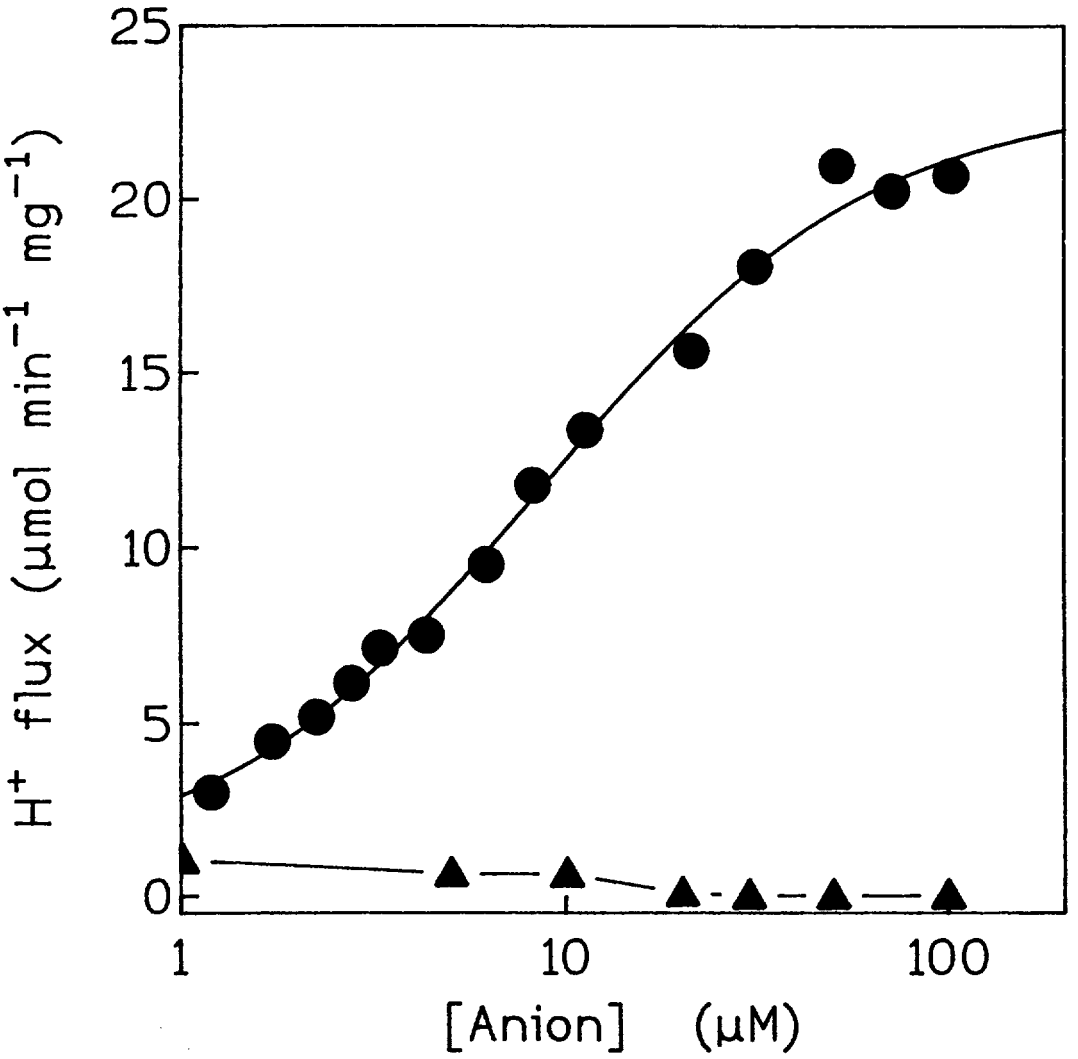

Figure 4.2 Laurate, but not undecanesulfonate, activates H^+ efflux from proteoliposomes reconstituted with UCP. H^+ flux, determined from changes in intraliposomal [TES^-], is plotted versus concentrations ([Anion]) of undecanesulfonate (▲) and laurate (●). Laurate or undecanesulfonate were added to the proteoliposomes in assay medium, followed by addition of 0.1 μM valinomycin to initiate H^+ efflux, as in Fig. 4.1A. Net fluxes are plotted, after subtraction of flux obtained in the presence of 1 mM external GDP. Non-linear regression (*solid line*) of the dose-response curve yielded a K_m of 9 μM for laurate. For undecanesulfonate, the *dashed line* merely connects the points. Media compositions were identical for the two anions and are described in Section 4.1.2.

4.2.3 Comparative kinetics of undecanesulfonate influx and laurate-induced H^+ efflux in proteoliposomes reconstituted with UCP

Fig. 4.3 contains Eadie–Hofstee plots of undecanesulfonate influx and of laurate-catalyzed H^+ efflux. Fluxes were obtained when the anions and valinomycin were added to assay medium containing proteoliposomes. Undecanesulfonate was transported rapidly, and its K_m and V_{max} are comparable to the values obtained for laurate-induced H^+ transport. The result with undecanesulfonate is consistent with experiments in brown adipose tissue mitochondria showing that transport of short-chain alkylsulfonates increased with increasing alkyl chain length (53). Table 4.1 contains a summary of kinetic parameters from experiments on anion transport and FA-induced H^+ transport in proteoliposomes reconstituted with UCP. The data in Table 4.1 confirm and extend the finding that hydrophobicity affects both the K_m and V_{max} (53).

4.2.4 Undecanesulfonate and laurate are competitive inhibitors of Cl^- flux through UCP

We have shown previously that laurate is a competitive inhibitor of Cl^- transport through UCP (115). The data in Fig. 4.4 show that undecanesulfonate is also a potent inhibitor of Cl^- transport through UCP. The effects of these analogues on the kinetics of Cl^- uptake are compared in Fig. 4.5. Competitive inhibition by both anions is demonstrated by the parallel Hanes plots (Fig. 4.5). This result extends previous findings that short- and medium-chain alkylsulfonates are competitive with Cl^- transport (53).

4.2.5 Undecanesulfonate is a competitive inhibitor of laurate-induced H^+ efflux in proteoliposomes reconstituted with UCP

Anions that do not quench SPQ fluorescence (104) can be investigated for their effects on H^+ transport because they do not interfere with the measurement. NO_3^- (59) and hexanesulfonate (53) are transported electrophoretically by UCP, and we have shown that they are competitive inhibitors of laurate-induced H^+ transport (115). The double reciprocal plots in Fig. 4.6 show that undecanesulfonate is also

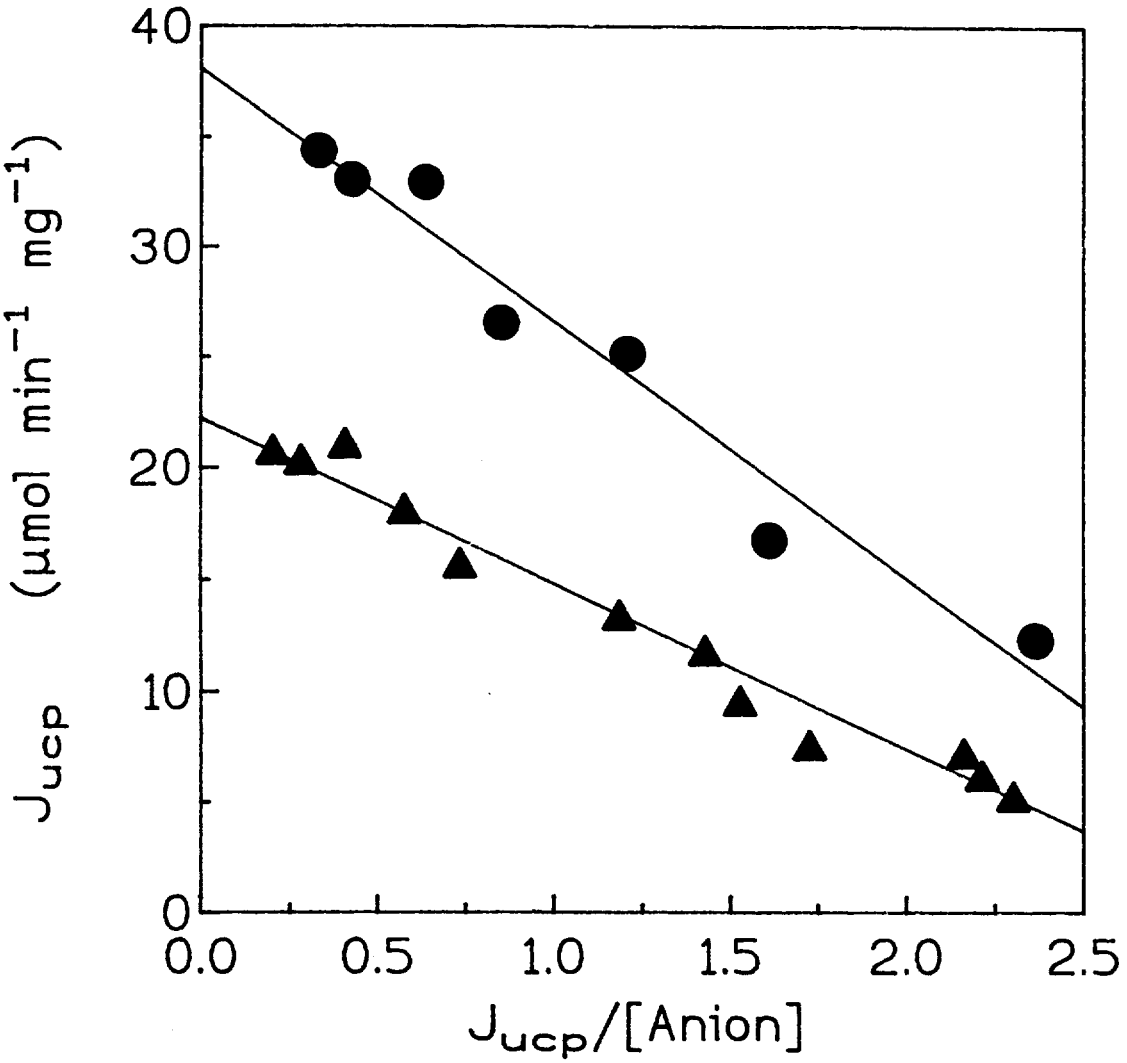

Figure 4.3 Kinetics of undecanesulfonate influx and laurate-induced H^+ efflux in proteoliposomes reconstituted with UCP. J_{UCP} refers to undecanesulfonate influx (▲), measured indirectly as K^+ influx, and laurate-induced H^+ efflux (●), measured directly. [Anion] refers to concentrations of undecanesulfonate and laurate, respectively. Figure contains Eadie–Hofstee plots for the two anions. Net fluxes are plotted after subtraction of flux obtained in the presence of 1 mM external GDP. Except for internal probe, media compositions were identical for the two anions and are described in Section 4.1.2. Linear regressions (*solid lines*) of the data yielded a K_m = 12 μM and a V_{max} = 37,600 nmol/min/mg protein for undecanesulfonate and a K_m = 8 μM and a V_{max} = 22,000 nmol/min/mg protein for laurate.

Table 4.1

Kinetic Parameters for Anionic Substrates of Uncoupling Protein

The table contains V_{max}, K_m and limiting permeabilities for a series of anions whose kinetics have been measured using UCP reconstituted into proteoliposomes. Limiting permeability is flux/[anion] as [anion] approaches zero and equals the ratio, V_{max}/K_m. SPQ fluorescence quenching was used to measure flux of Cl^- and flux of H^+ induced by laurate and oleate. PBFI fluorescence was used to measure K^+ flux as an indirect measure of hexanesulfonate and undecanesulfonate flux. $\Delta\psi$ varied between 120 and 140 mV for these measurements, and parameters have not been adjusted for the effects of these variations.

Anion	V_{max} (nmol/mg UCP · min)	K_m (M)	**Limiting permeability** (μl/mg UCP · min)
Cl^-	9,000	1.4×10^{-1}	6.4×10^{-5}
Hexanesulfonate	23,500	1.2×10^{-2}	2.0×10^{-3}
Undecanesulfonate	37,600	1.2×10^{-5}	3.1
Laurate	22,000	8.0×10^{-6}	2.8
Oleate	16,000	5.0×10^{-6}	3.2

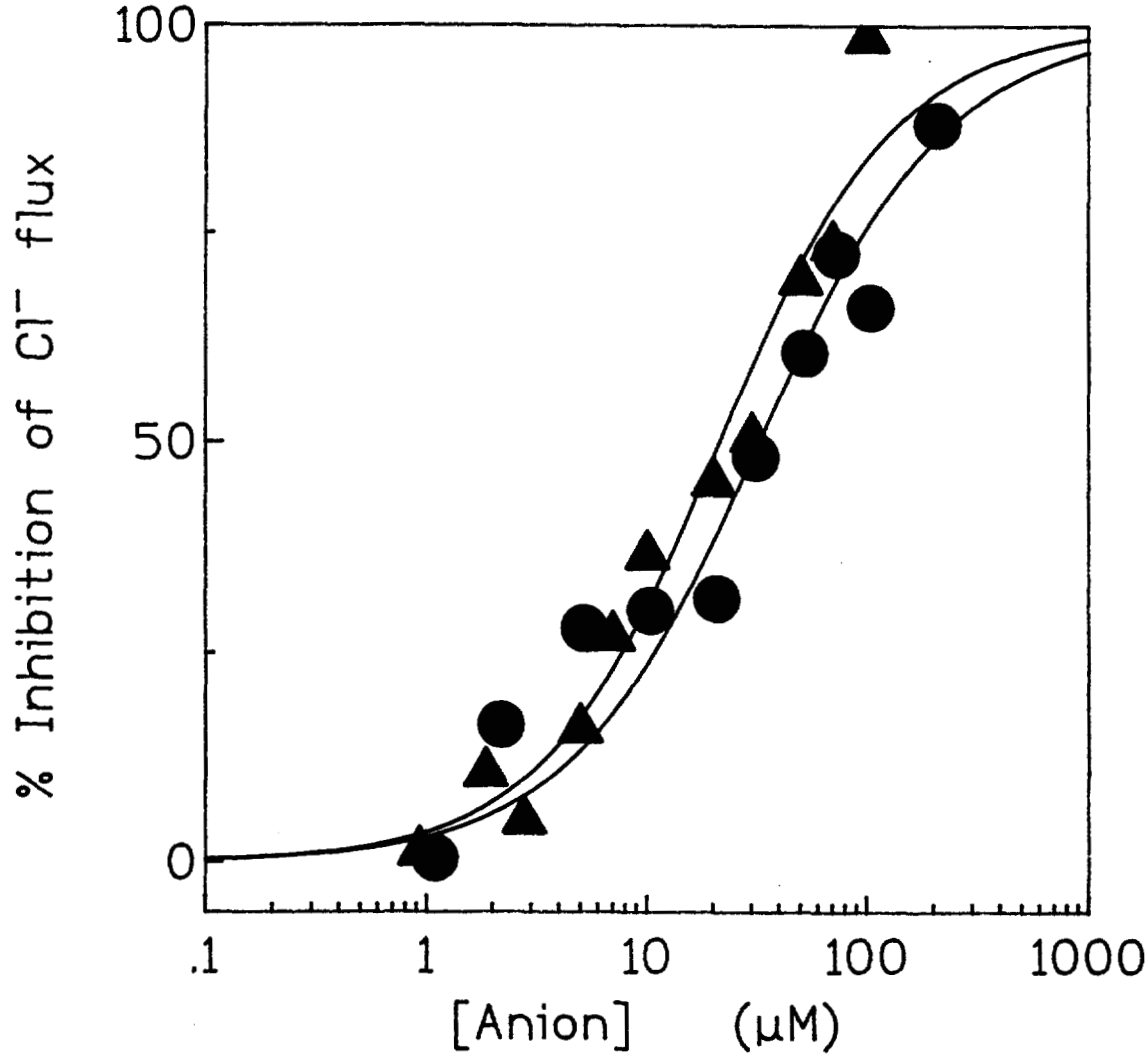

Figure 4.4 Laurate and undecanesulfonate inhibit Cl^- influx into proteoliposomes reconstituted with UCP. Percent inhibition of UCP-mediated Cl^- influx is plotted versus [laurate] (●) and [undecanesulfonate] (▲) ([Anion]). Non-linear regressions (*solid lines*) yielded IC_{50} values of 23 μM and 32 μM for undecanesulfonate and laurate, respectively. Hill coefficients for both curves are 1. Cl^- flux was determined from SPQ fluorescence as described in Section 4.1.2.

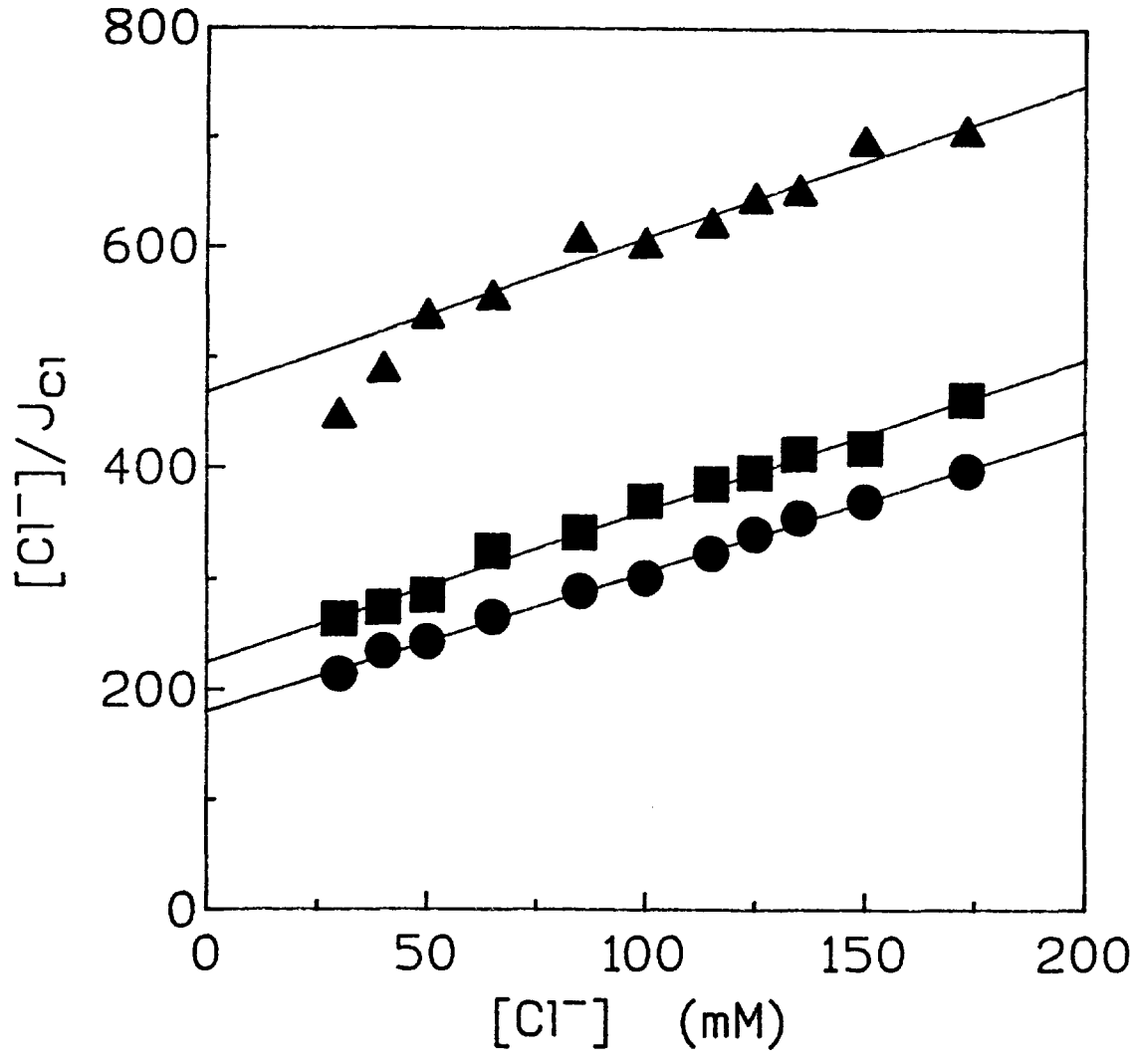

Figure 4.5 Laurate and undecanesulfonate are competitive inhibitors of UCP-mediated Cl^- transport. UCP-mediated Cl^- influx (J_{Cl}) was measured as described in Section 4.1.2. J_{Cl} was measured in varying Cl^- concentrations ($[Cl^-]$) without additions (●), and containing 10 μM laurate (■) or 50 μM undecanesulfonate (▲). $[Cl^-]$ was varied by mixing medium containing 175.5 mM KCl with medium containing 175.5 mM K-glucuronate. Internal medium was adjusted with TEA_2SO_4 to be isosmotic with external medium. Cl^- uptake was initiated with 0.1 μM valinomycin. Linear regressions (*solid lines*) of the initial rates yielded apparent K_m values for Cl^- of 140 mM (●), 164 mM (■), and 332 mM (▲). Corresponding V_{max} values (nmol Cl^-/min mg protein) were 9490 (●), 8800 (■), and 8530 (▲). Assuming fully competitive inhibition, the K_i values calculated for undecanesulfonate and laurate were 37 μM and 66 μM, respectively.

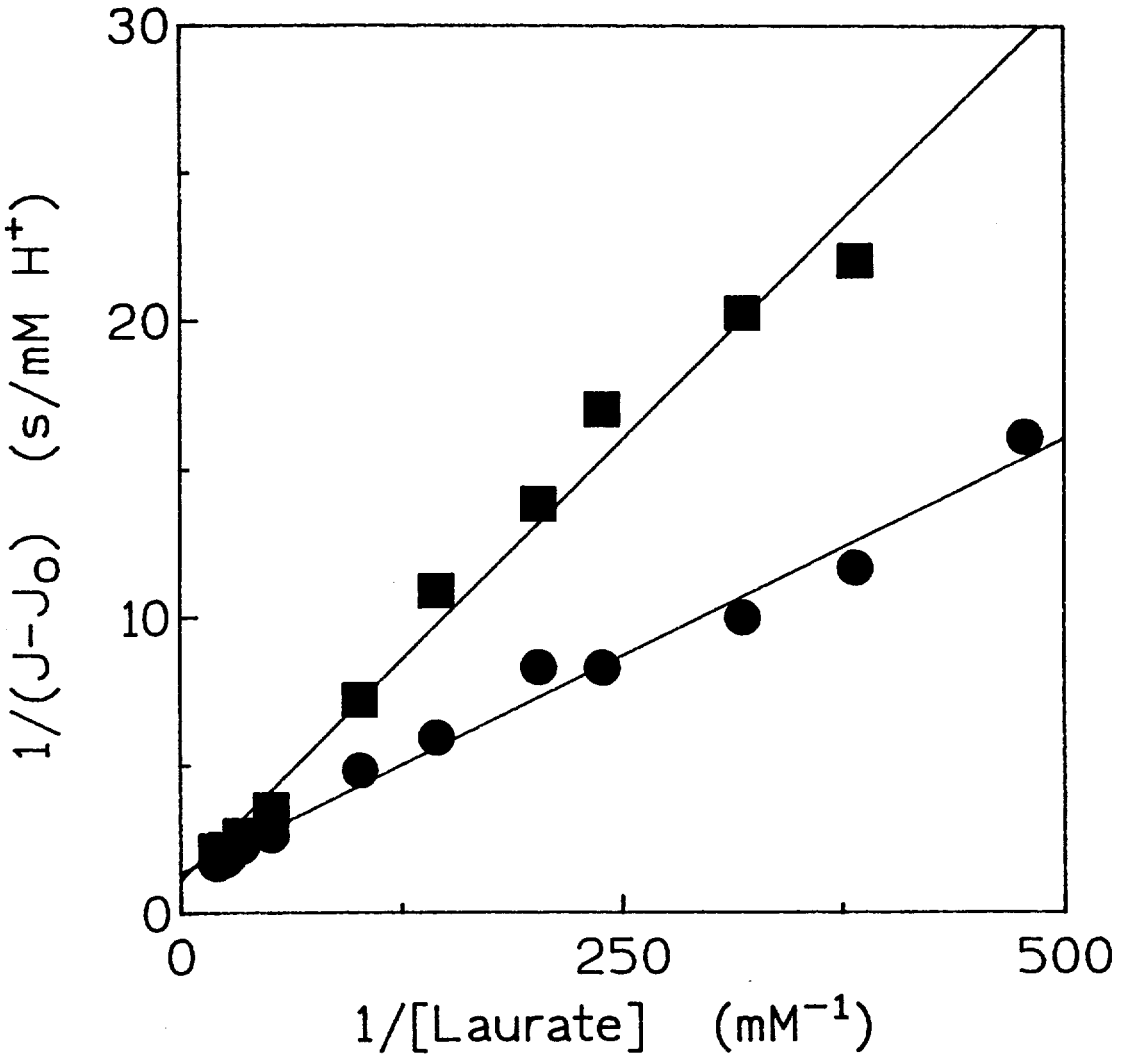

Figure 4.6 Undecanesulfonate is a competitive inhibitor of laurate-induced H^+ efflux in proteoliposomes reconstituted with UCP. The dependence of H^+ efflux on [laurate] is expressed as a double reciprocal plot without further addition (●) and in the presence of 100 μM undecanesulfonate (■). $J - J_0$ is the difference in flux in the presence (J) and absence (J_0) of laurate. H^+ efflux was measured as described in Section 4.1.2. Linear regressions of the data (*solid lines*) yielded apparent K_m values for laurate of 22 μM and 53 μM in the absence and presence of 100 μM undecanesulfonate, respectively. Based on purely competitive inhibition, the K_i value for undecanesulfonate was calculated to be 72 μM.

competitive with laurate as an inhibitor of UCP-mediated H^+ transport.

4.2.6 Undecanesulfonate is incapable of nonionic diffusion in liposomes

The preceding results show that undecanesulfonate and laurate behave similarly with respect to UCP. The notable exception is that laurate causes UCP-mediated proton transport, whereas undecanesulfonate does not. The likely structural basis for this exception is that FAs are weak acids, whereas the alkyl sulfonic acids are very strong acids, with pK $\sim$ 0 (130). Accordingly, lauric acid is more likely than undecanesulfonic acid to undergo nonionic diffusion across the membrane.

The traces in Fig. 4.7 demonstrate that lauric acid equilibrates rapidly across the membrane, resulting in the delivery of protons to the intraliposomal space of protein-free liposomes. In contrast, undecanesulfonate additions were without effect on intraliposomal pH. Thus, undecanesulfonic acid is not transported by nonionic diffusion, probably because its concentration is so low near neutral pH.

4.3 Discussion

4.3.1 The mechanism by which fatty acids induce UCP-mediated proton transport

Our understanding of the UCP transport mechanism is built on foundations laid by Nicholls and coworkers (39), beginning with the discovery that UCP conducts anions of strong acids (59). Nicholls (11) pointed out that anion transport is without physiological significance and concluded that Cl^- and other anions are accidental substrates of UCP. In our view, it is this very aspect of anion transport through UCP—the case of the dog that didn't bark (131)—that holds the key to the mystery of UCP-mediated H^+ transport. This view was strengthened by our finding that short-chain (C1–C8) alkylsulfonates are transported by UCP and that their flux increases with alkyl chain length (32). These results are now extended to long-chain alkylsulfonates: (i) undecanesulfonate is transported as the anion by UCP with K_m values of 10–15 μM (Fig. 4.3); (ii) laurate and undecanesulfonate are competitive inhibitors of Cl^- transport (Fig. 4.5); and (iii) undecanesulfonate is a competitive

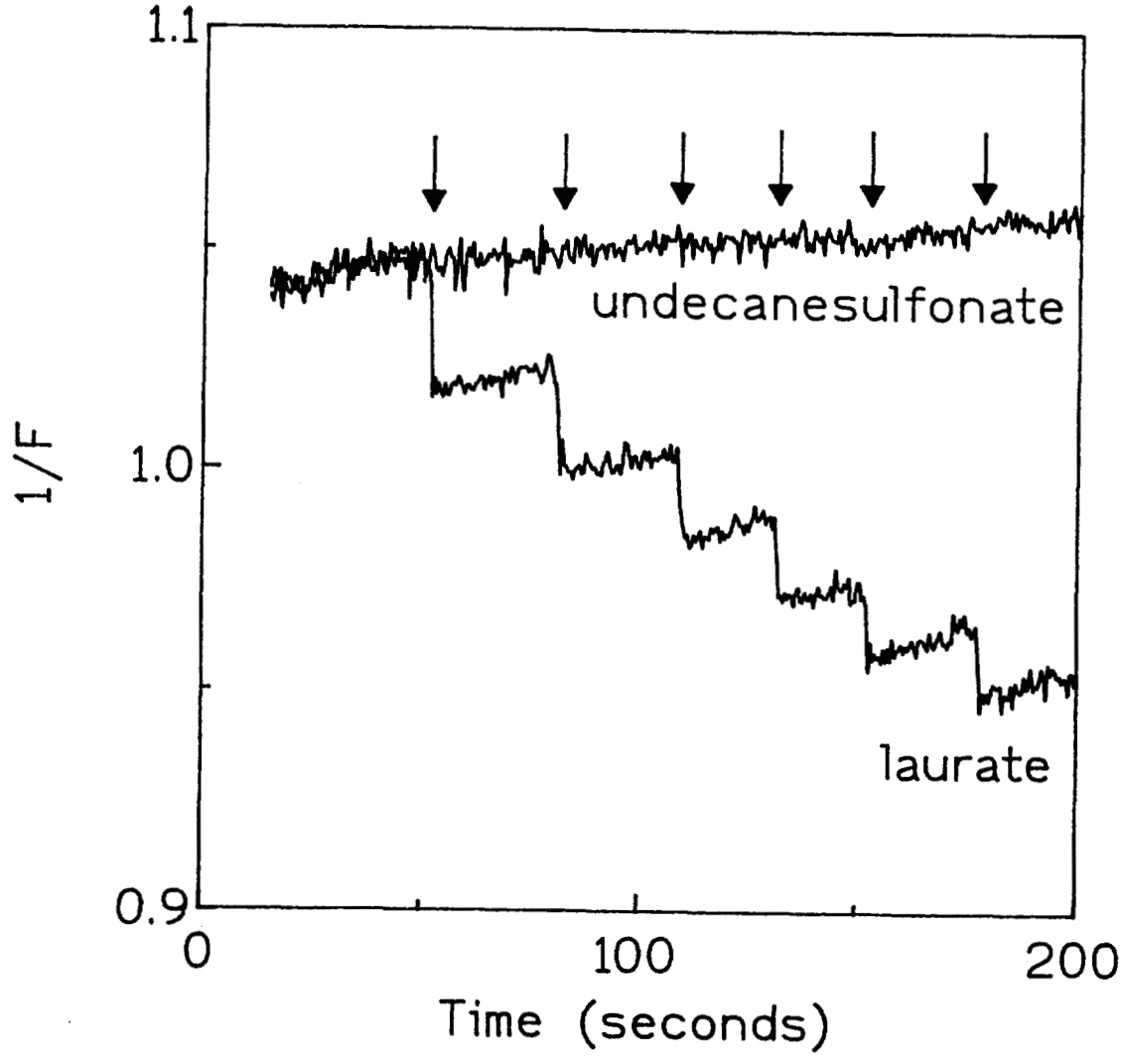

Figure 4.7 Lauric acid, but not undecanesulfonic acid, can diffuse across the liposomal membranes. Inverse SPQ fluorescence (1/F) is plotted versus time in liposomes lacking UCP and containing internal medium for H^+ transport (see Section 4.1.2). A decrease in 1/F indicates protonation of TES anion and, hence, delivery of protons across the liposomal membrane. Arrows indicate additions of 25 μM Na-laurate (laurate) or 50 μM Na-undecanesulfonate (undecanesulfonate).

inhibitor of laurate-induced H^+ transport (Fig. 4.6). These and other results strongly support the hypothesis that anions are transported through the FA docking site in UCP (32, 43, 115).

How do FAs activate UCP-mediated proton transport? This is the principal unsolved question surrounding the molecular basis of the UCP mechanism. Winkler and Klingenberg (34) propose that multiple FAs bind at sites within the UCP proton channel, thereby providing local acceptor/donor groups that facilitate H^+ transport (the buffering model). Based on work showing FA-induced H^+ transport via the ADP/ATP carrier, Skulachev (44) proposes that UCP transports FA anions directly, with protons transported via nonionic diffusion of the protonated FA (the Protonophoretic Model). Our experiments comparing the behavior of laurate and its close analogue, undecanesulfonate, provide a plausible means of distinguishing between these models.

Most features of undecanesulfonate behavior are consistent with either model. Interpreted according to the Buffering Model, the results imply that undecanesulfonate competes successfully with laurate in binding to the FA-binding sites within the UCP proton channel, thereby inhibiting laurate-induced H^+ transport (Fig. 4.6). Because it is a strong acid, it provides no buffering in the channel and therefore cannot support UCP-mediated H^+ transport (Fig. 4.2). Interpreted according to the Protonophoretic Model, undecanesulfonate, like other anions, is transported through the FA anion channel of UCP. It does not support UCP-mediated H^+ transport because it is incapable of nonionic delivery of protons across the bilayer (Fig. 4.7).

A crucial distinction between the two models is that FA binding and transport are stoichiometrically linked to H^+ transport in the Protonophoretic Model, whereas FAs remain bound to the protein in the Buffering Model and do not participate stoichiometrically in H^+ transport. In this respect, our data support the Protonophoretic Model on both qualitative and quantitative grounds: undecanesulfonate anion is *transported* by UCP. We are unaware of any physicochemical mechanism to explain why the laurate anion should remain bound without also undergoing transport. Furthermore, undecanesulfonate, as a stand-in for the laurate anion, is transported with V_{max} and K_m values that are fully sufficient to

account for laurate-induced H^+ transport via a stoichiometric, protonophoretic mechanism (Table 4.1). Applying Occam's razor, we infer that FAs catalyze UCP-mediated proton conductance, because the FA anion is transported by UCP and the protonated FA is rapidly transported across the lipid bilayer by nonionic diffusion (see model in Fig. 4.8). This proton cycling mechanism is entirely analogous to uncoupling by weak acid protonophores. It differs in that a specific protein is required in order to provide a conductance pathway for back-diffusion of the FA anion.

4.3.2 The UCP-catalyzed protonophoretic cycle

The protonophoretic FA cycle consists of the following steps, as diagrammed in Fig. 4.8.

(i) The FA anion partitions in the lipid bilayer with its head group at the level of the acyl glycerol linkages and *below* the surface of the phospholipid head groups. This shielded location, driven by the free energy of partitioning of the alkyl chain, is responsible for the long-standing observation that the pK_a values of FAs in membranes are 3–4 units higher than their values in solution (132). Despite high electrical gradients, there is no significant flux of the FA anion, because the bilayer energy barrier is too high.

(ii) The FA anion diffuses laterally in the bilayer to reach the protein. UCP may contain a weak binding site to concentrate the anion in the conductance pathway. If so, this site must also be partly buried, because kinetic studies show that it is shielded from the bulk aqueous phase (53).

(iii) The energy barrier to anion transport is lowered by a weak binding site located about halfway through the UCP transport pathway. [The existence of this energy well was deduced from the dependence of UCP-mediated Cl^- flux on $\Delta\psi$ (43)]. The anionic head group is driven to this energy well by the electric field created by redox-linked proton ejection. Given the preference for hydrophobic substrates, it seems likely that all or part of the conductance pathway lies on the *outer* surface of the protein at the lipid–protein interface.

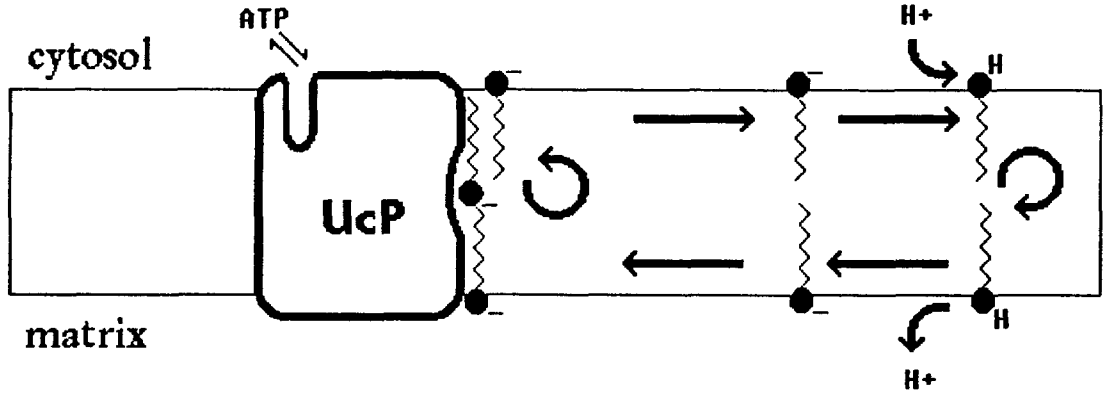

Figure 4.8 Proposed protonophoretic mechanism of uncoupling protein. Fatty acid partitions in the membrane and diffuses laterally to the UCP. The fatty acid anion is driven to the center of the membrane by the electric field along the UCP anion conductance pathway. The anion flip-flops, and COO^- reaches the opposite interface. It then picks up a proton and rapidly flip-flops again, delivering protons by nonionic diffusion to the other side. This catalyzed protonophoretic cycle dissipates redox energy and produces heat. Alkylsulfonates are anions of strong acids and cannot undergo nonionic diffusion; therefore, UCP-mediated alkylsulfonate transport does not lead to proton transport. For more details, see Section 4.3.2.

(iv) The anionic carboxyl group moves to the other side of the membrane by a flip-flop mechanism such as occurs during nonionic transmembrane diffusion of protonated FAs (133). The FA anion then diffuses laterally away from the conductance pathway.

(v) The FA is protonated and rapidly flip-flops again, delivering protons by nonionic diffusion to the mitochondrial matrix and completing the cycle.

4.3.3 Properties of the UCP anion transport pathway

V_{max} values reflect the rate constant for crossing the second energy barrier as anions leave the saturated energy well and move to the other side. Cl^- exhibits the lowest V_{max} among the anions in Table 4.1, suggesting that the alkyl chain facilitates transport along the hydrophobic protein–lipid interface. The limiting permeabilities (V_{max}/K_m), which equal J/[anion] as [anion] approaches zero, reflect the rate constants for passage over the first energy barrier and also contain the coefficients of anion partitioning into the pathway. The limiting permeabilities of undecanesulfonate, laurate and oleate are very nearly the same (Table 4.1). The lower value for hexanesulfonate can be rationalized by its lower partition coefficient. Small polar anions, such as halides (32, 59), acetate (115) and nitrate (53, 59), cannot partition into the hydrocarbon at all and must gain additional thermal energy to reach the same starting location as hydrophobic anions. This is acquired through normal thermal bombardment of the total membrane surface. Thus, their limiting permeabilities are very low, and their K_m values are correspondingly high.

4.3.4 Bioenergetic aspects of the fatty acid protonophore hypothesis

In mitochondria containing 10% UCP protein, the V_{max} for laurate (Table 4.1) translates to about 2000 nmol/(mg mitochondrial protein · min), roughly equal to the maximum rate of proton ejection by the redox chain. This is not unexpected, because mitochondrial transporters are normally synthesized in quantities more than sufficient to carry out their tasks. The maximum turnover number estimated from these data is about 20 s^{-1}. This rather sluggish rate emphasizes another physiological control

mechanism for UCP. When the need for thermogenesis is great, mammals synthesize more UCP, to the extent that UCP levels reach 15% of mitochondrial protein (9, 10).

It should be emphasized that long-chain FAs that reach the matrix by nonionic diffusion cannot enter the β-oxidation pathway, because the matrix doesn't contain long-chain acyl-CoA synthetase (134). Instead, acylcarnitine is transported to the matrix where it is activated by carnitine acyl transferase II. Since FAs rapidly equilibrate across the inner membrane, it may be useful to view carnitine/acylcarnitine translocase as being required for *channeling* of long-chain FAs into the β-oxidation pathway.

4.3.5 Summary

The uncoupling protein of brown adipose tissue mitochondria mediates electrophoretic transport of anions and protons, and proton transport requires fatty acids for activation. Transported anions and FAs interact with a common site on UCP which we have called the FA docking site (43, 53). The differential effects of laurate and its analogue, undecanesulfonate, support the hypothesis that the protonophoretic mechanism of UCP relies on FA anion transport. That is, UCP contains a conductance pathway for anions and does not transport protons. We propose that this pathway lies in the protein–lipid interface.

---

[2] This material has been published in this or similar form in *The Journal of Biological Chemistry* and is used here by permission of The American Society for Biochemistry and Molecular Biology:

Garlid, K. D., Orosz, D. E., Modriansky, M., Vassanelli, S., and Jezek, P. (1996) On the mechanism of fatty acid-induced proton transport by mitochondrial uncoupling protein. *J. Biol. Chem.* **271**, 2615–2620.

Chapter 5

A STRUCTURE-ACTIVITY STUDY OF FATTY ACID INTERACTION WITH LIPID MEMBRANE AND MITOCHONDRIAL UNCOUPLING PROTEIN[3]

The mitochondrial uncoupling protein (UCP), expressed in mammalian brown adipose tissue (BAT), is the terminal regulated unit of the catabolic cascade of non-shivering thermogenesis (8, 40). UCP allows for H^+ backflow across the mitochondrial inner membrane in the presence of free fatty acids (FA), thus dissipating the protonmotive force and generating heat (8, 40). The consensus is that the free FAs participate in the process, but are considered to act as a buffering agent without being transported themselves (40). We have published evidence (33, 35, 37, 115, 135) in support of the mechanism of FA cycling, hypothesized originally by Skulachev (44) who described UCP as an anion channel which transports FA anions unidirectionally, implying that H^+ translocation originates from the return of protonated FAs through the lipid bilayer. Such a mechanism would be possible under the following three circumstances:

(i) *UCP must be an anion uniporter.* This condition is fulfilled (32, 53), but the structural requirement for the monovalent noncarboxylic substrates and their maximum size is yet to be investigated.

(ii) *UCP must transport anionic FAs.* Such a uniport (apparent as the H^+ counterflux due to presumed FA cycling) should exhibit properties very similar to the uniport of other UCP substrates, since the internal binding site mediating translocation, a *docking site* (53), was found to be common for anions and FAs (33, 35, 37, 115, 135).

(iii) *Nonionic FAs in the membrane must undergo a rapid flip-flop.* It would balance the reported activities of UCP, i.e., account for at least 11–22 mol

H^+/min/mg protein which is equivalent to 726–1452 min^{-1} turnover for a dimeric UCP (33–35, 69, 115).

Indeed, long chain FAs are capable of rapid nonionic flip-flop across biological membranes (133, 136). Kamp and Hamilton (133, 136) have shown that only the protonated FAs can flip-flop very rapidly, while flip-flop or diffusion of the negatively charged FAs was several orders of magnitude slower. Rates of flip-flop were inferred from the internal acidification of liposomes upon addition of FAs. Interestingly, the FAs with bulky groups such as 5-DOXYL-stearic acid and 1-pyrenenonanoic acid exhibited the same fast flip-flop with $t_{1/2} < 1$ s (136). Only flip-flop of 12-(9-anthroyloxyl) stearic acid proceeded with $t_{1/2}$ of 200 s (136).

Garlid et al. (33) demonstrated that a pair of similar amphiphiles, undecanesulfonate and laurate, can both undergo a GDP-sensitive uniport mediated by UCP, but only laurate in its protonated form is capable of rapid flip-flop across the liposomal membrane. The flip-flop results in acidification of the liposomal interior after H^+ dissociates from laurate at the inner surface. Moreover, the GDP-sensitive H^+ flux in UCP proteoliposomes can be induced only with laurate, but not with undecanesulfonate. Applying Occam's razor, the laurate-induced UCP-mediated H^+ flux was explained by the FA cycling mechanism.

This study deals with the structural features that affect the ability of FAs to flip-flop. We found several FA derivatives which were unable to flip-flop, at least in the time course of our experiments. Their flip-flop rates, if they exist at all, must correspond to $t_{1/2} > 30$ min. We designated these FAs as *inactive* and suggested them as a tool for studying FA-induced uncoupling. The inactive FAs share the inability to flip-flop with alkylsulfonates even though the carboxy group is preserved. We also examined the interaction of the inactive FAs with reconstituted UCP. The inability of the FA to flip-flop was strongly correlated to its inability to be transported by UCP and to induce UCP-mediated H^+ translocation, and with the lack of FA inhibition of Cl^- transport via UCP. Such correlation supports the FA cycling mechanism.

5.1 Materials and Methods

The fluorescent probes PBFI, SPQ, and ADIFAB were purchased from Molecular Probes, (Eugene, OR). Various FA derivatives were purchased from Sigma (St. Louis, MO) and Fluka (Germany or Lancaster, UK). The materials for reconstitution were from the same sources as previously described (32, 33, 53, 115, 116). BAT mitochondria were isolated from Golden Syrian hamsters in 250 mM sucrose, 10 mM TEA–TES, 1 mM K–EGTA, pH 6.7, containing 2 mg BSA/ml. UCP was purified and reconstituted into lipid vesicles, and all H^+, Cl^-, and K^+ fluxes were measured using a SLM Aminco 8000C fluorometer as described elsewhere (32, 33, 53, 115). The transport rates were calculated in mM of ion/s. Our results have shown that the effects of FAs do not depend on the data treatment when either net rates or GDP-sensitive rates are taken into account. UCP reconstituted into liposomes (32, 33, 53) has equal distribution with respect to the GDP-binding site orientation (outward or inward). Hence, GDP added externally results in a maximum of 50% inhibition and when added to both sides results in 100% inhibition (32, 33, 53). Therefore, every test was performed in pairs, with and without external GDP (calibrated separately), and the difference was taken as the net GDP-sensitive flux. The amount of reconstituted UCP was estimated by the Amido Black method (103), and the vesicle volume was determined from probe distribution (33, 115). FAs (either in the form of free acid or sodium salt) were prepared in ethanol and added in 1-μl aliquots for assays with ADIFAB.

5.1.1 SPQ detection of H^+ flux

SPQ is quenched by TES anion, but not by TES zwitterion (104), which allows for monitoring of H^+ fluxes after rigorous calibration (33, 104). Vesicles (25 μl/assay) contained 84.4 mM TEA–SO_4, 29 mM TES (TEA-salt), pH 7.2, 0.6 mM TEA–EGTA and 2 mM SPQ. External medium contained 84.4 mM K_2SO_4, 29 mM TES (TEA-salt), pH 7.2, and 0.6 mM TEA–EGTA. UCP-mediated H^+ efflux in the presence of FAs was initiated by addition of 0.1 μM valinomycin.

5.1.2 PBFI detection of FA uniport

A K^+ gradient was established across the liposomal membrane to drive the electrophoretic UCP-mediated transport. The K^+ uptake can be used as an indirect measurement of UCP-mediated transport by assuming it is equivalent to the net charge flux facilitated by UCP. The process was initiated by addition of 0.1 μM valinomycin while change in internal [K^+] was detected by following PBFI fluorescence (3). The system was calibrated by adding aliquots of 2 M KCl in the presence of 0.5 μM nigericin and 5 μM tributyltin. Composition of internal and external media was the same as for measurements of H^+ flux (see Section 5.1.1), except for 0.15 mM K_2SO_4 and 300 μM PBFI in the internal medium.

5.1.3 SPQ detection of Cl^- uptake

Vesicles contained 2 mM SPQ, 79.4 mM TEA_2-SO_4, 0.6 mM TEA-EGTA, and Tris-P_i, pH 7.2 (24.7 mM Tris, 12.8 mM P_i). External medium for a higher Cl^- gradient contained 119.25 mM KCl, 0.6 mM TEA-EGTA, and Tris-P_i (as above), pH 7.2. Alternative external medium had only 74.8 mM [Cl^-], but [K^+] was 201.2 mM in 126.4 mM glucuronate, 32.5 mM $SO_4$2- salts, 0.6 mM TEA-EGTA, and Tris-P_i (as above) pH 7.2, were also present. Cl^- uptake was initiated by addition of 0.1 μM valinomycin. Calibration of SPQ quenching by Cl^- was done by μl additions of 2 M KCl in the presence of 0.5 μM nigericin and 5 μM tributyltin (32), permitting fluorescence traces to be transformed into *Cl-traces* according to the Stern-Vollmer equation:

$$[Cl^-] = \mathbf{m}^{-1} \{F_0exp - F\}/\{F - L\} \qquad \text{(Eq. 4.1)}$$

where L is light scattering (i.e., background) of a given sample, F_0exp is the maximum fluorescence intensity at zero [Cl^-] corrected for light scattering, and **m** is the experimental Stern-Vollmer constant of calibration.

5.1.4 HPLC measurement of FA partitioning between water and liposomes

FA (8 nmol) were added to liposomes (40 mg lipids) and the aqueous portion of the FA was estimated as the difference between the original (total) amount of FA and the amount retained in the vesicles after gel filtration on Sephadex G25–300 spin columns. The amount of FA was analyzed after sample derivatization by phenylacylbromide (137) on a Waters HPLC system with an automated gradient controller, Model 510 pumps, and W490E absorbance detector (242 nm) using a 10 M Nucleosil 250 × 4 mm column (Macherey–Nagel, Düren, Germany) at 46°C. Elution was done with a linear gradient of water and acetonitrile, from 70% acetonitrile to 100% acetonitrile for 30 min at a flow rate of 2 ml/min.

5.1.5 Fluorescent measurement of FA partitioning between water and liposomes

To estimate free FA, we used a decrease in the slope (138) of a plot of the ADIFAB fluorescence ratio, R, at 505–432 nm versus the total amount of FA, $[FA]_{total}$. Excitation was set at 477 nm. The assay medium contained 150 mM NaCl, 1 mM TEA–EGTA, 10 mM Tris–Cl, pH 8, with 0.2 mM ADIFAB (139, 140). The amount of free FA was calculated from the experimentally obtained ratios as described (139, 140):

$$[FA]_{free} = K_d\, Q\, (R - R_0)/(R_{max} - R) \qquad \text{(Eq. 4.2)}$$

where K_d is an equilibrium constant for binding of the given FA to ADIFAB, Q is the ratio of fluorescence at 432 nm at zero and saturating FA concentrations, and R_0 and R_{max} are the ratios at zero and saturating FA concentrations, respectively. We had to calculate our own parameters, Q (14.5) and R_{max} (5), while using the Marquardt algorithm to fit Eq. 4 in ref. 140 onto our data obtained with oleic acid. This procedure yielded K_d values close to those published for oleic acid binding to ADIFAB (0.39 μM, and 0.22 μM) (140). Eq. 4.2 also was used to calculate $[FA]^L_{free}$ at the equilibrium that shifted due to the addition of liposomes. The respective K_d

calculated from the data of the experiments without liposomes were used. We then evaluated the partition coefficient K_P from the data around K_d according to Anel et al. (139) as follows:

$$K_P = (V_a/V_m)\ (1/[FA]^L_{free})\ ([FA]_{total} - [FA]^L_{free}) \qquad \text{(Eq. 4.3)}$$

where V_a/V_m is the ratio of volumes of the aqueous and membrane phases. V_m/V_a = 0.001/1 μM phospholipids was used (139).

5.2 Results

5.2.1 Flip-flop is observed only with *active* FAs

Fig. 5.1 illustrates internal acidification in liposomes upon addition of 50 μM heptylbenzoic acid (trace C_7bz $-UCP$). The acidification occurred independent of the presence of UCP (Fig. 5.1, trace C_7bz $+UCP$) and can be interpreted as the flip of the protonated FA from outer to inner leaflet of the lipid membrane, according to Kamp and Hamilton (133, 136). The flip-flop behavior was not observed with all FA derivatives, as demonstrated for 12-hydroxylaurate (Fig. 5.1, traces $12OHC_{12}$). The addition of solvent alone, i.e., pure ethanol, in the μl volume used in adding FA, resulted in traces identical to those obtained with 12-hydroxylaurate (Fig. 5.1, traces $12OHC_{12}$). Addition of 0.1 μM valinomycin in the presence of any inactive FA caused negligible alkalization of the vesicle interior. The FA-induced H^+ leak was therefore very low (33) and equal to the H^+ leak existing in the absence of FAs, despite the existence of the K-diffusion potential of over 180 mV. The leak magnitudes were between 0.007 and 0.03 nmol H^+/s with the inactive FA, and 0.016 to 0.04 nmol H^+/s with the active FA. For comparison, the H^+ leak in the presence of ethanol was 0.013 to 0.025 nmol H^+/s. Extrapolating to 0 mV (108), permeability coefficients derived from these data were 1.10^{-4} to 4.10^{-4} cm/s. Only with 12-hydroxystearic and hexadecanedioic acids was the H^+ leak significantly higher (not shown).

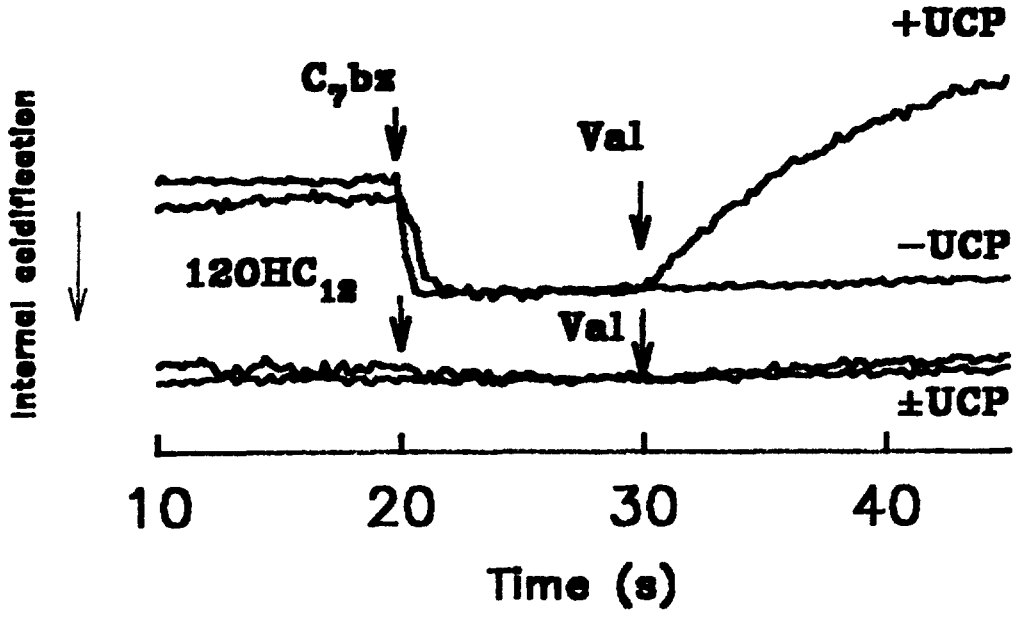

Figure 5.1 Fatty acid cycling requires the presence of the uncoupling protein and the active fatty acid. Net H^+ fluxes in proteoliposomes containing UCP (+UCP) and in liposomes (–UCP) were monitored as quenching of SPQ fluorescence by TES^- anion as described in Section 5.1.1. Either 100 nmol of the active FA, heptylbenzoic acid (C_7bz), or the inactive FA, 12-hydroxylauric ($12OHC_{12}$), were added (50 μM final concentrations) as indicated by the arrows. 0.1 μM valinomycin (Val) was added at 30 s.

All physiologically abundant FAs and their derivatives demonstrated the ability to acidify the vesicle interior with a $t_{1/2}$ well below 1 s, as reported (136). Nevertheless, we found several FA derivatives (Table 5.1), which did not acidify the vesicle interior at concentrations up to 200 μM. No significant changes in pH_{in} were observed for up to 5 min. We conclude that these FAs were unable to flip-flop at a significant rate, designating them as *inactive* FAs to distinguish them from the *active* FAs which do possess the ability to fast flip-flop.

5.2.2 UCP-mediated H^+ transport is induced by active but not by inactive FAs

Addition of long-chain FAs followed by addition of valinomycin to liposomes containing UCP induced internal alkalization of vesicles indicating UCP-dependent H^+ efflux (33, 115). This alkalinization was not observed for all FA derivatives and lead us to distinguish between active and inactive FA derivatives (Fig. 5.2, Table 5.2). Participation of UCP is confirmed by GDP sensitivity of the H^+ flux (Fig. 5.2).

Our interpretation attributes the observed H^+ efflux to the return of the protonated FA while the UCP mediates influx of the anionic FA (33). The flip-flop rates were positively correlated with the rates of H^+ efflux. The inactive FA induced neither vesicle acidification, i.e., did not flip-flop, nor UCP-mediated H^+ efflux (Figs. 5.1, 5.2, Table 5.2). Typically, they were bipolar compounds, such as 12-hydroxylauric acid and 12-dodecanedioic acid, or compounds with a benzene ring at the tail, such as phenylvaleric acid. The inactive FA had no influence on the transport induced by the active FA. For example, H^+ efflux induced by lauric acid in UCP proteoliposomes was neither inhibited nor increased by addition of 12-hydroxylauric acid before lauric acid (not shown). H^+ transport induced by all active FAs tested was inhibited by 150 μM undecanesulfonate, as reported previously for laurate (33).

5.2.3 Inactive FAs are not UCP substrates

Net charge movement in vesicles can be measured with the fluorescent probe PBFI (3), and was used to monitor UCP-mediated transport of various anionic

Table 5.1

Flip-flop of Various Fatty Acids across the Lipid Bilayer as Indicated by Internal Acidification in Liposomes

Experiments were performed in duplicate if not indicated otherwise (n = number of measurements) in the presence of 50 μM FA. The inactive FA were also tested at 200 μM concentration.

Compound		Acidification (*nmol H^+/100 nmol FA added*)[a]	$t_{1/2}$ (*s*)
1. Active fatty acids:			
lauric	(n=7)	2.54	0.387
2-hydroxylauric		1.76	0.5
12-bromo-lauric		2.57	1.0
12-TNT-lauric		2.20[b]	4.0[b]
myristic		4.20	0.4
2-hydroxymyristic		5.67	0.1
3-hydroxymyristic	(n=3)	4.57	0.28
palmitic		3.34	0.45
2-hydroxypalmitic		8.20	0.55
stearic		0.91	2.5
2-hydroxystearic		4.64	1.6
12-hydroxystearic		4.28	0.5
heptylbenzoic	(n=4)	3.92	0.3
dodecyloxybenzoic		1.12	2.4
16-hydroxypalmitic		1.68	0.5
hexadecanedioic[c]	(n=4)	0.44	1.7
2. Inactive fatty acids:		**50 μM[d]**	**200 μM[d]**
12-hydroxylauric		>60 min	>60 min
12-aminolauric		>60 min	>30 min
dodecanedioic	(n=4)	>2 min	>2 min
tetradecanedioic	(n=3)	>200 min	
phenylhexanoic		>200 min	>200 min
phenylvaleric		>200 min	>200 min
9,10,16-trihydroxypalmitic			>4 min
biphenyl-2-carboxylic	(n=3)	>30 min	>200 min
3,3-diphenylpropionic		>200 min	>60 min
2-naphtoic		>30 min	>60 min

[a] With 100 nmol FA added, this is numerically equal to the % of FA molecules partitioning in the lipid bilayer. In the case of inactive FAs, the extent is not related to partitioning.
[b] Increased H^+ leak.
[c] Measured with 10 μM, separately calibrated, and accounting for shift due to absorbance.
[d] Calculated with regard to the extent of H^+ release for lauric acid.

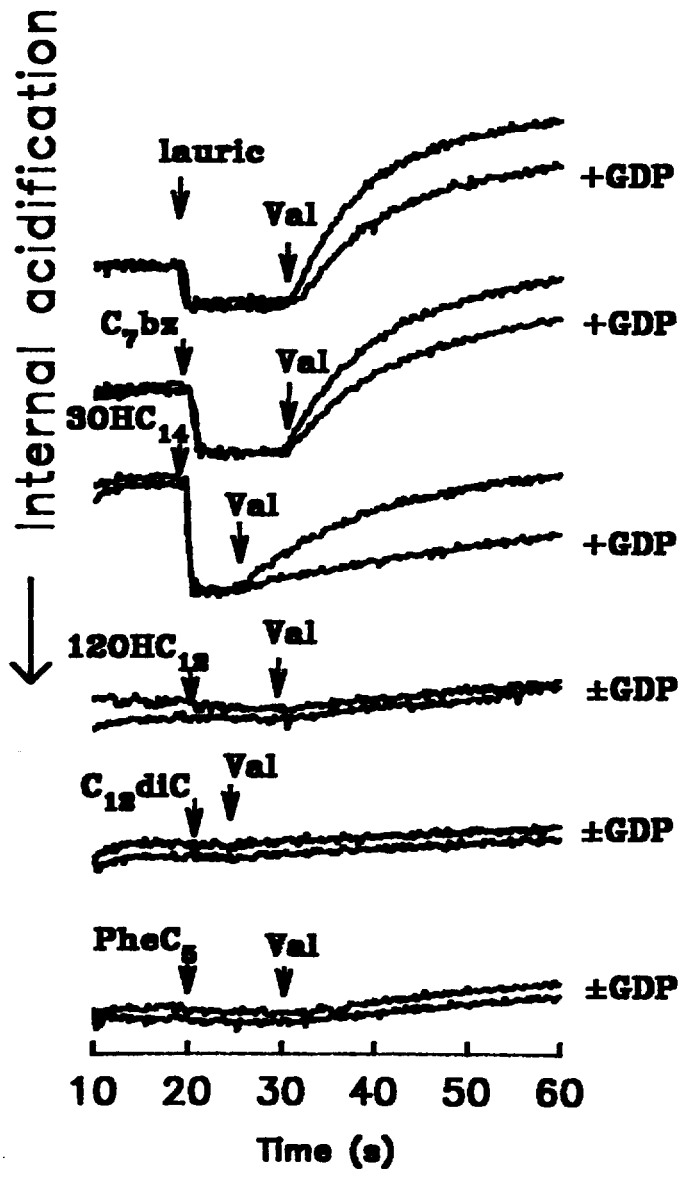

Figure 5.2 GDP inhibition of fatty acid cycling. Net H^+ fluxes in proteoliposomes containing UCP were monitored as quenching of SPQ fluorescence by the TES^- anion as described in Section 5.1.1. Each panel shows a pair of traces expressed as H^+ versus time, measured in the absence (no label) or presence of 0.5 mM GDP (traces +GDP), when 50 μM fatty acid was added at 20 s and 0.1 μM valinomycin (Val) at 30s (or 25 s) to initiate UCP-mediated transport. Top half contains traces obtained in the presence of active FA, lauric, heptylbenzoic (C_7bz), and 3-hydroxymyristic (3-OHC_{14}) acids; bottom-half contains traces obtained in the presence of inactive FA, 12-hydroxylauric (12OHC_{12}), dodecanedioic (C_{12}diC), and phenylvaleric (PheC_5) acids.

Table 5.2

Effects of Active and Inactive Fatty Acids in Liposomes and UCP Proteoliposomes

For comparison, effects of 50 μM lauric acid were set as 100% of the flip-flop rate or the GDP-sensitive transport rate. The % inhibition of Cl^- uniport by FA is listed in absolute values.

	LIPOSOMES	UCP PROTEOLIPOSOMES		
	flip-flop application (%)	H^+ transport (%)	charge transport (%)	inhibition of Cl^- transport (%)
1. ACTIVE FA:	**YES**	**YES**	**YES**	**YES**
lauric	100	100	100	78, 90*
2-hydroxylauric	75	58	135	66
12-bromo-lauric	37	72	116	40
12-TNT-lauric**	9–19		87	58
myristic	93	140	112	81
2-hydroxymyristic	370	149	136	64
3-hydroxymyristic	124	86	83	50, 99*
palmitic	83	134	112	73
2-hydroxypalmitic	68	149	150	75
stearic	15	30	33	25
2-hydroxystearic	23	154	70	52
12-hydroxystearic	75	67	81	17, 61*
heptylbenzoic	107	68	90	60, 97*
dodecyloxybenzoic	16	21	30	N.D.
16-hydroxypalmitic	75	27	49	7
hexadecanedioic	37	17	27	9
2B. INACTIVE FA:	**NO**	**NO**	**NO**	**NO**
12-hydroxylauric	0.01	0	4	0, 1*
12-aminolauric	0.01	4	3	0
dodecandedioic	0.3	3	2	0, 1*
tetradecanedioic	0.003	7	16	0
phenylhexanoic	0.03	2	6	7
phenylvaleric	0.003	3	0.5	0, 0.4*
aleuritic	0.16	1.7	1.2	0
biphenyl-2-carboxylic	0.03	3.4	4.7	8
3,3-diphenylpropionic	0.003	4.6	5.3	0
2-naphtoic	0.03	5.3	6.4	0
ethanol	0	5	6	0–5
2B. INACTIVE FA:	**YES**	**NO**	**NO**	**NO**
None found				
3. TRANSPORTED ANIONS:	**NO**	**NO**	**YES**	**YES**
undecanesulfonate	0	0	200	98*
4. MODEL VIOLATION:	**NO**	**YES**	**YES**	**YES/NO**
None found				

* 200 μM FA instead of 50 μM. ** 10 μM.

substrates (33, 53). A GDP-sensitive K^+ uptake was observed in UCP proteoliposomes in the presence of various active FAs, while no such uptake was observed with the inactive FAs (Fig. 5.3, Table 5.2). Rates of FA uniport were correlated with the rates of the H^+ efflux induced by a given FA (Table 5.2).

5.2.4 UCP-mediated Cl^- uptake is inhibited only by active FAs

Net Cl^- uptake can be measured with SPQ in vesicles containing phosphate buffer instead of TES, allowing unobscured SPQ quenching by Cl^- (104). Cl^- transport in UCP proteoliposomes was competitively inhibited by lauric acid (Fig. 5.4). We observed a strong inhibition caused by various 50 μM FAs (Table 5.2). Without exception, inhibitory ability was pronounced only with active FAs, some of which nearly completely inhibited the Cl^- uniport via UCP (Table 5.2). The inactive FAs were unable to inhibit the Cl^- uniport through the reconstituted UCP (Fig. 5.4, Table 5.2). The extent of inhibition by active FAs correlated with their relative activity in other tests (Table 5.2).

5.2.5 Interaction of FAs with the lipid bilayer

The inability of any particular FA to exhibit a fast flip-flop is a very important property, the trivial explanation being its low partitioning into the lipid bilayer. We have, however, observed otherwise. Using HPLC, we estimate that 15.5% of 12-hydroxylauric acid is retained in liposomes after their passage through a Sephadex G25-300 column, as compared to 27.8 % retention of lauric acid. Data presented in Fig. 5.5 demonstrate the partitioning of 12-hydroxylauric (*diamonds*), tetradecanedioic (*triangles*), oleic (*circles*), and lauric (*squares*) acids into liposomes, with the first two being the inactive and the latter two the active FAs. The binding equilibrium between the intestinal FA-binding protein modified by acrylodan (ADIFAB) and the aqueous phase is strongly disturbed by the presence of liposomes (20 μM lipid concentration). The partitioning into lipids is also implied from calculations of the respective partition coefficients K_P (Table 5.3). Interestingly, the evaluated K_d values for FA binding to ADIFAB (Table 5.3) were not correlated to the FA's ability to flip-flop. Thus, for example, while the binding of α- or β-hydroxy-FA to ADIFAB was very poor (not

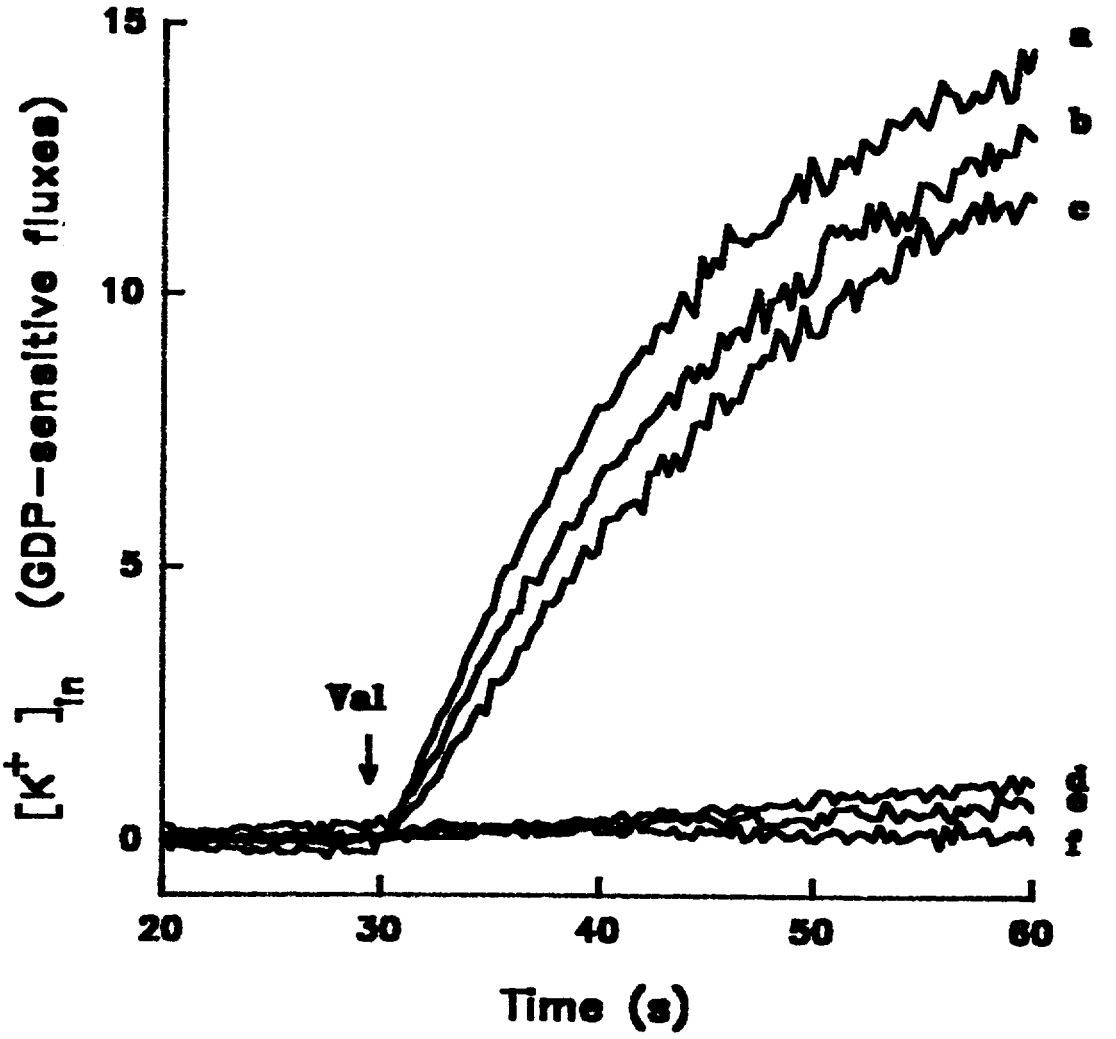

Figure 5.3 GDP-sensitive fatty acid uniport proceeds with the active but not with the inactive fatty acids. Fatty acid anion uptake (or concomitant H^+ efflux via protonated FA) was detected using PBFI as K^+ uptake into proteoliposomes containing PBFI. Transport was initiated by adding 0.1 μM valinomycin. The GDP-sensitive "K-traces" were constructed from PBFI fluorescence recorded for each sample in the absence of GDP and in the presence of 0.5 mM GDP. The differential K-traces are shown for active FA, lauric (*trace a*), 3-hydroxymyristic (*b*) and 12-hydroxystearic (*c*) acids, and for the inactive FA, 12-hydroxylauric (*d*), dodecanedioic (*e*) and phenylvaleric (*f*) acids.

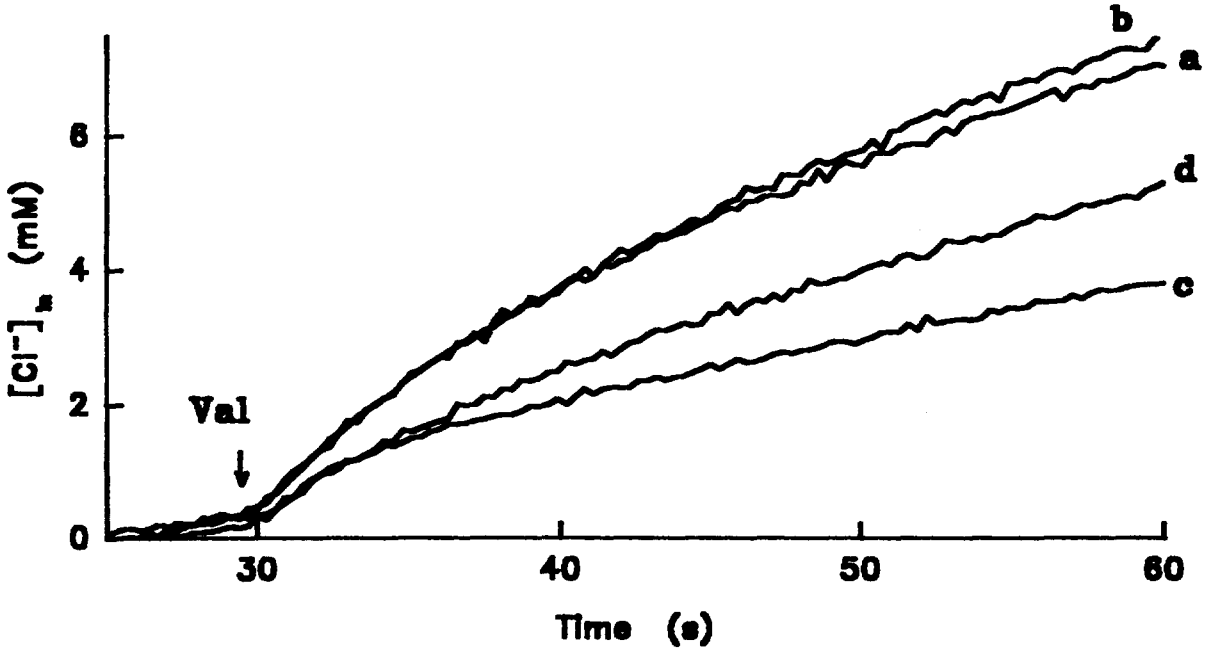

Figure 5.4 Effect of FAs on the inhibition of Cl^- uptake into proteoliposomes containing UCP. Cl^- transport was detected as quenching of SPQ fluorescence by Cl^- in TES-free media containing phosphate buffer as described in Section 5.1.3. Traces show Cl^- transport in the absence of added FAs (*trace a*, control) and in the presence of 200 μM 12-hydroxylauric (*b*), lauric (*c*), and heptylbenzoic (*d*) acids. % Inhibition of the initial rate was estimated as 0% (*b*), 65% (*c*), and 57% (*d*). When GDP-sensitive parts were compared (traces with GDP are not shown), the resulted inhibition reached 0%, 88% and 97%, respectively.

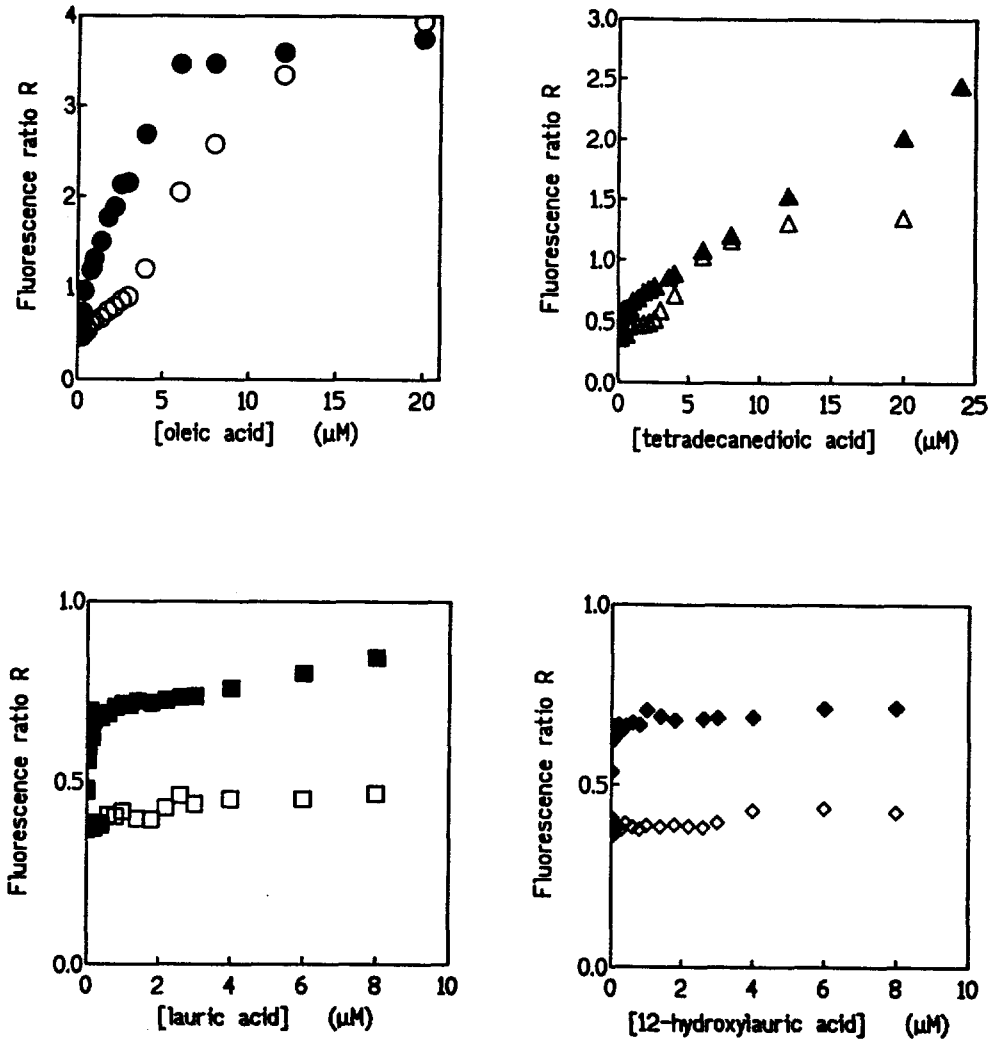

Figure 5.5 Fatty acid binding to ADIFAB in the presence and absence of liposomes. Binding of FAs to ADIFAB was measured in the absence (filled symbols) and presence (open symbols) of liposomes (20 μM lipid) for oleic acid (*circles*), tetradecanedioic acid (*triangles*), lauric acid (*squares*), and 12-hydroxylauric acid (*diamonds*). The fluorescence ratio R (432 nm/505 nm) is plotted versus the total FA concentration (for details see Section 5.1.5.). Measurements were done with Na-salts of FAs in a medium containing 150 mM NaCl, 1 mM TEA-EGTA, 10 mM Tris-Cl, pH 8, with 0.2 mM ADIFAB. The derived K_d values are listed in Table 5.3, as well as the calculated partition coefficients K_p.

Table 5.3

Partitioning of the Selected Fatty Acids into the Lipid Bilayer as Evaluated using ADIFAB

Binding of FA to ADIFAB was measured in the absence or presence of liposomes (18 μM) formed from L-α-phosphatidylcholine, cardiolipin and 1% L-α-phosphatidic acid. The corresponding K_d values and partition coefficients were calculated as described in Section 5.1.5.

Fatty acid	Binding to ADIFAB K_d (μM)	Partition coefficient K_d
oleic acid	0.39 0.22	51,000
myristic acid	1.44	81,000
lauric acid	1.2 4.5	220,000
tetradecanedioic acid	2.33	66,000
12-hydroxylauric acid	9	50,000
3-hydroxymyristic acid	20	11,000
2-hydroxylauric acid	infinite*	—

* 2-hydroxy-lauric acid did not bind to ADIFAB, and addition of liposomes did not change the ADIFAB fluorescence at any 2-hydroxy-lauric acid concentration. This provides evidence that liposomes *per se* are not affecting ADIFAB.

shown), these FAs manifested significant flip-flop, as inferred from their ability to acidify liposomes (Table 5.1).

5.3 Discussion

The coherence of structural patterns of FAs required for *trans*-membrane flip-flop and interaction with the UCP (Table 5.2) is consistent with the model of the FA cycling mechanism (33, 44). Cycling of the active FAs is given by the ability of UCP to translocate the FA's anionic form (Fig. 5.3) and by the ability of active FAs to flip-flop in a protonated form (Figs. 5.1, 5.2) which leads to H^+ translocation. This FA protonophore model for the mechanism of UCP-mediated H^+ transport (33) requires that UCP translocate the anionic FA carboxylate headgroup from one side of the membrane to the other. FA anion transport is driven by H^+ ejection via the redox chain and may be facilitated by an internal energy well in the transport pathway of UCP located near the center of the membrane (33, 53). Protons are then delivered by nonionic flip-flop of the neutral FA back to the other side. Thus, the role of UCP is to enable FAs to act as cycling protonophores in BAT mitochondria (33, 115). This mechanism has certain advantages, not the least of which is providing an explanation for the long-standing observation that UCP transports a variety of monovalent anions in addition to mediating H^+ transport (33, 115).

The existence of inactive FAs that are unable to flip-flop and unable to activate UCP-mediated H^+ transport supports the existence of a FA cycling mechanism. Lack of flip-flop of the inactive FAs would clearly prevent the whole FA cycling process. Moreover, we have shown that the pathway of FA uniport and the pathway of protonated FAs must both be present. The uniport pathway is not used by the inactive FAs (they are not transported by UCP in a uniport mode; Fig. 5.3) since they do not show a charge compensation by K^+ in UCP proteoliposomes. Also, no UCP-related H^+ efflux was induced with the inactive FAs. We must then exclude the possibility that such an H^+ efflux can be allosterically activated either from a *docking site* (35, 53) or by a local buffering mechanism as suggested by Klingenberg (34, 40).

If such a mechanism existed, the inactive FAs should provide local buffering of the same strength as the active FAs.

Inactive FAs are incapable of flip-flop and of reaching the internal anion binding site of UCP (energy well), even though they do partition into the bilayer (Fig. 5.5, Table 5.3). Their inability to reach the internal anion binding site can be deduced from the lack of their uniport via UCP. More directly it is reflected by their lack of inhibition of UCP transport of Cl^- and other anions. In contrast, the active FAs competitively inhibit uniport of Cl^- (33, 115) and alkylsulfonates (33) via UCP. To achieve this inhibition, the active FAs have to interact with the internal binding site (33). We also imply they are translocated as demonstrated by the GDP sensitivity. This is valid also in the case of noncarboxylic transport substrates of UCP (53).

Noting that most of the inactive FAs have a bipolar character or have a terminal phenyl, we hypothesize that their inability to flip-flop may be due to an unusual conformation when present in a lipid bilayer. The assay using the fluorescent probe ADIFAB indicates that these FAs do partition into the bilayer, but they do not interact with UCP. A possible explanation is that its conformation or location within the bilayer prevents the FA from reaching the internal translocation binding site of UCP, which might be formed by a cluster of positively charged or polar amino acid residues. Alternatively, the inactive FA can reach the internal site, but could not be translocated for structural reasons, such as a highly polar or bulky tail. The second explanation appears unlikely as it would constitute a case of a nontransportable substrate analog which would inhibit transport of other substrates. As yet, we have not found such a case.

Physiologically, the negatively charged carboxyls (33) of the active, naturally abundant, FAs (100) which possess a unipolar character are attracted to UCP's energy well. By this interaction, UCP discharges all polarities, and the nonpolar hydrophobic tail may emerge into the hydrophobic bilayer core as does the neutral active FA during flip-flop in the lipid bilayer. The structural requirements for FAs to be UCP substrates (Table 5.2) are similar to those found for the noncarboxylic substrates of UCP (53): (i) monovalent charge is strictly required; (ii) unipolarity is

required—an additional polar group might be present only if it is in close proximity to the charge or carboxyl, or is shielded by an additional hydrophobic chain or a nonpolar group; and (iii) so-called bulky groups are allowed along the aliphatic chain or at its end, provided they do not bear polar groups or charges. Thus, "Good" buffer-type anions are not UCP substrates (53), while groups like nitroxy of DOXYL (36), nitro, and bromo are tolerated, as is the secondary amino group (-NH-) (35). A benzene ring is tolerated, either when positioned close to the carboxyl or when it is shielded by a nitro group (TNP-lauric, or compounds described in refs. 35 and 135). Contrary to the findings of Winkler and Klingenberg (34), we found that both phenylvaleric and phenylhexanoic acids were inactive (Figs. 5.2, 5.3, and 5.4; Table 5.2), while a *mirror* derivative, heptylbenzoic acid, was one of the most active.

The previous evidence for the FA cycling mechanism includes the comparison of behavior of laurate and its close analogue undecanesulfonate (33, 115). The single factor that may explain the failure of undecanesulfonate to deliver H^+ electroneutrally by flip-flop is that it is a very strong acid. If so, the inactive FAs may be similarly regarded as amphiphiles which lack the flip-flop ability, as does undecanesulfonate. The important difference is that the latter is transported by UCP while the inactive FAs are not.

The evidence for the FA cycling mechanism reported here, while indirect, is currently the best available. It was not possible to measure FA anion transport directly because the rapid flip-flop of the acid precludes internal accumulation of FA anions. It is, however, possible to test and refute the model, which was a motivating factor for the presented series of experiments. The FA protonophore model would become invalid if a FA analogue was found that catalyzed UCP-mediated H^+ transport without acidification of the liposome interior by flip-flop (case 4 in Table 5.2). The important outcome of this study is that no such violation was found. A second motivation for this study was to develop an understanding of the structure–activity relationships that exist among the vast family of FAs and their derivatives and analogues. This has led to some interesting results. The crucial indicator of an active FA, i.e., those able to induce UCP-mediated H^+ flux, is the ability to deliver protons by flip-flop to the intraliposomal medium. Of all the FAs

surveyed in our experiments, flip-flop was invariably associated with the ability to induce UCP-mediated H^+ flux. And while it would not violate the model to have found FAs capable of flip-flop but unable to induce UCP-mediated H^+ transport, we found no such example among the FAs tested.

---

[3] This material has been published in this or similar form in *FEBS Letters* and is used here by permission of Elsevier Science - NL:

Jezek, P., Modriansky, M., and Garlid, K. D. (1997) Inactive fatty acids are unable to flip-flop across the lipid bilayer. *FEBS Lett.* **408,** 161–165.

Jezek, P., Modriansky, M., and Garlid, K. D. (1997) A structure-activity study of fatty acid interaction with mitochondrial uncoupling protein. *FEBS Lett.* **408,** 166–170.

Chapter 6

SINGLE CYSTEINE RESIDUES ARE NOT ESSENTIAL FOR UCP FUNCTIONING

Non-shivering thermogenesis is the result of the activity of uncoupling protein (UCP) which increases proton conductance of the inner mitochondrial membrane. UCP does so by transporting free fatty acid (FA) anions, which then act as protonophores (33, 44). While the FA cycling hypothesis continues to gain supporting evidence (35, 135, Chapter 5), little is known of the nature of a FA binding site that would make this mechanism possible. UCP activity is regulated by purine nucleotides (8, 34, 50), which bind to a distinct binding site (31) and inhibit the transport allosterically (34, Chapter 3). Site-directed mutagenesis experiments identified the Arg276 residue as essential for GDP inhibition of UCP-mediated transport (79). These experiments were designed based on a previously published chemical modification study of UCP (31) and a site-directed mutagenesis study of the AAC (78). Adopting a similar approach, the aim of these experiments was to identify the residues essential for FA anion transport in UCP.

Cysteine, a residue with a highly reactive hydrophobic side chain (141), seemed a good candidate as a potential key residue in FA anion transport. Peptide sequencing revealed seven cysteine residues present in UCP (84), each of which is conserved in the UCP of all species (8), as confirmed by UCP cDNA sequences (83, 85–87).

Chemical modification studies using various sulfhydryl reagents provided evidence that supports the importance of cysteines in UCP (64–67). A single water-accessible cysteine on the cytosolic side, Cys304 at the C-terminus, was suggested as essential for proton transport (64, 65). Klingenberg and Appel (73) showed otherwise by cross-linking the C-termini of a UCP dimer and demonstrating the cross-link had

no effect on either nucleotide binding or UCP-mediated H^+ transport. Though not essential for UCP-mediated transport, Cys304 may modulate the K_m for FA as suggested by Gonzalez-Barroso et al. (74). The differential effects of various reagents on both proton and chloride transports, and on GDP inhibition, lead Jezek to propose two distinct pathways for each of the transports (65). In a later publication, Jezek and Drahota distinguished three groups of cysteine residues that are essential for UCP activity (67).

Mayinger and Klingenberg (70) explored amino acid residues essential for UCP-nucleotide interactions by experimenting with the covalent binding of azido-labeled ATP derivatives to UCP. Partial peptide sequencing of the azido-labeled polypeptide identified the stretch of residues 238–283 as a *nucleotide binding site*. Two amino acids within that stretch, Thr263 and Cys253, were proposed as essential for nucleotide binding (70).

In the studies presented here, yeast expression system and site-directed mutagenesis were employed to create and express seven UCP mutants, each of which had a single cysteine residue replaced by serine. Since Cys253 is present within the predicted nucleotide binding site, we designed two additional mutants, Cys253Ala and Cys253Phe, to further examine the role of this particular residue. Finally, we prepared three random multiple Cys → Ser mutants which were tested for FA-induced H^+ transport and for GDP sensitivity of UCP-mediated transport. All single cysteine mutants except Cys253Phe showed negligible differences from wild-type UCP with respect to proton transport and GDP inhibition thereof. In contrast, all multiple mutants showed a decrease in proton transport activity and in GDP inhibition, the observed decrease being proportional to the number of cysteine residues mutated.

6.1 Materials and Methods

6.1.1 Materials

The fluorescent probes SPQ and PBFI were purchased from Molecular Probes (Eugene, OR). Fatty acid-free bovine serum albumin (BSA), ionophores, and GDP (Tris-salt) were from Sigma Chemical (St. Louis, MO). Zymolyase 100T was

purchased from Seikagaku America (Ijamsville, MD). All other materials, including those used for molecular cloning, yeast cell growth, yeast mitochondria isolation, and UCP purification and reconstitution were the same as described previously (32, 33, 79, 95).

6.1.2 Site-directed mutagenesis

Mutants were prepared using the method developed by Kunkel et al. (142). Briefly, a phosphorylated mutagenic oligonucleotide was annealed to single-stranded template DNA containing uracil instead of thymine. Following primer extension and ligation, the now double-stranded DNA was introduced into *ung*$^+$ *E. coli* cells, where the DNA strand containing uracil was degraded. Library efficient cells were then transformed with the full-thymine double-stranded DNA and plated onto a cell lawn. Randomly selected plaques were used for the preparation of single-stranded DNA, which was sequenced to confirm the introduced mutation. Positive clones were released by *Sac*I/*Sph*I digestion and subsequently re-inserted into a *Sac*I/*Sph*I pre-cut pCGS110 shuttle vector, as described previously (79). Multiple mutants were obtained by introducing all seven mutagenic oligonucleotides at once. Three clones containing three (C188S, C287S, and C304S), four (C24S, C188S, C253S, and C287S), and six (C188S, C213S, C224S, C253S, C287S, and C304S) changes were selected for H^+ flux assays.

6.1.3 Isolation, purification, and reconstitution of UCP

Yeast mitochondria from cells grown for 10 h in a medium containing 0.2% galactose were isolated according to Gasser (143). The final mitochondrial pellet was resuspended in a medium originally used for BAT mitochondria isolations (32, 53) and contained 250 mM sucrose, 5 mM TES, pH 6.7, 1 mM EGTA (K^+ salts), and 2 mg BSA/ml. UCP was purified from yeast mitochondria on an HTP column in the presence of detergent and lipids, as described previously (32). The flow-through fraction was collected, adjusted to internal medium composition, and applied to a Bio-Beads SM-2 (Bio-Rad) column to form proteoliposomes by slow detergent removal. The formed liposomes were passed once through a Sephadex G25-300 column to

remove external SPQ, which had been added to the lipid/detergent/protein mixture prior to the liposome formation step. The internal medium contained 84.4 mM SO_4, 29 mM TES, pH 7.2, 0.6 mM EGTA (all TEA salts), and 2 mM SPQ.

6.1.4 Measurements of H^+ flux

The method developed by Orosz and Garlid (104) was used to measure H^+ flux in UCP proteoliposomes. This ingenious method takes advantage of the fluorescence probe SPQ interaction with many of the "Good" buffers. SPQ is quenched by TES anion, but not by TES zwitterion, which allows the monitoring of H^+ fluxes after rigorous calibration by the addition of μl aliquots of KOH in the presence of nigericin. The system is well buffered while maintaining high sensitivity to changes in $[H^+]$ with a high signal/noise ratio. Laurate was added to the UCP proteoliposomes as μl aliquots of a stock solution in ethanol. Internal medium composition is described above. External medium contained 84.4 mM K_2SO_4, 29 mM TEA-TES, pH 7.2, and 1.5 mM TEA-EGTA. The resulting potassium gradient is used for driving the UCP-mediated transport after it is clamped by addition of 0.1 μM valinomycin. When used, GDP was added to the assay medium prior to the addition of liposomes.

6.1.5 Measurements of UCP-mediated hexanesulfonate transport

The potassium flux, which is necessary to drive the electrophoretic UCP-mediated transport, can be used for indirect measurement of anion transport through UCP (33, 53). Potassium-sensitive fluorescent probe PBFI (300 μM) is trapped in the liposome interior much like the above described SPQ, but unlike SPQ, PBFI fluorescence increases in direct proportion to internal $[K^+]$. In case of electroneutral transport, the K^+ influx is accompanied by anion, in this case hexanesulfonate, entering through UCP. The UCP-mediated hexanesulfonate influx is then estimated assuming it is the rate limiting step. All other conditions and media compositions were exactly the same as described above in Section 6.1.4.

6.2 Results

6.2.1 Effect of single Cys → Ser mutations

All seven single-Cys UCP mutants were tested for their ability to mediate fatty acid-induced H^+ transport and GDP inhibition of this transport. The results are summarized in Table 6.1. The kinetic parameters of all single-Cys mutants showed negligible differences from the wild type. Mutants Cys212Ser and Cys304Ser were also tested for their ability to mediate the transport of hexanesulfonate, a well-known monovalent anion substrate of UCP (53). The dose-response curves in Fig. 6.1 demonstrate that both of these mutants retained GDP-sensitive hexanesulfonate transport. The non-linear curve fits (*solid lines*) yielded K_i values of 23 μM and 14 μM for the Cys213Ser and Cys304Ser mutants, respectively. The K_i for wild type was 16 μM (not shown). That all the K_i values are slightly higher than those observed for GDP inhibition of proton transport is due to weak interference of hexanesulfonate with GDP binding (54).

6.2.2 Effect of mutations of Cys253 → Ala and Phe

The Cys253 residue, located within the postulated nucleotide binding site, was suggested to be responsible for nucleotide regulation of UCP activity (70). Because our experiments with the Cys253Ser mutant showed negligible difference from the wild type, we designed two additional mutations, to alanine and to phenylalanine, to test how much steric interference could be introduced without affecting UCP activity and GDP inhibition of UCP-mediated transport. Fig. 6.2 is a representation of proton fluxes obtained with the wild-type, Cys253Ala, and Cys253Phe mutants in the presence of 30 μM laurate and in the presence or absence of 1 mM GDP. The Cys253Ala maintained wild-type activity and was fully GDP-sensitive. On the other hand, activity of the Cys253Phe mutant was the same as the proton flux obtained in protein-lacking liposomes upon addition of 30 μM laurate (not shown). This comparison to a protein-independent proton leak emphasizes the apparent inactivity of the mutant. Experiments on intact yeast mitochondria containing the Cys253Phe mutant UCP showed an oleate-induced uncoupling of respiration that was reversed by the addition of GDP (144).

Table 6.1

Phenotypes of Single Cys → Ser Mutants

Table lists K_m, V_{max}, and K_i values measured for laurate-induced H^+ transport mediated by wild type and seven single-cysteine mutants.

Uncoupling protein	K_m (μM)	V_{max} ($nmol\ min^{-1}\ mg^{-1}$)	K_i (μM)
wild-type	19	7500	11
Cys24Ser	22	7500	14
Cys188Ser	21	7200	11
Cys213Ser	20	7250	10
Cys224Ser	19	7100	14
Cys253Ser	22	7300	10
Cys287Ser	20	7200	12
Cys304Ser			16

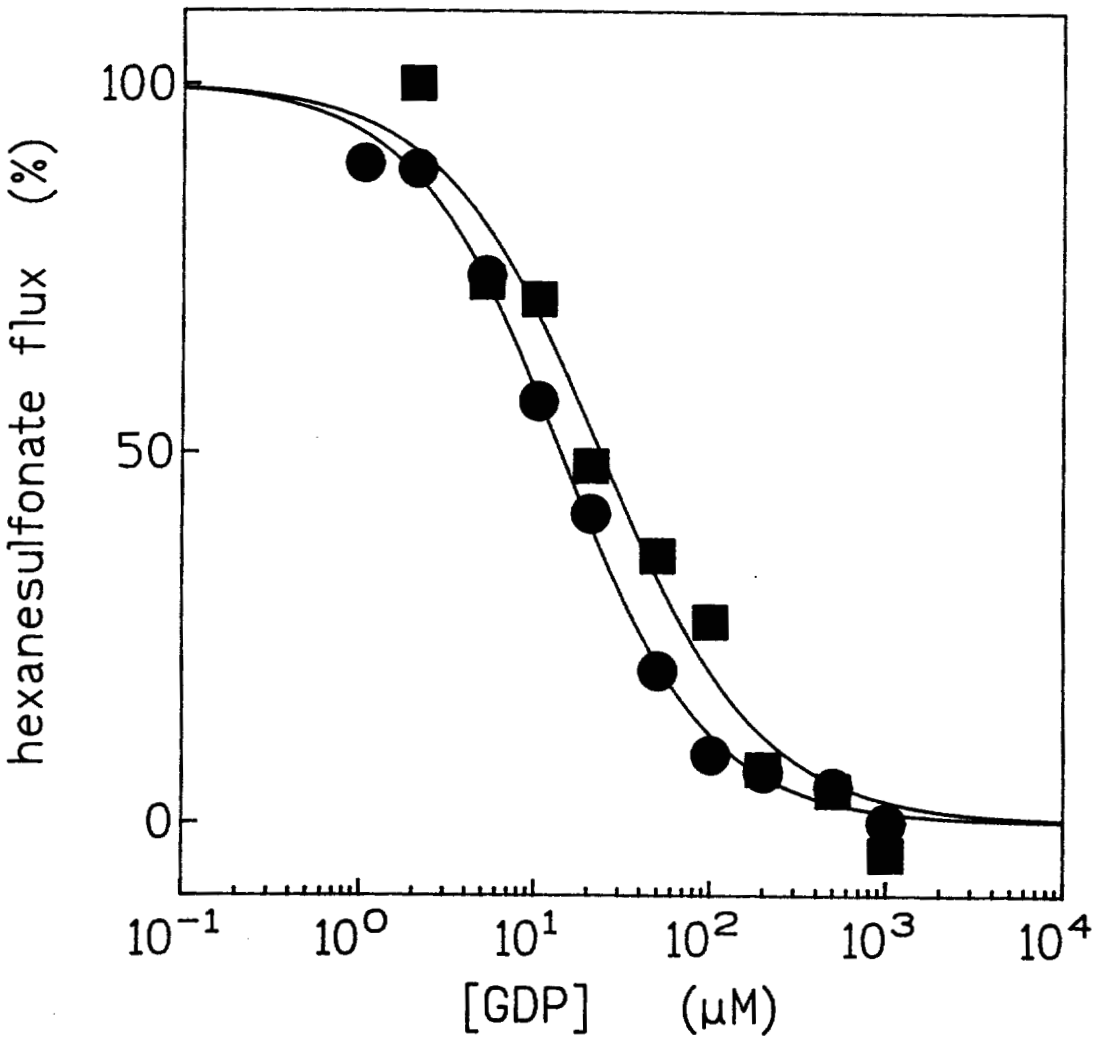

Figure 6.1 Cys213Ser and Cys304Ser mutant UCPs mediate GDP-sensitive hexanesulfonate transport. GDP dose–response curves were obtained in the presence of 20 mM hexanesulfonate for Cys213Ser (■) and Cys304Ser (●) mutants. The curve fits (*solid lines*) were drawn with Hill coefficient = –0.9. The derived K_is for both mutants are noted in Section 6.2.1.

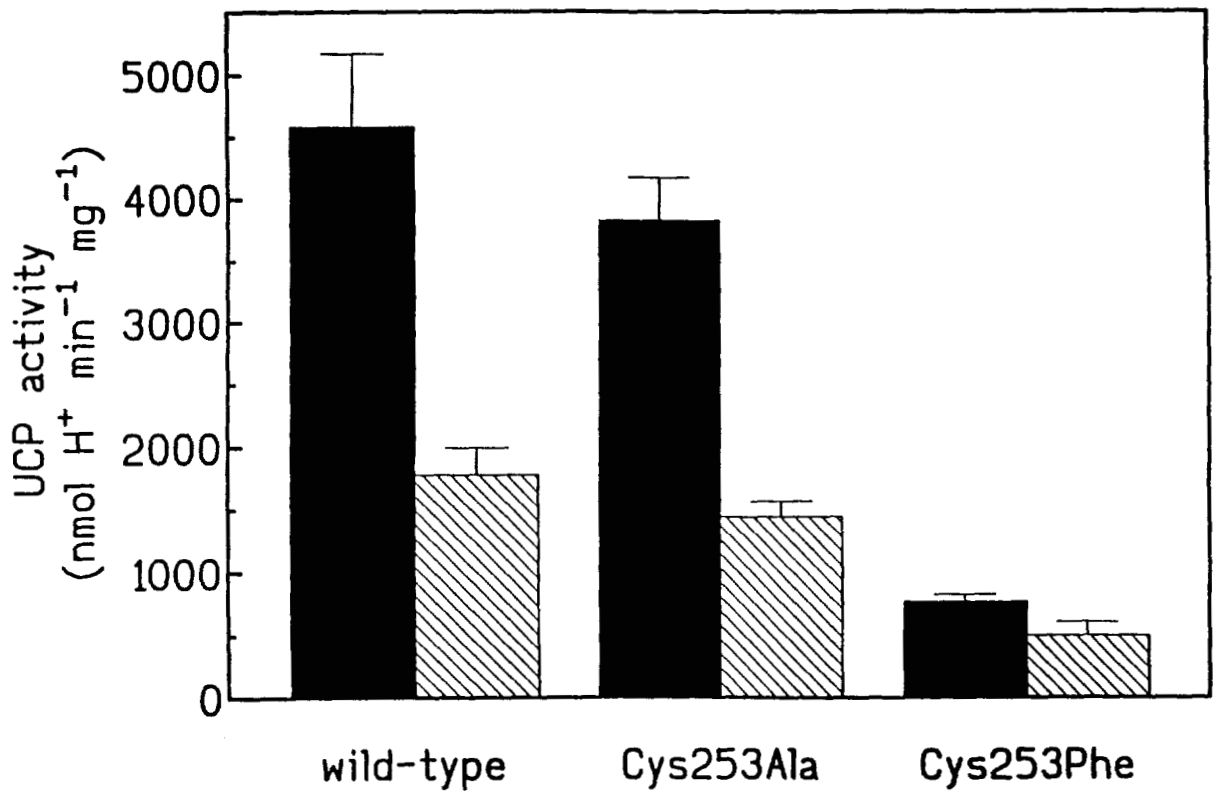

Figure 6.2 The isolated Cys253Phe mutant UCP lacks activity. Figure compares the activity of wild-type, Cys253Ala, and Cys253Phe mutant UCPs in the presence of 30 μM laurate. Bars represent normalized activity (nmol H^+ min^{-1} mg^{-1}) obtained for each UCP in the absence (*solid* bar) and in the presence of 1 mM GDP (*diagonal fill-in* bar). Values are means $\pm$ SE from five independent measurements.

6.2.3 Effect of multiple Cys → Ser mutants

We prepared three multiple Cys → Ser mutants, each containing a random combination of mutated residues. Each of these three mutants showed diminished transport activity, characterized by an increase of K_m for laurate when compared with the wild type. These effects became more pronounced as the number of mutations increased (Fig. 6.3). The GDP-sensitivity of enzymes containing multiple mutations was also diminished; the K_i for GDP increased as the number of mutations increased (Fig. 6.4). The mutant Cys253Ser represents the single mutants in both Figs. 6.3 and 6.4. The remaining single Cys → Ser mutants show the same characteristics (Table 6.1).

Table 6.2 compares kinetic parameters of the single and multiple Cys → Ser mutants to the wild type. The V_{max} values for mutants containing four and six changes are estimates due to diminishing GDP sensitivity of the transport. The mutant lacking four cysteines showed about 80% inhibition by 2 mM GDP (Fig. 6.4). The V_{max}, estimated from a baseline GDP-sensitive rate measured in the presence of 2 mM GDP, is 5400 nmol/min/mg protein. The mutant lacking six cysteines shows no sensitivity to GDP. Undecanesulfonate, a substrate of UCP (53) and a competitive inhibitor of laurate-induced H^+ flux (33, 79), could not be used for establishing a UCP-specific rate because its K_m was also increased. Therefore, the V_{max} estimate is based on uncorrected data which is not UCP-specific.

6.3 Discussion

The aim of these experiments was to test the role of the cysteine residues of UCP. Serine, an amino acid with a hydrophilic side chain containing a terminal -OH group, can substitute for cysteine without disrupting the hydrogen bonds with neighboring residues while barring any -SH specific reactions. In the case of UCP, serine is fully capable of replacing any single cysteine without affecting UCP-mediated transport or the GDP sensitivity thereof. Thus, -SH chemistry is not essential for UCP-mediated transport or GDP inhibition of the transport, as anticipated from published chemical modification experiments (64–67). While our

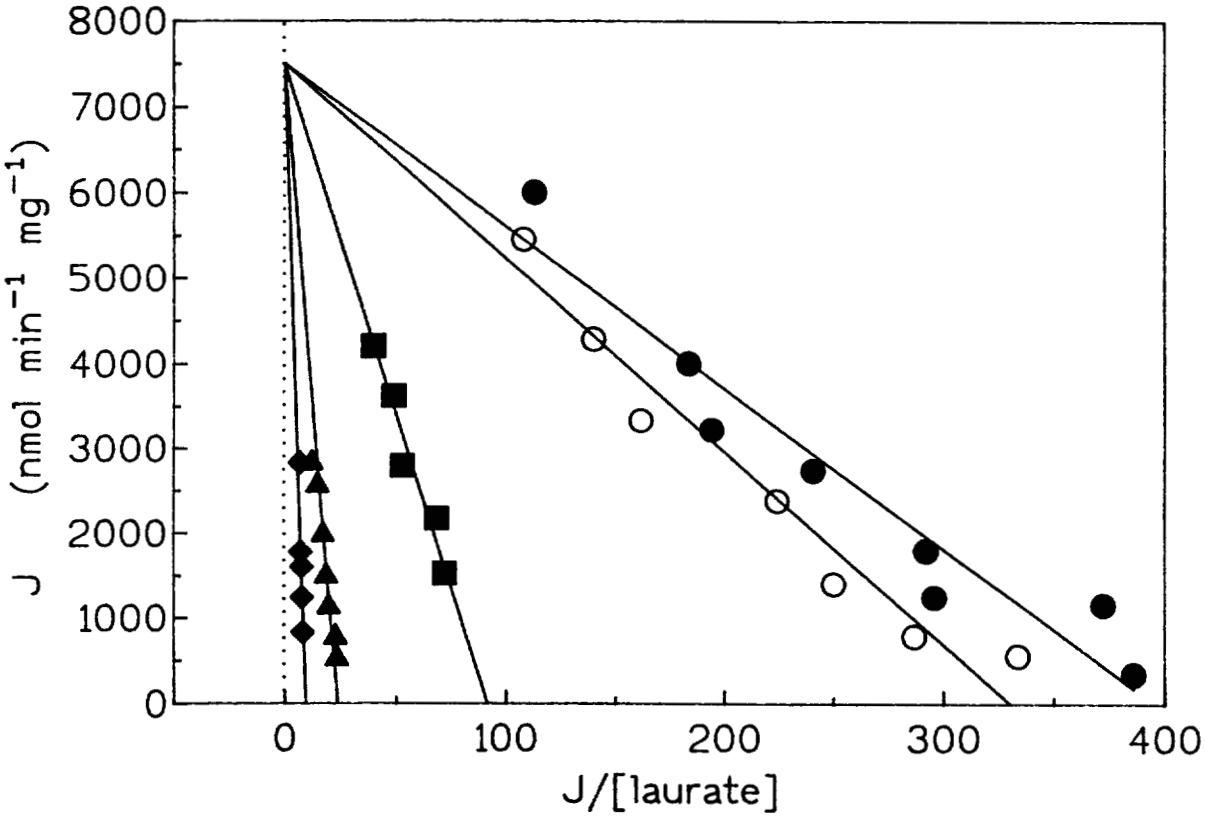

Figure 6.3 Laurate-induced H^+ transport mediated by multiple Cys → Ser mutant UCPs. Eadie–Hofstee plots were constructed from values of H^+ flux measured at different [laurate] for wild-type (●), 1Cys (○), 3Cys (■), 4Cys (▲), and 6Cys (◆) mutants. Regressions of the data (*solid lines*) yielded K_m and V_{max} parameters that are summarized in Table 6.2.

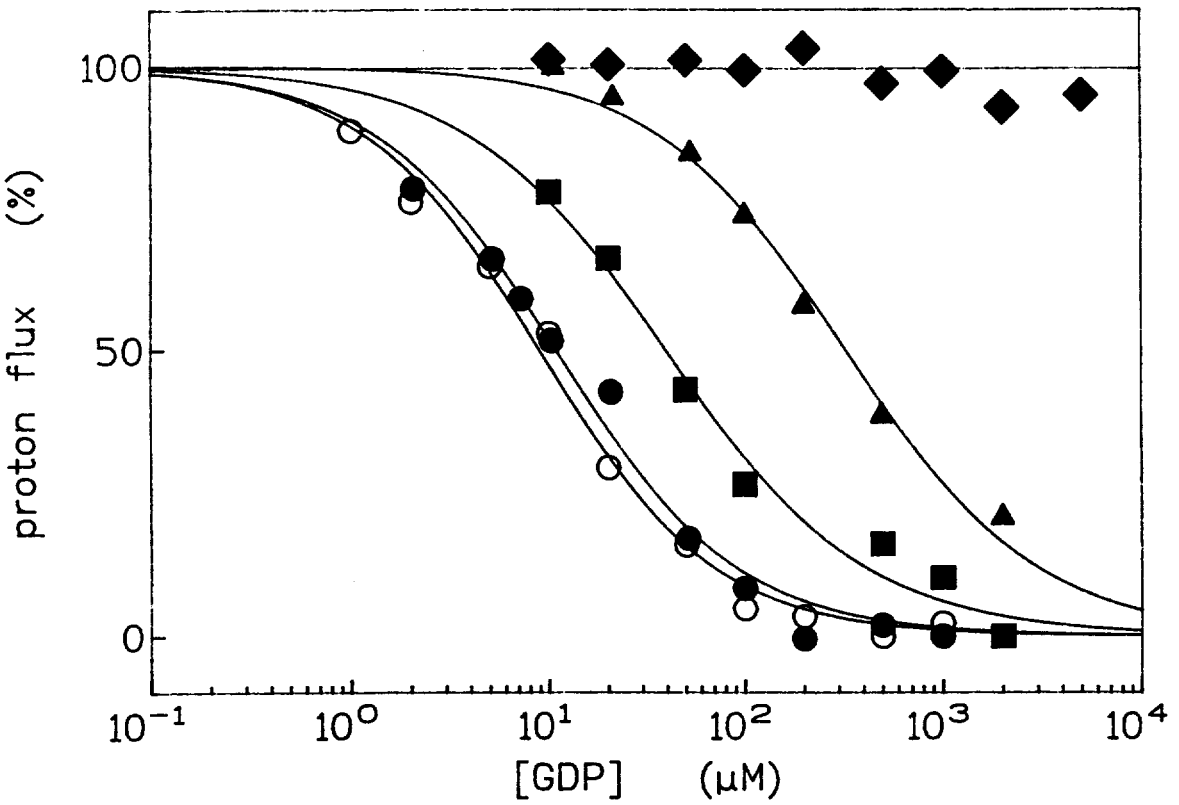

Figure 6.4 GDP inhibition of laurate-induced H^+ transport mediated by multiple Cys → Ser mutants. GDP dose-response curves were obtained in the presence of 30 μM laurate for wild-type (●), 1Cys (○), 3Cys (■), 4Cys (▲), and 6Cys (◆) mutants. The curve fits (*solid lines*) were drawn with Hill coefficient = -0.9 , except for the 6Cys mutant (straight line). The derived K_is are summarized in Table 6.2.

Table 6.2

Kinetic Parameters for Yeast-Expressed UCPs

Table summarizes parameters derived from the kinetic plot and dose-response curves obtained for respective UCPs. The three-letter abbreviation for cysteine preceded by a number indicates the number of cysteine residues mutated in a particular UCP. For exact positions of introduced mutations, see Section 6.1.2.

Uncoupling protein	K_m *(μM)*	V_{max} *(nmol min^{-1} mg^{-1})*	V_{max}/K_m *(ml min^{-1} mg^{-1})*	K_i *(μM)*
Wild-type	19	7500	395	11
1 Cys	22	7320	333	10
3 Cys	77	7200	94	39
4 Cys	312*	7500*	24	326
6 Cys	780*	7500*	10	n.a.

* Estimated values, for details see Section 6.2.3.
n.a. = not available

observations have been confirmed by an independent research group (97), a more recent publication contains data indicating that Cys304 is involved in modulation of FA interactions with UCP (74). No pattern is obvious regarding hydrophobicity, polarity, or charge of the substituting residue; for example Cys304Gly shows the highest affinity for FA and Cys304Ala the lowest affinity for FA.

To investigate the influence of the spatial arrangement of the residues surrounding the Cys253 on UCP activity or regulation, this residue was replaced with either alanine or phenylalanine.

Alanine, an amino acid with a non-reactive single-carbon side chain, should not introduce any steric interference. While the side chain of alanine is spatially much smaller than that of cysteine, the number of available hydrogen bonds is roughly equal in both. There should be no effect when alanine is substituted for a cysteine that resides in a conformationally non-specific connecting loop. Cys253 is located within such a loop that connects the fifth and sixth α-helices of UCP and can be replaced by alanine without any effects on UCP activity or nucleotide regulation. Besides rendering Cys253 as a non-essential residue, alanine demonstrates that strict maintenance of spatial arrangement is not necessary. Indeed, alanine was found a better substitute than serine in cysteine-less mutant variants of the citrate carrier (81). Activity of a citrate carrier construct containing all Cys → Ser mutations maintained only about 5% of wild-type activity. This low-activity construct was rescued by introducing two Cys → Ala mutations, out of a total of four original cysteines, to about 40% of wild-type activity. Another single change into valine improved the activity to 60% of wild-type (81). As a result, the reactive, hydrophilic serine substitution appears to be more of an impediment rather than an advantage if more than one residue is mutated.

In contrast to alanine, phenylalanine contains a bulky benzene ring side chain, that would be expected to disrupt local conformation around Cys253, even though the loop containing it is predicted to protrude into the transmembrane region of UCP and thus to be quite mobile (70). Experiments with isolated yeast mitochondria containing the over-expressed Cys253Phe mutant UCP showed oleate-stimulated uncoupling of respiration that was reversed by GDP (144). The mutant UCP is either capable of

accommodating the bulky phenylalanine, or the side chain of residue 253 plays no role whatsoever. Surprisingly, this same mutant UCP lost activity after its isolation and reconstitution into liposomes, so that no conclusions can be drawn on GDP sensitivity. Our current explanation of the loss of activity is that the isolated UCP folds incorrectly into the artificial bilayer during the reconstitution, perhaps due to an interaction with the detergent or the particular lipid composition. However, we are unaware of any circumstance that would prevent such a misfolding in yeast mitochondria.

Protein misfolding is a possible explanation for the low activity and lack of GDP inhibition in the mutant UCP with six Cys → Ser changes. This is because the degree of misfolding would seem likely to depend on the number of introduced mutations. Data presented here support this explanation. As seen in Table 6.2, UCP activity decreased as the number of cysteines mutated increased; GDP sensitivity followed the same pattern. Because GDP acts at a different binding site than FA (31), the multiple Cys → Ser mutations must introduce a global misconformation of UCP. A similar pattern of behavior was observed in the citrate carrier (81).

In summary, the -SH chemistry *per se* is not essential for UCP activity or nucleotide regulation of UCP. Even though no disulfide bonds are found in the UCP dimeric structure (40), the cysteine residues appear crucial for overall conformational integrity of the protein.

Chapter 7

A SINGLE MUTATION IN UNCOUPLING PROTEIN OF RAT BROWN ADIPOSE TISSUE MITOCHONDRIA ABOLISHES GDP SENSITIVITY OF H^+ TRANSPORT[4]

Uncoupling protein (UCP) belongs to a family of mitochondrial anion porters involved in energy metabolism, including the ADP/ATP translocator, the phosphate-H^+ symporter, and the oxoglutarate carrier. These porters do not exhibit prominent homologies at the level of amino acid sequence; however, they have similar molecular masses, and all contain three homologous domains of about 100 amino acid residues, each of which contains two transmembrane helical sequences (40, 84, 86, 145). UCP has the specific role of generating heat in mammalian brown adipose tissue, either by permitting proton flux directly or by catalyzing fatty acid anion transport across the mitochondrial inner membrane, thus enabling the fatty acids to act as protonophores (40, 44).

Chemical modification studies on UCP using sulfhydryl reagents or arginine-modifying reagents have suggested that these residues might have functional significance, but in this approach the specific residues could not be identified (31, 65). Moreover, these effects could be due to introduction of bulky side groups resulting in steric interference with function. In a different approach, photoaffinity labeling with purine nucleotide analogs shows that the third domain of UCP is involved in nucleotide binding but does not identify functionally important residues (69, 70).

We have approached the question of locating such residues in UCP by developing a system of high-level expression of functional rat UCP in yeast (95) and sensitive fluorescent assays of proton (104) and anion (32) transport in proteoliposomes reconstituted with expressed UCP purified from yeast. These

protocols were used to evaluate the effects of changing the individual cysteine residues to serine and Arg276 to glutamine or leucine on GDP-sensitive proton transport. Mutation of Arg276 resulted in complete loss of GDP inhibition of proton transport mediated by reconstituted UCP.

7.1 Materials and Methods

7.1.1 Materials

The *Escherichia coli/Saccharomyces cerevisiae* shuttle vector pCGS110 was the kind gift of Dr. D. T. Moir, Collaborative Research Inc. M13mp19 was from Life Technologies, Inc. Zymolyase 100T was obtained from ICN Biochemicals. D-(+)-galactose (catalog #G 0750) and fatty acid-free bovine serum albumin (catalog #A 6003) were obtained from Sigma. Oligonucleotides were purchased from the Central Facility of the Institute for Molecular Biology and Biotechnology at McMaster University. SPQ was purchased from Calbiochem. Bovine serum albumin (Factor IV), fatty acids, and ionophores were purchased from Sigma. Alkylsulfonates were purchased from Research Plus, Inc. Materials for protein purification and liposome formation were obtained from sources described in Jezek et al. (32).

7.1.2 Mutagenesis

Rat UCP cDNA altered around the 5′-translation start site for efficient translation in yeast was originally constructed in pGEM5Zf (95). The *Sal*I–*Sph*I fragment containing the altered rat UCP cDNA from this construct was cloned into *Sal*I–*Sph*I-cut M13mp19 for site-directed mutagenesis. Oligonucleotides were designed to alter UCP codons for Arg276 (CGA) to Gln (CAA) and Leu (CTA) and Cys253 (TGT) to Ala (GCT). Site-directed mutagenesis was carried out using the method of Kunkel (146). A unique *Sac*I site was engineered into the *E. coli/S. cerevisiae* shuttle vector pCGS110 between the *Bam*HI and *Sph*I sites of the vector. This permitted subcloning of *Sac*I–*Sph*I fragments from M13mp19 containing wild-type or mutated forms of UCP cDNA into *Sac*I–*Sph*I-cut pCGS110 such that the cDNAs were under transcriptional control of the inducible *Gal*I promoter. The *S.*

cerevisiae strain JB516 (*MATa*, *ura*3, *ade*1, *leu*2, *his*4, *gal*$^+$) was transformed by electroporation with the shuttle vector constructs at 1.5 kV, 25 μF, 200 Ω. The yeast transformants were grown at 30°C in selective medium as previously described (95).

7.1.3 Mitochondrial isolation

Expression of UCP was induced in yeast transformants with 0.2% galactose for 12 h, after which mitochondria were isolated and resuspended in a solution containing 0.6 M sucrose, 20 mM HEPES–KOH (pH 6.5), and 0.1% fatty acid-free bovine serum albumin as previously described (95).

7.1.4 Preparation of proteoliposomes containing the expressed, purified mutant and wild-type UCPs

Purification and reconstitution followed protocols previously described (32). Briefly, yeast mitochondria were solubilized in 13% octylpentaoxyethylene in the presence of L-α-phosphatidylcholine, cardiolipin, and L-α-phosphatidic acid; this mixture was applied to a hydroxyapatite column. The internal medium was adjusted to the desired concentrations, and the fluorescent probe SPQ was added. Vesicle formation and external probe removal were accomplished by treatment with Bio-Beads SM-2 and Sephadex G-25, respectively. Final lipid concentration was approximately 40 mg/ml.

7.1.5 Proton flux measurements using SPQ

Proteoliposomes were added to 2 ml of assay medium to a final concentration of 0.5 mg of lipid/ml. The intravesicular medium contained 1 mM GDP and tetraethylammonium salts of TES (28.8 mM), EGTA (0.6 mM), and SO_4 (84.4 mM), pH 7.2. The external medium, also at pH 7.2, contained tetraethylammonium salts of TES (28.8 mM), EGTA (0.6 mM), and SO_4 (84.4 mM), and 120 mM K^+ as the SO_4 salt. Proton efflux from the liposomes was initiated by adding 30 μM laurate followed by 0.1 μM valinomycin. As we have reported (104), the TES anion quenches SPQ fluorescence whereas the TES zwitterion does not; therefore, changes in fluorescence in this medium result from changes in total acid, i.e., from proton

flux across the liposomal membrane. In each experiment, the quench coefficient was determined by calibration curves carried out on the proteoliposomes. Internal liposomal volume, determined from the volume of distribution of SPQ, was 1.1–1.6 μl/mg of lipid. Protein content, estimated by the Amido Black method, was 1–3 μg of protein/mg of lipid.

7.2 Results

7.2.1 Proton transport phenotype of wild-type UCP

Fig. 7.1 contains typical traces of H^+ efflux from vesicles reconstituted with wild-type UCP. The large internal acidification following laurate addition is due to partitioning of laurate/lauric acid in the membrane, followed by rapid flip-flop equilibration and delivery of protons to the internal medium (133). Addition of valinomycin caused internal alkalinization (Fig. 7.1, *trace a*), which implies an underlying movement of protons and charge. This electrophoretic proton efflux may be the result of proton transport directly by UCP (40) or laurate anion transport by UCP, with the proton carried by nonionic diffusion of lauric acid (44). That proton efflux required mediation of UCP is demonstrated by its inhibition by external GDP (Fig. 7.1, *trace b*). The K_i values for GDP inhibition of proton transport by wild-type UCP ranged between 8 and 10 μM in three experiments where it was measured. Proton efflux was also inhibited by the laurate analogue undecanesulfonate (Fig. 7.1, *trace c*). Undecanesulfonate is transported by UCP, and its inhibition of UCP-catalyzed H^+ transport is competitive with laurate.

7.2.2 Proton transport phenotypes of cysteine mutants of UCP

We mutated all cysteines to serines independently, and we also mutated Cys253 to alanine. For each mutant, we assayed proton transport and its inhibition by GDP and undecanesulfonate. As we reported in a preliminary communication (96), each of these mutations was without effect on transport and inhibition (data not shown; see Chapter 6).

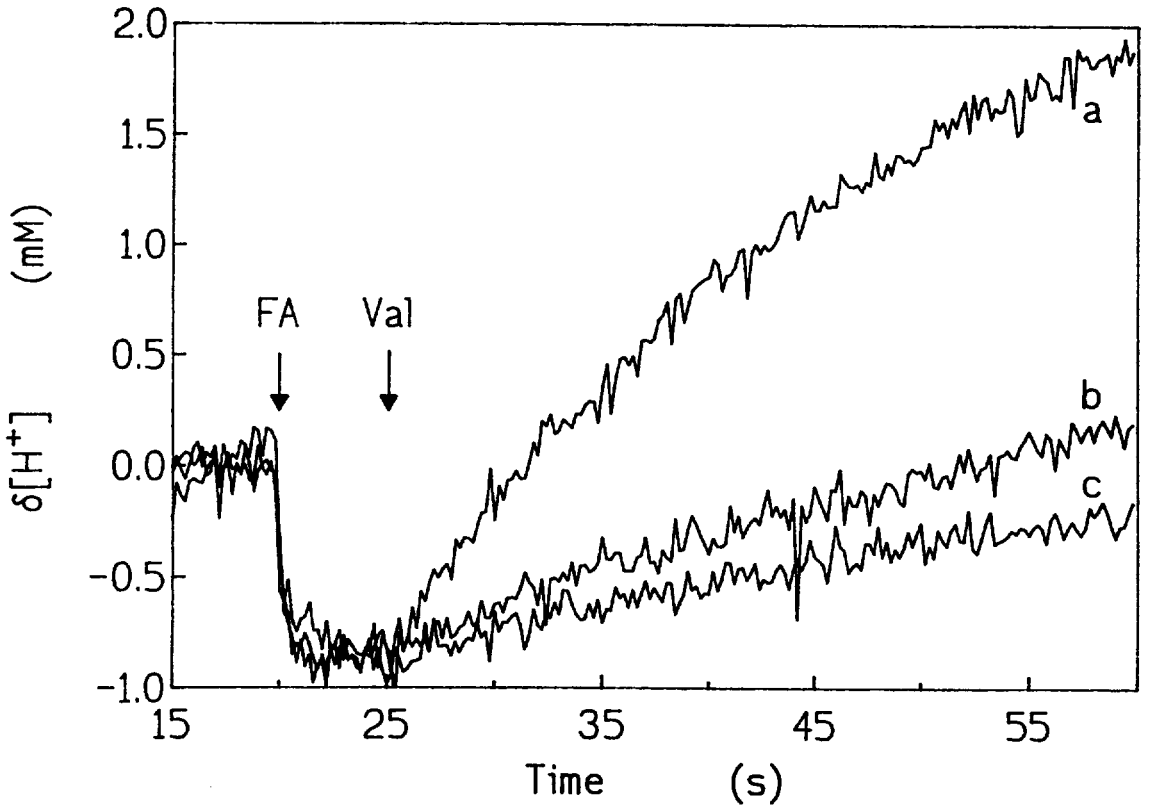

Figure 7.1 Electrophoretic H^+ efflux from proteoliposomes reconstituted with expressed, purified wild-type UCP. Fluorescence traces from proteoliposomes containing SPQ and 1 mM GDP were converted to changes in intraliposomal acidity ($d[H^+]$) and plotted versus time. Proton efflux was initiated by addition of valinomycin (Val) in the presence of 30 μM laurate (FA). *Trace a*, no further additions; *trace b*, 1 mM GDP was present in the assay medium; *trace c*, 300 μM undecanesulfonate was present in the assay medium.

7.2.3 Proton transport phenotypes of Arg276 mutants of UCP

We mutated Arg276 to leucine and glutamine. Fig. 7.2 contains representative traces from an Arg276Leu mutant reconstituted into liposomes. UCP-catalyzed H^+ transport (Fig. 7.1, *trace a*) was unaffected in the leucine mutant, and it was reduced by about 50% in the glutamine mutant (see Table 7.1). The striking feature of these mutants is that GDP had no effect on H^+ transport (Fig. 7.1, *trace b*), and this defect was apparent at doses up to 1 mM, as shown in the GDP dose–response curves of Fig. 7.3. Confirming that laurate-induced H^+ transport was qualitatively unaffected by these mutations, the competitive inhibitor undecanesulfonate was effective in inhibiting transport (Fig. 7.2, *trace c*; Table 7.1).

7.3 Discussion

7.3.1 Mechanism of UCP-catalyzed proton transport

It is agreed that fatty acids cause UCP to catalyze electrophoretic proton transport and that UCP also catalyzes electrophoretic transport of monovalent anions, including undecanesulfonate (8, 29, 30, 32, 40, 41, 53, 147). Undecanesulfonate is an analogue of lauric acid, but it is incapable of inducing H^+ transport through UCP. These analogues differ in that lauric acid rapidly equilibrates across lipid membranes, whereas undecanesulfonic acid is incapable of nonionic diffusion (Fig. 7.1). Finally, undecanesulfonate is competitive with laurate in inhibiting UCP-mediated H^+ transport. These results favor a mechanism proposed by Skulachev (44), in which UCP is an anion channel whose physiological substrate is fatty acid anions. In this model, fatty acids act as protonophores, and regulation of H^+ back flux is provided by nucleotide inhibition of the anion uniport half-cycle.

The mechanism of UCP-catalyzed proton transport is still under active investigation, but the present results are most simply understood using the Skulachev model. Thus, the data in Fig. 7.1 show that H^+ efflux can be inhibited either by GDP, an allosteric non-competitive inhibitor of fatty acid anion transport, or by undecanesulfonate, a channel substrate and competitive inhibitor of laurate anion transport. The data in Fig. 7.2 show a dissociation of these effects. Protonophoretic

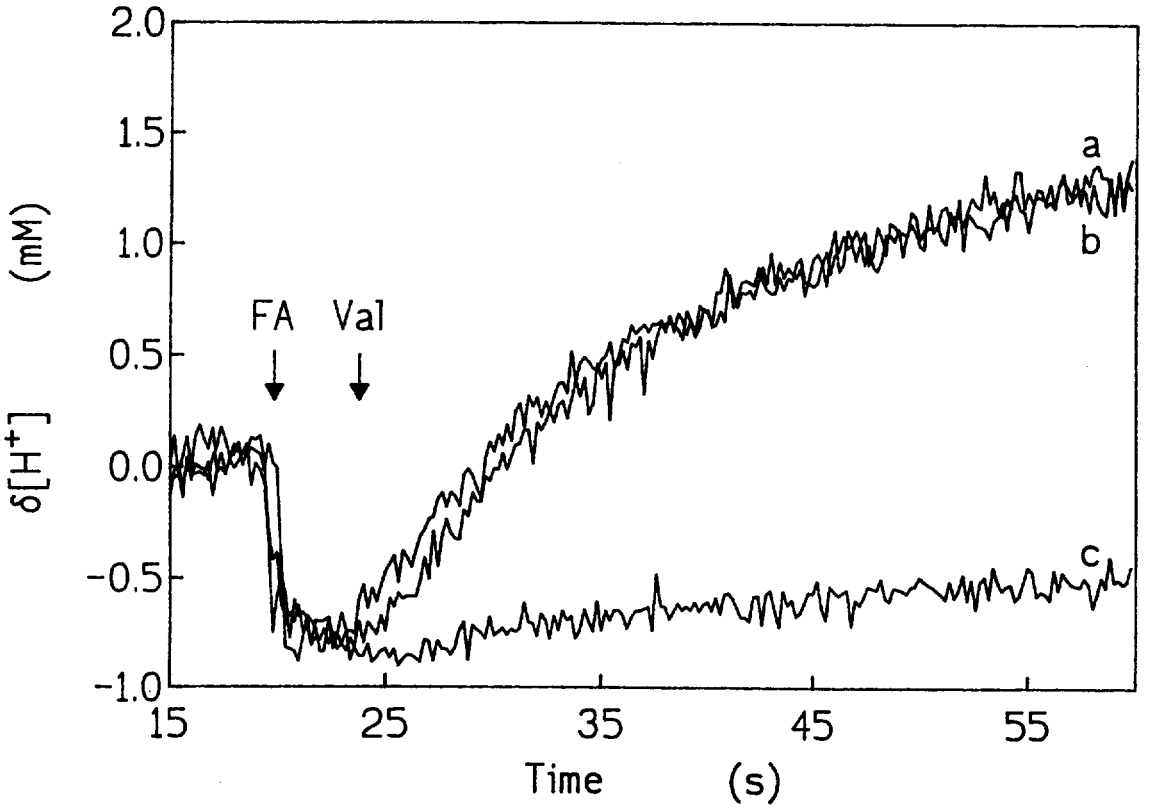

Figure 7.2 Electrophoretic H^+ efflux from proteoliposomes reconstituted with expressed, purified Arg276→Leu mutant UCP. Fluorescence traces from proteoliposomes containing SPQ and 1 mM GDP were converted to changes in intraliposomal acidity ($d[H^+]$) and plotted versus time. Proton efflux was initiated by addition of valinomycin (Val) in the presence of 30 μM laurate (FA). *Trace a*, no further additions; *trace b*, 1 mM GDP was present in the assay medium; *trace c*, 300 μM undecanesulfonate was present in the assay medium.

Table 7.1

Transport Activity of Reconstituted, Yeast-Expressed Rat Uncoupling Protein

Proton fluxes were measured as described under in Section 7.1.5. Fluxes are given as means ± S.E. of *n* independent experiments for each uncoupling protein genotype. Proton fluxes were measured in the presence or absence of either external GDP or undecanesulfonate. Rates for Arg276→Gln are averages of two separate experiments.

Uncoupling protein	**n**	**Undecanesulfonate** (μM)	**GDP** (μM)	**Proton flux** ($nmol\ min^{-1}\ mg^{-1}$)
Wild type	4	0	0	3860 ± 310
		0	1	1240 ± 180
		300	0	720 ± 280
Arg276→Leu	3	0	0	4250 ± 490
		0	1	4230 ± 440
		300	0	280 ± 280
Arg276→Gln	2	0	0	1940
		0	1	2040
		300	0	600

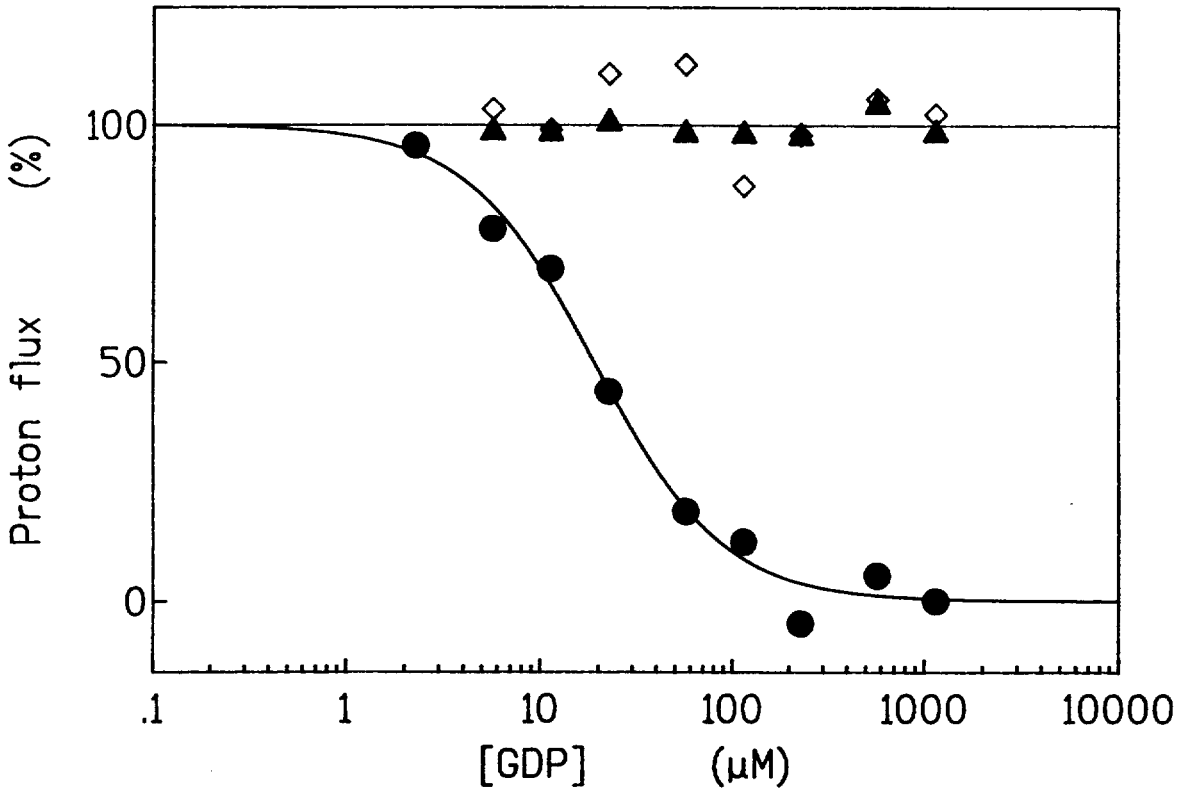

Figure 7.3 Effects of GDP on H^+ efflux from proteoliposomes reconstituted with wild-type and mutant UCPs. Proton fluxes, as percent of control rate in the absence of external GDP, are plotted versus external [GDP]. The figure contains data from three separate preparations: ●, wild-type UCP; ▲, Arg276→Leu mutant UCP; ◇, Arg276→Gln mutant UCP. The K_i for GDP inhibition of proton transport in the wild type was 10 μM. Control rates and rates in the presence of 1 mM GDP are contained in Table 7.1.

cycling of laurate and lauric acid is unaffected by the mutation, as is inhibition by the competitive substrate undecanesulfonate. On the other hand, GDP is no longer able to inhibit laurate transport through the mutant protein. Thus, the Arg276Leu mutation is unimpaired in transport function but has completely lost its nucleotide regulatory capacity.

7.3.2 Role of cysteines in UCP transport and regulation

The seven cysteines in UCP are conserved in UCP of all known species. Past chemical studies have implied that cysteines may be involved in both ion transport and GDP inhibition of this transport (65). However, changing all cysteines to serines independently was without effect on GDP inhibition of UCP-mediated proton or anion transport (96), indicating that a hydroxyl group can functionally substitute for each thiol group in UCP. Curiously, five of the seven cysteines are found in the third domain of UCP, the region containing the GDP binding site. Because Mayinger and Klingenberg (70) deduced that Cys253 was the most likely residue covalently labeled by the ATP analog FDNP-ATP, we replaced this residue with alanine to remove its hydrogen-bonding ability while maintaining the hydrophobic nature of the side chain. This mutation was also without effect on transport function or regulation. These results show that the thiol group *per se* is not decisive for these functions. We are carrying out further studies, using bulkier substitutions, to determine whether the effects of thiol reagents on function may be steric rather than chemical.

7.3.3 Role of arginine 276 in UCP transport and regulation

Based on the pH dependence of nucleotide binding to UCP, Klingenberg and co-workers (84) proposed that both acidic and basic residues are present in the purine nucleotide binding site of UCP. Chemical studies using arginine-modifying reagents had previously indicated that arginine is a critical functional residue for purine nucleotide binding (31). The most likely location of the arginine is in the third domain of UCP, because labeling studies using ATP analogs have localized the purine nucleotide binding region of UCP to this area. Peptides labeled by the ATP analogs contained amino acids 258-283 and 238-255 (69, 70). From membrane disposition

models of UCP, these peptides reside in helix 6 and in the matrix region connecting transmembrane helices 5 and 6, respectively (8,70). It has been proposed that this region comprises a nucleotide binding pocket accessible to the cytosol side, because it is known that purine nucleotides regulate UCP from this side of the inner membrane (70).

Of the three arginine residues in the third domain of UCP, we chose to modify Arg276. Based on the size of ATP in its extended *anti* conformation and the location of residues covalently labeled by the ATP analogs, it is unlikely that Arg299 could interact with ATP. Although Arg238 is about the same linear distance from the covalently labeled residues as Arg276, the transmembrane arrangement of the third domain proposed by Mayinger and Klingenberg (70) depicts Arg276 as being present in the proposed nucleotide binding pocket, spatially close to residues covalently labeled by ATP analogs and accessible to cytosolic purine nucleotides. Arg238 is excluded from this binding pocket and is inaccessible to nucleotides in this arrangement. Further, Arg276 is conserved in all mitochondrial carrier family members except the phosphate carrier, and the homologous residue in the yeast ADP/ATP translocator has recently been found to be required for growth, although its role in the transport function of the ADP/ATP translocator was not tested (78).

The functional role of Arg276 was investigated by replacing the arginine with glutamine and leucine. The glutamine substitution maintains some hydrogen-bonding ability but removes positive charge. Leucine removes both these characteristics. In each case, the substituted side chain was shorter to minimize steric interference of function. Our results with purified, reconstituted UCP show that both mutations caused total abolition of GDP inhibition of proton transport. On the other hand, both mutant forms of UCP catalyzed proton efflux, and this transport was completely inhibited by the competitive inhibitor undecanesulfonate. Because transport was normal with the Arg276→Leu mutant, the results are difficult to reconcile with gross conformation change in the protein structure. They indicate that the effect of the mutation was on purine nucleotide sensitivity and not on transport function.

This is the first identification of a single residue that is directly involved in purine nucleotide regulation of UCP transport function and the first evidence that directly relates functionally important residues between the ADP/ATP translocator and UCP.

---

[4] This material has been published in this or similar form in *The Journal of Biological Chemistry* and is used here by permission of The American Society for Biochemistry and Molecular Biology:

Murzda-Inglis, D. L., Modriansky, M., Patel, H. V., Woldegiorgis, G., Freeman, K. B., and Garlid, K. D. (1994) A single mutation in uncoupling protein of rat brown adipose tissue mitochondria abolishes GDP sensitivity by H^+ transport. *J. Biol. Chem.* **269,** 7435–7438.

Chapter 8

IDENTIFICATION BY SITE-DIRECTED MUTAGENESIS OF THREE ARGININES IN UNCOUPLING PROTEIN THAT ARE ESSENTIAL FOR NUCLEOTIDE BINDING AND INHIBITION[5]

Uncoupling protein (UCP) from brown adipose tissue mitochondria mediates proton flux from the cytosol back into the matrix, thereby producing heat (39, 40). UCP contains an anion transport pathway which permits the charged fatty acid (FA) anion head group, to which the membrane is normally impermeable, to flip-flop in the membrane. The cycle is completed by flip-flop of the protonated FA head group in the bilayer, resulting in energy-dissipating back flux of protons into the matrix (33). This uncoupling cycle is regulated by purine nucleotides, which bind to UCP and allosterically inhibit transport.

UCP does not contain a consensus nucleotide binding sequence, and relatively little is known about the location of the nucleotide binding site. Klingenberg's laboratory (69, 70) has shown by chemical labeling that the base and ribose moieties are positioned near the matrix loop connecting the fifth and sixth transmembrane domains. Lysine and arginine residues have long been suspected of participation in nucleotide regulation, and Katiyar and Shrago (31) showed that phenylglyoxal abolished GDP binding to UCP. However, none of the residues that interact with the phosphate groups have been identified.

The introduction of a high-level expression system for UCP in *Saccharomyces cerevisiae* (95) opened the door to a study of these interactions using site-directed mutagenesis. Thus, we were able to show that mutation of a single arginine residue (Arg276) abolished GDP inhibition without affecting UCP-mediated proton transport (79). We have now extended this study to Arg83, Arg182, Lys268 and His214, which are positioned within the membrane-spanning helices of UCP, and Lys72,

which lies outside the transmembrane domain (84). The mutant proteins were over-expressed in yeast (79, 95), then purified and reconstituted into liposomes. FA-induced, UCP-mediated H^+ transport, and its sensitivity to nucleotides, was assayed by fluorescence (104), and GDP binding was assayed using [^{3}H]GDP.

Each of the three arginine mutations caused complete loss of GDP inhibition of transport without affecting transport itself. This finding implies an extensive nucleotide interaction domain, because the three arginines are located on three different transmembrane segments. A surprising finding was that the Arg276 mutant, despite complete loss of sensitivity to GDP inhibition (79), retained normal binding affinity for GDP. We propose a three-stage model for binding-induced conformational change in which Arg276 interacts with the nucleotide after it is tightly bound, causing a conformational change that prevents transport of the FA anion head group. This result confirms that FA anion transport and nucleotide inhibition are separate features of UCP, implying two distinct binding sites (31, 115).

8.1 Materials and Methods

8.1.1 Materials

Zymolyase 100T was purchased from Seikagaku America (Ijamsville, MD). Tritiated GDP was purchased from New England Nuclear (Boston, MA). Dowex 1X8, 200–400 mesh anion exchanger (chloride form) was obtained from Sigma Chemical (St. Louis, MO). All other materials for cloning, site-directed mutagenesis, yeast growth and mitochondria isolation, and UCP isolation and reconstitution were from the same sources as described previously (79).

8.1.2 Site-directed mutagenesis

A M13mp19 plasmid containing the rat UCP cDNA fragment was used to prepare the site-directed mutants by the method of Kunkel (146). Oligonucleotides were designed to alter UCP codons for Arg83 (AGG) to Gln (CAG), Arg182 (AGA) to Thr (ACA), Lys72 (AAA) to Gln (CAA), Lys268 (AAA) to Gln (CAA), and His214 (CAT) to Gln (CAA). The *Sac*I–*Sph*I fragments from M13mp19 containing

either the wild-type or the mutant forms of UCP cDNA were subcloned into the *Sac*I–*Sph*I-cut pCGS110 *Escherichia coli–S. cerevisiae* shuttle vector. The cDNAs were under transcriptional control of the inducible *Gal*I promoter. The *S. cerevisiae* strain JB516 (*MATa*, *ura*3, *ade*1, *leu*2, *his*4, *gal*$^+$) was transformed by electroporation with the shuttle vector constructs and plated onto uracil-lacking selective plates. The resulting yeast transformants were grown at 30°C in the selective medium, and over-expression of UCP was induced by addition of 0.2% galactose, as previously described (95).

8.1.3 Purification and reconstitution of mutant UCPs

Yeast cells were harvested after growing in the presence of galactose for 11 hours, and yeast mitochondria were isolated by a modified protocol developed by Gasser (143). The final mitochondrial pellet was resuspended and stored at -20°C in buffer consisting of 250 mM sucrose, 5 mM K-TES, pH 6.7, and 1 mM K-EGTA. UCP was extracted, purified, and reconstituted into liposomes using the protocols described in detail in ref. 32.

8.1.4 Assay of H^+ transport mediated by mutant UCPs

The fluorescent probe SPQ is quenched by the TES anion, but not by the TES zwitterion, allowing measurement of changes in proton concentration (104). SPQ (2 mM) trapped inside liposomes containing the mutant UCPs was used to assay transport and GDP sensitivity of the transport, as before (79). The intravesicular medium contained TES (28.8 mM), EGTA (0.6 mM), and SO_4 (84.4 mM), pH 7.2, all TEA salts, and 1 mM GDP. The external medium, also at pH 7.2, contained TES (28.8 mM) and EGTA (0.6 mM) as TEA salts, and SO_4 (84.4 mM) as K^+ salt. Proton efflux from the liposomes was initiated by the addition of 30 μM laurate, followed by 0.1 μM valinomycin. Each proteoliposome preparation was individually calibrated to obtain the quench constant and liposomal volume. The protein content of the liposomes was estimated by the Amido-Black method (103).

8.1.5 Assay of GDP binding to mutant UCPs

We used a modified anion-exchange method developed by Klingenberg et al. (148) to assay GDP binding. A pasteur pipette tip was packed with glass wool and then filled with 30 mg of wet Dowex 1X8, 200–400 mesh (chloride form). A 75-μl volume of sample containing 6–9 μg of UCP was then applied to the resin. The assay medium was the same composition as the internal medium described above, except [^{3}H]GDP in concentrations from 1 to 15 μM was present. The sample was immediately chased with 2 $\times$ 100 μl of water, the entire eluate was collected and subjected to scintillation counting. In a parallel control assay, 100 μM non-radioactive GDP was included with each concentration of the radiolabeled nucleotide.

8.2 Results

8.2.1 Effects of Arg and Lys mutations on GDP inhibition of proton transport

Fig. 8.1 shows a typical GDP concentration dependence for inhibition of wild-type UCP (●) and Arg182Thr mutant UCP (○). As shown in Table 8.1, each of the arginine mutations completely abolished GDP inhibition, whereas the lysine and histidine mutants retained full GDP sensitivity. The K_i for GDP inhibition of proton flux in wild-type and native UCP under these conditions was 10 μM (79) and was not affected in the mutants exhibiting GDP inhibition.

Upon reconstitution, UCP is distributed randomly in the bilayer (32). It transports anions in both directions, but 1 mM GDP is present in the liposome interior so that 50% of the wild-type UCP is always inhibited. Loss of GDP-regulation should therefore free up both orientations of the protein and cause doubling of transport activity. This expectation was met in the Arg83Gln mutant, but not in the other two Arg mutants.

The undecanesulfonate anion is transported by UCP and is a competitive inhibitor of laurate-induced proton flux (33). 300 μM undecanesulfonate inhibited proton flux in all mutants to the level of proton leak, consistent with normal behavior of the FA anion transport pathway in the mutant UCPs.

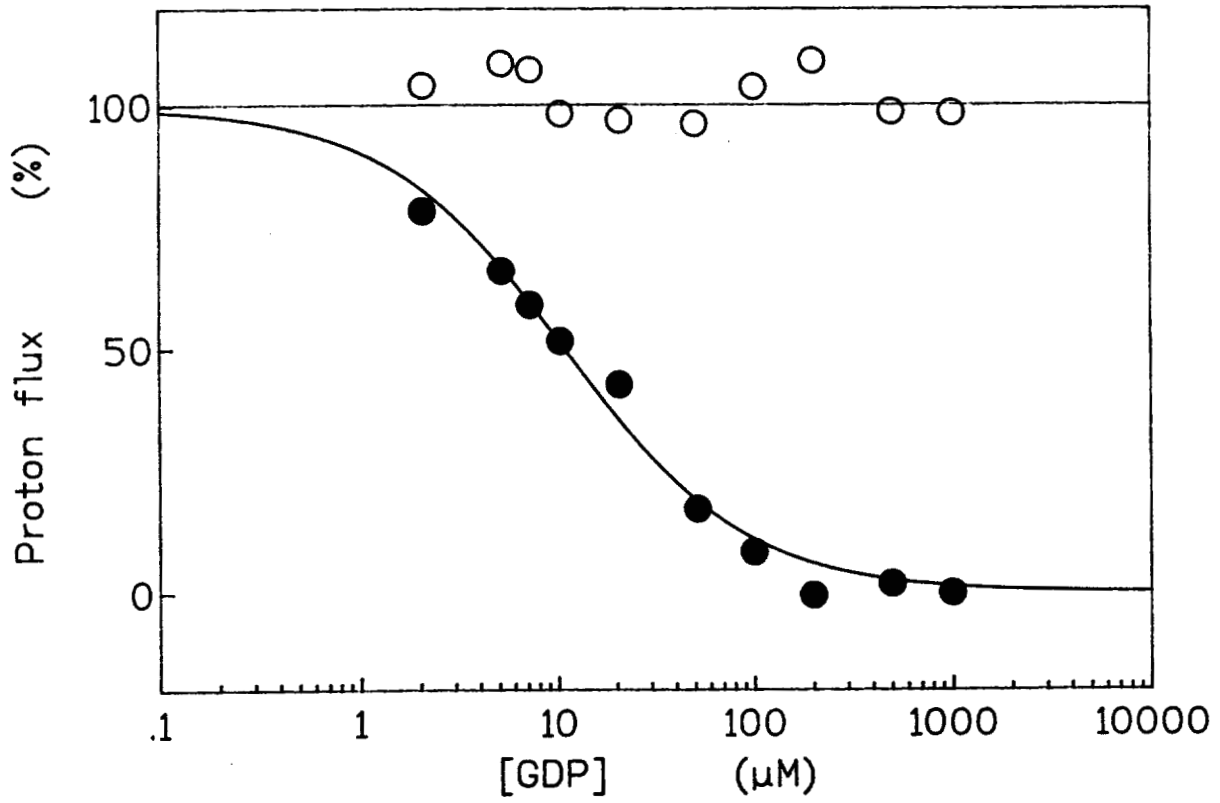

Figure 8.1 GDP inhibition of wild-type and Arg182Thr mutant UCPs. Proton fluxes, as percent of control rate in the absence of external GDP, are plotted versus external [GDP]. The data shown were obtained with the wild type (●) and Arg182Thr (○) mutant in the presence of 30 μM laurate. The difference between the maximum flux (100% flux) and the minimum flux (0% flux) corresponds to rates shown in Table 8.1.

Table 8.1

GDP Inhibition of Proton Fluxes Mediated by Mutant and Wild-Type UCP

The table contains values for proton flux (± S.E.) in the presence and absence of 1 mM GDP [normal K_i = 10 μM (79)]. Proton flux in proteoliposomes was induced by 30 μM laurate. Rates are corrected for proton leak, estimated at 28 ± 2 μM H^+/s (n = 30). This was also the level to which 300 μM undecanesulfonate, a competitive inhibitor of laurate-induced proton flux (33), reduced proton flux.

UPC	n	proton flux ($\mu mol\ H^+\ min^{-1}\ mg^{-1}$)		% inhibition
		$[GDP]_{out}$ = 0	$[GDP]_{out}$ = 1 mM	
wild-type	7	2.89 ± 0.13	0.24 ± 0.08	93
Lys72Gln	5	2.33 ± 0.44	0.19 ± 0.08	92
Lys268Gln	3	2.43 ± 0.22	0.16 ± 0.15	93
His214Gln	4	2.33 ± 0.56	0.13 ± 0.16	94
Arg83Gln	4	6.70 ± 0.38	6.66 ± 0.39	1
Arg182Thr	5	3.23 ± 0.46	3.02 ± 0.45	7
Arg276Leu	3	3.16 ± 0.59	3.14 ± 0.52	1

8.2.2 Effects of Arg and Lys mutations on GDP binding

Fig. 8.2 contains mass-action plots of GDP binding data obtained with reconstituted wild-type, Arg276Leu, and Lys268Gln mutants. Binding constants for each of the mutants are contained in Table 8.2. In comparing the data in Tables 8.1 and 8.2, there is agreement between GDP binding and inhibition in each case except one. Thus, the Arg83Gln and Arg182Thr mutants lost both GDP inhibition and GDP binding, whereas the Lys72Gln and Lys268Gln mutants retained both functions. The Arg276Leu mutant is unique in that it binds GDP normally but cannot be inhibited by GDP. Retention of normal GDP binding by the Arg276Leu mutant has been confirmed in isolated yeast mitochondria (144). As pointed out by Huang and Klingenberg (149), the protocol used to assay binding captures only the tightly bound state. Thus, GDP is tightly bound in the Arg276 mutant.

The dissociation constants, K_d, obtained for each of the mutant UCPs capable of binding GDP (Table 8.2), were higher than published values pertaining to native rat UCP (51); however, the K_d values are close to the observed K_i for GDP inhibition of UCP-mediated transport, which is generally 11 μM. This agreement may reflect our use of identical conditions for both H^+ flux and binding measurements.

Lysine 268 is located within the third domain of the tripartite structure among residues 238–283, which have long been identified with nucleotide interactions (70), and Lys72 is located in the second domain. As shown in Tables 8.1 and 8.2, neither residue affected GDP binding or GDP inhibition.

8.2.3 The role of His214 in pH regulation of nucleotide inhibition

The pH dependence of nucleoside triphosphate binding to UCP has a pK_a of 7.2, which suggests involvement of a histidine residue (150). If His214 plays this role, the His214Gln mutation should exhibit an increased K_i for GTP inhibition at neutral pH. In fact, this mutation had no effect on the K_i for GTP inhibition at pH 7.2 or 7.6 when compared to the wild type (three experiments, data not shown).

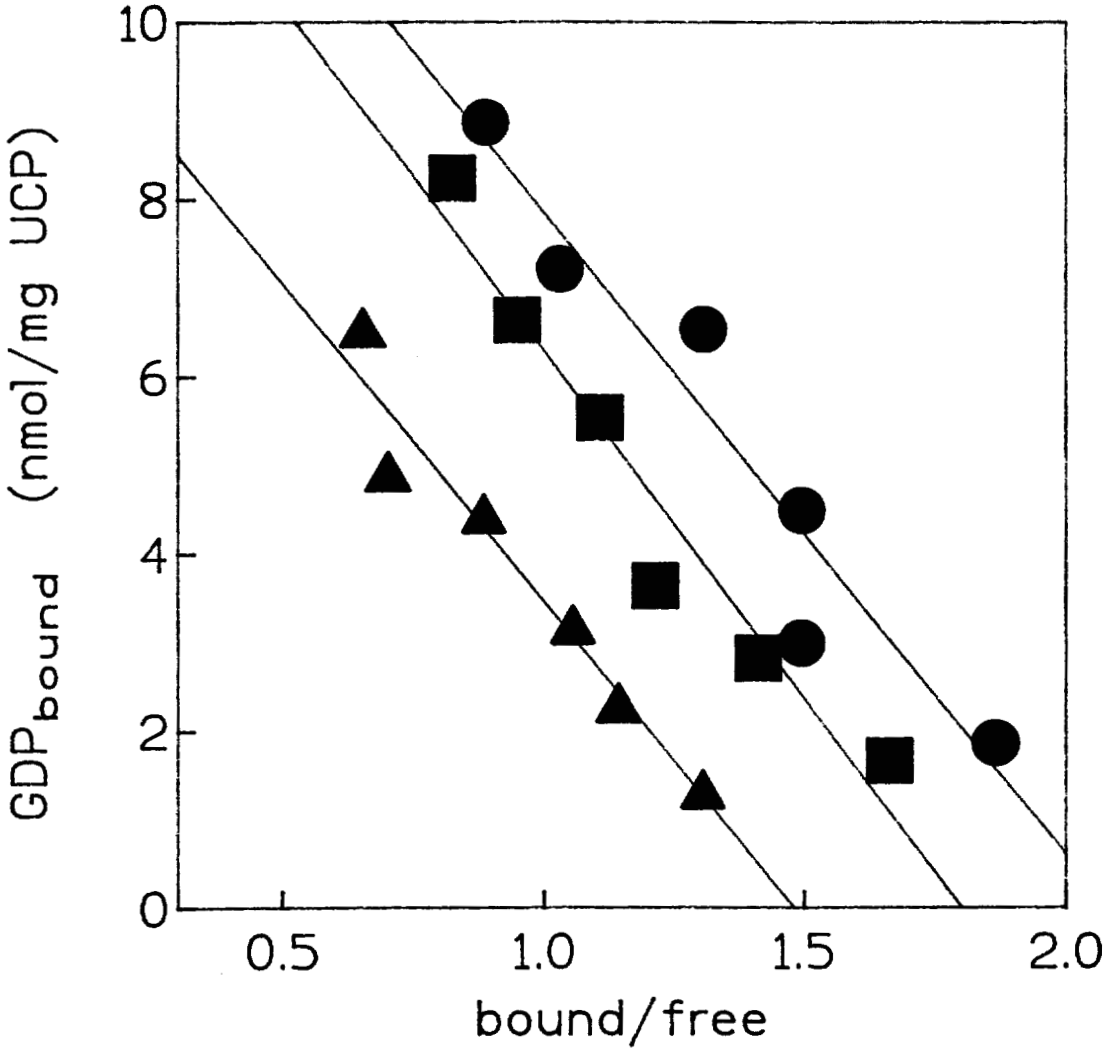

Figure 8.2 Arg276Leu mutant retains GDP binding. Mass-action plots of GDP binding to wild-type (●), Lys268Gln (▲), and Arg276Leu (■) mutant UCPs are shown. The derived parameters of K_d and B_{max} are summarized in Table 8.2.

Table 8.2

GDP Binding to Mutant and Wild-Type UCP

Table contains the dissociation constants, K_d, and binding capacity, B_{max}, derived from Eadie–Scatchard plots for each of the mutants. The value for wild-type protein translates to 0.9 mol GDP/mol UCP, assuming that one-half of the sites are available for binding due to random insertion. This stoichiometry is in agreement with that of Rafael et al. (51).

Uncoupling protein	**K_d** *(μM)*	**B_{max}** *(nmol/mg protein)*
wild-type	7.2	15.1
Lys72Gln	9.2	12.3
Lys268Gln	7.2	10.6
Arg276Leu	7.8	14.1
Arg83Gln	no binding	no binding
Arg182Gln	no binding	no binding

8.3 Discussion

Inhibition of uncoupling by nucleotides is the only known regulation of UCP. Because of their polyanionic character, nucleotides are expected to bind to positively charged amino acid residues. Arg276 was the first such residue to be identified (79), and we now show that Arg83 and Arg182 are also essential for normal nucleotide binding and inhibition.

8.3.1 Structural implications for UCP and UCPH

The three arginines that we mutated are located on three different transmembrane helices (Fig. 8.3), implying an extensive interaction region involving at least three of the six transmembrane helices in UCP. These helices very likely form the walls of a dead-end aqueous pocket for nucleotides, which are known to enter and exit from the cytosolic side and to interact with residues located on the matrix loop between helices 5 and 6 (70). Moreover, each of the three arginines is conserved in UCPH, suggesting that this protein is also regulated by nucleotides. UCPH is a recently discovered gene sequence encoding a protein thought to be involved in prevention of obesity and diabetes (7, 151). Its primary amino acid sequence is 56% identical with that of UCP, and the expressed protein appears to uncouple mitochondrial respiration.

8.3.2 Proposed three-stage mechanism of nucleotide regulation

Klingenberg and co-workers (149, 150, 152) have elaborated an elegant kinetic model of the interactions of nucleotide phosphates with UCP. Access to the phosphate binding region is controlled by protonation of Glu190, presumably by releasing a salt bridge that occludes the binding site. Huang and Klingenberg (149) proposed a two-stage mechanism in which nucleotides are first loosely bound, and then the protein undergoes a slow, spontaneous conformational change to a *tight* state in which nucleotides are tightly bound and H^+ transport is inhibited. Our results show, however, that the tightly bound state is not sufficient for transport inhibition. Thus, the tight binding exhibited by the Arg276 mutant is ineffective in inhibiting H^+

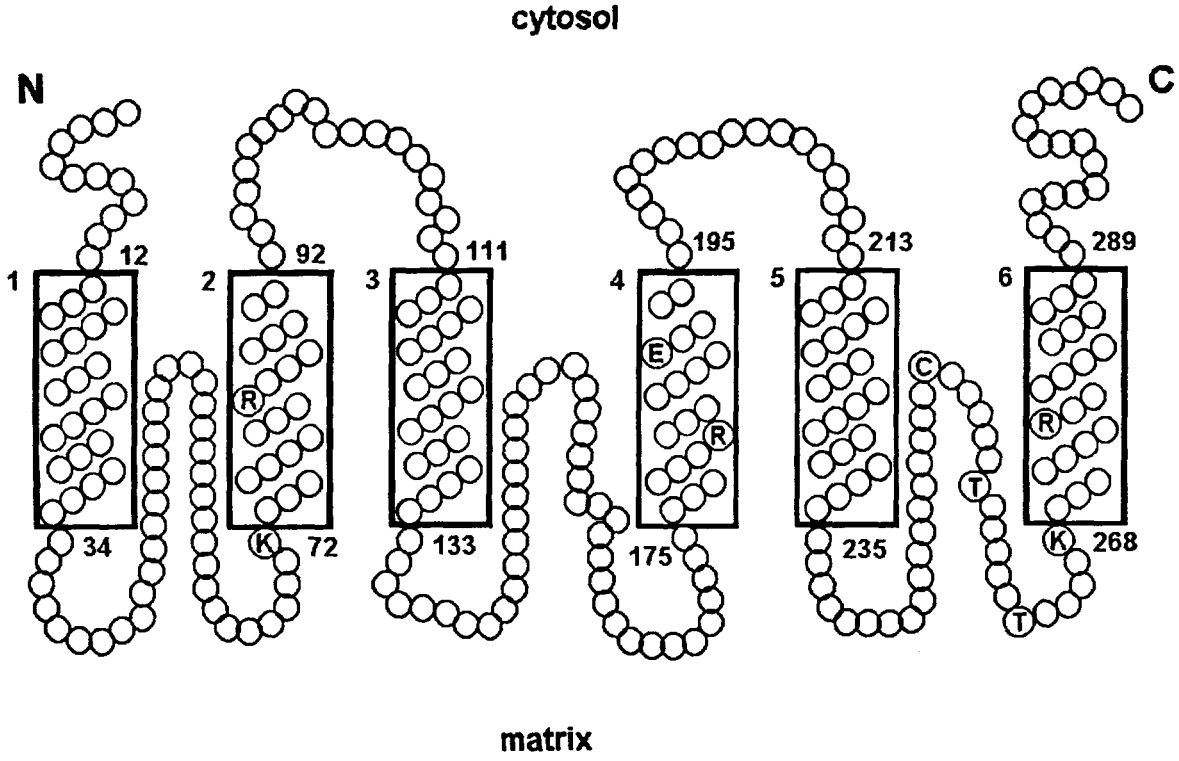

Figure 8.3 Membrane spanning model of uncoupling protein. UCP contains six transmembrane domains, which are designated by the single digit numbers. The amino acids at the cytosolic and matrix ends of the α-helices are numbered, based on models of Klingenberg (40) and Winkler et al. (152). The membrane topology is consistent with that reported by Miroux et al. (155). K72 and K268 were mutated without effect (this study). The remaining designated residues have been shown to participate in nucleotide binding to UCP. T259, T264, and C253 interact with the sugar-base moiety of the nucleotide (152). R83, R182, and R276 are essential for nucleotide binding and/or inhibition (this study), as is E190 (152). Each of the four transmembrane residues, R83, R182, R276, and E190, is conserved in UCPH, as is C253. UCPH contains substitutions at position 259 (Q instead of T) and 264 (R instead of T).

transport. These findings require modifications of the Huang and Klingenberg model (149), as described below and in Fig. 8.4.

8.3.2.1 Loose binding. The nucleotide enters the aqueous pocket in UCP, and its sugar-base moiety binds to the matrix loop connecting the fifth and sixth helices (69, 70). This interaction may be responsible for discrimination between purine and pyrimidine nucleotides (49, 51, 153). The nucleotide β-phosphate binds to Arg182, and the sum of these interactions results in a loose binding conformation.

8.3.2.2 Tight binding. The switch to a tight binding conformation is initiated by protonation of Glu190, making Arg83 available for binding to the second charge on the β-phosphate of diphosphates and the γ-phosphate of triphosphates. A histidine binds to the second charge on the γ-phosphate of triphosphates (154). The tightly bound conformation prevents trypsin cleavage of the C-terminus of UCP at Lys292 (149). This step is necessary, but not sufficient, for inhibition of transport.

8.3.2.3 Inhibited conformation. The nucleotide is now bound stably and positioned so that the α-phosphate can bind to Arg276. This final interaction induces a conformational change that occludes or removes the internal FA binding site (33, 43), causing inhibition of transport. This extension of Huang and Klingenberg's model (149) is consistent with our finding that mutation of Arg276 to Leu did not affect the K_d for binding but completely prevented nucleotide inhibition of transport.

---

[5] This material has been published in this or similar form in *The Journal of Biological Chemistry* and is used here by permission of The American Society for Biochemistry and Molecular Biology:

Modriansky, M., Patel, H. V., Murdza-Inglis, D. L., Freeman, K. B., and Garlid, K. D. (1997) Identification by site-directed mutagenesis of three arginines in uncoupling protein that are essential for nucleotide binding and inhibition. *J. Biol. Chem.* **272,** 24759–24762.

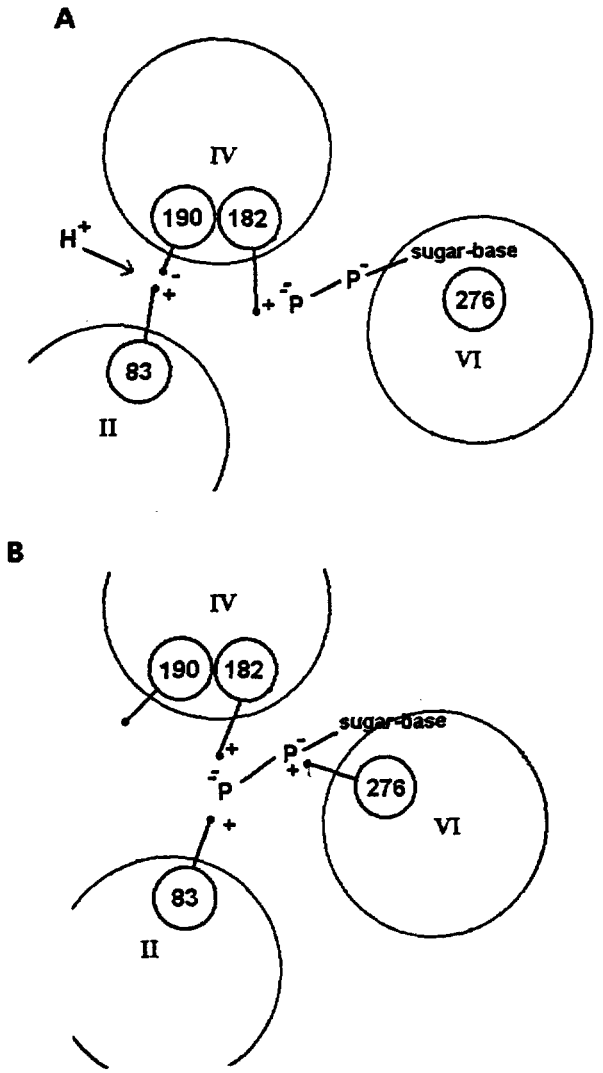

Figure 8.4 Model of the phosphate binding pocket in UCP. ***(A) Loose Conformation.*** The nucleotide sugar-base moiety binds loosely to the loop between transmembrane helices 5 and 6, and the terminal phosphate binds to Arg182 on helix 4. Binding to Arg83 is prevented by a salt bridge from Glu190 to a neighboring Arg or Lys. The figure tentatively identifies this residue as Arg83 itself. ***(B) Tight Conformation.*** Protonation of Glu190 causes the phosphate binding cleft between helices 2 and 4 to open and frees Arg83 to bind to the terminal phosphate of nucleoside diphosphates. [For triphosphates, Arg83 and an unidentified histidine bind to the terminal phosphate (not shown).] The tight binding pulls the bound nucleotide, together with its sugar-base attachments at the N-terminus of helix 6, into a new position. Tight binding causes a demonstrable conformational change at the C-terminus of helix 6 (149) but is not sufficient to inhibit transport. This occurs when Arg276 binds to the α-phosphate, causing the inhibitory conformational change.

Chapter 9
SUMMARY OF RESULTS

Several influential publications coming from our laboratory preceded the work presented here. A rapid, reproducible, GDP-sensitive chloride transport in liposomes containing purified, reconstituted UCP was reported (32). New anionic substrates of UCP were identified (53). The collaboration with Dr. Karl Freeman's laboratory resulted in functional reconstitution of a yeast-expressed rat UCP (95). A sensitive fluorescent technique was developed that utilizes a previously unknown phenomenon of SPQ quenching by "Good" buffers (104). The protocols developed during this time were used for obtaining data presented here.

Chapter 2 is a discussion of several long-standing hypotheses that needed to be tested, because they directly or indirectly conflicted with the fatty acid cycling hypothesis proposed by Skulachev (44). Chapter 3 is a supplement of Chapter 2 in that it clarifies the nature of nucleotide inhibition of UCP and suggests a possible role of palmitoyl-CoA in UCP activation. The data presented in Chapters 4 and 5 support the fatty acid cycling hypothesis (33, 44). Although Winkler and Klingenberg (34) offered an intriguing alternative model for the mechanism of UCP-mediated proton transport, they failed to explain why UCP transports monovalent anions, such as chloride or undecansulfonate.

The information available so far established the fatty acid cycling hypothesis as a sound model for the mechanism of UCP-mediated proton transport. The next step was to associate functional properties of UCP with its structural features, namely to identify essential amino acids. To find the amino acid residues responsible for transport will be more difficult than initially anticipated, mainly because cysteines, the major candidate (64-67), were found to be non-essential (Chapter 6, 97). The progress in uncovering residues essential for nucleotide inhibition of UCP-mediated

proton transport was much greater and some residues have been identified (Chapters 7 and 8, 79, 149), allowing mechanistic models of the UCP-nucleotide interaction to be developed (Chapter 8, 149).

Future research will probably focus on testing the remaining two lysine residues in the transmembrane regions and refining the model for nucleotide inhibition of UCP. Another open venue is to study the effects of mutations of polar residues within the transmembrane regions, which are likely to be essential for proton transport. An active cysteine-less UCP construct would allow re-introduction of single cysteines at different positions. These can be spin-labeled with EPR probes and tested for depth of immersion in the lipid bilayer or for interaction with a spin-labelled ligand. It is also important to realize that all or any part of the knowledge can be applied to other proteins, such as UCP2.

LITERATURE CITED

1. Himms-Hagen, J. (1985) Brown adipose tissue metabolism and thermogenesis. *Annu. Rev. Nutr.* **5**, 69–94.

2. Mitchell, P. (1979) Keilin's respiratory chain concept and its consequences. *Science* **206**, 1148–1159.

3. Jezek, P., Mahdi, F., and Garlid, K. D. (1990) Reconstitution of the beef heart and rat liver mitochondrial K^+/H^+ (Na^+/H^+) antiporter. *J. Biol. Chem.* **265**, 10522–10526.

4. DiResta, D. J., Kutschke, K. P., Hottois, M. D., and Garlid, K. D. (1986) K^+–H^+ exchange and volume homeostasis in brown adipose tissue mitochondria. *Am. J. Physiol.* **251**, R787–R793.

5. Palmieri, F. (1994) Mitochondrial carrier proteins. *FEBS Lett.* **346**, 48–54.

6. Nicholls, D. G., and Ferguson, S. J. (1992) *Bioenergetics 2*, p. 85, Academic Press, San Diego, CA.

7. Fleury, C., Neverova, M., Collins, S., Raimbault, S., Champigny, O., Levi-Meyrueis, C., Bouillaud, F., Seldin, M. F., Surwit, R. S., Ricquier, D., and Warden, C. H. (1997) Uncoupling protein-2: a novel gene linked to obesity and hyperinsulinemia. *Nat. Genet.* **15**, 269–273.

8. Nedergaard, J., and Cannon, B. (1992) The uncoupling protein thermogenin and mitochondrial thermogensis. In *New Comprehensive Biochemistry: Molecular Mechanisms in Bioenergetics* (Ernster, L., Ed.) Vol. 23, pp. 385–420, Elsevier Science Publishers B.V., Amsterdam.

9. Ricquier, D., Mory, G., Bouillaud, F., Thibault, J., and Weissenbach, J. (1984) Rapid increase of mitochondrial uncoupling protein and its mRNA in stimulated brown adipose tissue. *FEBS Lett.* **178**, 240–244.

10. Rehnmark, S., Nechad, M., Herron, D., Cannon, B., and Nedergaard, J. (1990) α- and β-adrenergic induction of the expression of the uncoupling protein thermogenin in brown adipocytes differentiated in culture. *J. Biol. Chem.* **265**, 16464–16471.

11. Nicholls, D. G., and Locke, R. M. (1984) Thermogenic mechanisms in brown fat. *Physiol. Rev.* **64**, 1–64.

12. Ohlson, K. B. E., Mohell, N., Cannon, B., Lindahl, S. G. E., and Nedergaard, J. (1994) Thermogenesis in brown adipocytes is inhibited by volatile anesthetic agents. *Anesthesiology* **81**, 176–183.

13. Douglas, R. J. (1992) Could a lowered level of uncoupling protein in brown adipose tissue mitochondria play a role in SIDS aetiology? *Med. Hypotheses* **37**, 100–102.

14. Lowell, B. B., Susulic, V. S., Hamann, A., Lawitts, J. A., Himms-Hagen, J., Boyer, B. B., Kozak, L. P., and Flier, J. S. (1993) Development of obesity in transgenic mice after genetic ablation of brown adipose tissue. *Nature* **366**, 740–742.

15. Huttunen, P., and Kortelainen, M. L. (1990) Long-term alcohol consumption and brown adipose tissue in man. *Eur. J. Appl. Physiol.* **60**, 418–424.

16. Kortelainen, M. L., Pelletier, G., Ricquier, D., and Bukowiecki, L. J. (1993) Immunohistochemical detection of human brown adipose tissue uncoupling protein in an autopsy series. *J. Histochem. Cytochem.* **41**, 759–764.

17. Zhao, J., Unelius, L., Bengtsson, T., Cannon, B., and Nedergaard, J. (1994) Coexisting β-adrenoceptor subtypes: significance for thermogenic process in brown fat cells. *Am. J. Physiol.* **267**, C969–C979.

18. Susulic, V. S., Frederich, R. C., Lawitts, J., Tozzo, E., Kahn, B. B., Harper, M.-E., Himms-Hagen, J., Flier, J. S., and Lowell, B. B. (1995) Targeted disruption of the β_3-adrenergic receptor gene. *J. Biol. Chem.* **270**, 29483–29492.

19. Prusiner, S. B., Cannon, B., and Lindberg, O. (1968) Oxidative metabolism in cells isolated from brown adipose tissue. 1. Catecholamine and fatty acid stimulation of respiration. *Eur. J. Biochem.* **6**, 15–22.

20. Bukowiecki, L. J., Follea, N., Lupien, J., and Paradis, A. (1981) Metabolic relationships between lipolysis and respiration in rat brown adipocytes. *J. Biol. Chem.* **256**, 12840–12848.

21. Drahota, Z., Honova, E., and Hahn, P. (1968) The effect of ATP and carnitine on the endogenous respiration of mitochondria from brown adipose tissue. *Experientia* **24**, 431–432.

22. Hittelman, K. J., Lindberg, O., and Cannon. B. (1969) Oxidative phosphorylation and compartmentation of fatty acid metabolism in brown fat mitochondria. *Eur. J. Biochem.* **11**, 183–192.

23. Nicholls, D. G. (1974) Hamster brown adipose tissue mitochondria: the control of respiration and the proton electrochemical potential gradient by possible physiological effectors of the proton conductance of the inner membrane. *Eur. J. Biochem.* **49**, 573–583.

24. Rafael, J., Ludolph, H. J., and Hohorst, H. W. (1969) Mitochondria from brown fat: uncoupling of oxidative phosphorylation by long chain fatty acids and recoupling by guanosine triphosphate. *Hoppe-Seyler's Z. Physiol. Chem.* **350**, 1121–1131.

25. Cannon, B., Nicholls, D. G., and Lindberg, O. (1973) Purine nucleotides and fatty acids in energy coupling of mitochondria from brown adipose tissue. In *Mechanism in Bioenergetics* (Azzone, G. F., Ernster, L., Papa, S., Quagliarello, E., and Siliprandi, N., Eds.) pp. 357–363, Academic Press, New York.

26. Heaton, G. M., and Nicholls, D. G. (1976) Hamster brown adipose tissue mitochndria. The role of fatty acids in the control of the proton conductance of the inner membrane. *Eur. J. Biochem.* **67**, 511–517.

27. Locke, R. M., Rial, E., and Nicholls, D. G. (1982) The acute regulation of mitochondrial proton conductance in cells and mitochondria from the brown fat of cold-adapted and warm-adapted guinea pigs. *Eur. J. Biochem.* **129**, 381–387.

28. Locke, R. M., Rial, E., and Nicholls, D. G. (1982) Fatty acids as acute regulators of the proton conductance of hamster brown-fat mitochndria. *Eur. J. Biochem.* **129**, 373–380.

29. Cunningham, S. A., Wiesinger, H., and Nicholls, D. G. (1986) Quantification of fatty acid activation of the uncoupling protein in brown adipocytes and mitochondria from the guinea-pig. *Eur. J. Biochem.* **157**, 415–420.

30. Strieleman, P. J., Schalinske, K. L., and Shrago, E. (1985) Fatty acid activation of the reconstituted brown adipose tissue mitochondria uncoupling protein. *J. Biol. Chem.* **260**, 13402–13405.

31. Katiyar, S. S., and Shrago, E. (1989) Reconstitution of purified brown adipose tissue mitochondria uncoupling protein: Demonstration of separate identity of nucleotide binding and proton translocation sites by chemical probes. *Proc. Natl. Acad. Sci. U.S.A.* **86**, 2559–2562.

32. Jezek, P., Orosz, D. E., and Garlid, K. D. (1990) Reconstitution of the uncoupling protein of brown adipose tissue mitochondria. *J. Biol. Chem.* **265**, 19296–19302.

33. Garlid, K. D., Orosz, D. E., Modriansky, M., Vassanelli, S., and Jezek, P. (1996) On the mechanism of fatty acid-induced proton transport by mitochondrial uncoupling protein. *J. Biol. Chem.* **271**, 2615–2620.

34. Winkler, E., and Klingenberg, M. (1994) Effect of fatty acids on H^+ transport activity of the reconstituted uncoupling protein. *J. Biol. Chem.* **269**, 2508–2515.

35. Jezek, P., Hanus, J., Semrad, C., and Garlid, K. D. (1996) Photo-activated azido fatty acid irreversibly inhibits anion and proton transport through the mitochondrial uncoupling protein. *J. Biol. Chem.* **271**, 6199–6205.

36. Jezek, P., and Freisleben, H.-J. (1994) Fatty acid binding site of the mitochondrial uncoupling protein. Demonstration of its existence by EPR spectroscopy of 5-DOXYL-stearic acid. *FEBS Lett.* **343**, 22–26.

37. Jezek, P., Bauer, M., and Trommer, W. E. (1995) EPR spectroscopy of 5-DOXYL-stearic acid bound to the mitochondrial uncoupling protein reveals its competitive displacement by alkylsulfonates in the channel and allosteric displacement by ATP. *FEBS Lett.* **361**, 303–307.

38. Nicholls, D. G. (1974) Hamster brown adipose tissue mitochondria. The chloride permeability of the inner membrane under respiring conditions, the influence of purine nucleotides. *Eur. J. Biochem.* **49**, 585–593.

39. Nicholls, D. G. (1979) Brown adipose tissue mitochondria. *Biochim. Biophys. Acta* **549**, 1–29.

40. Klingenberg, M., (1990) Mechanism and evolution of the uncoupling protein of brown adipose tissue. *TIBS* **15**, 108–112.

41. Klingenberg, M., and Winkler, E. (1985) The reconstituted isolated uncoupling protein is a membrane potential driven H^+ translocator. *EMBO J.* **4**, 3087–3092.

42. Kopecky, J., Guerrieri, F., Jezek, P., Drahota, Z., and Houstek, J. (1984) Molecular mechanism of uncoupling in brown adipose tissue mitochondria. The non-identity of proton and chloride conducting pathways. *FEBS Lett.* **170**, 186–190.

43. Garlid, K. D., (1990) New insights into mechanism of anion uniport through the uncoupling protein of brown adipose tissue mitochondria. *Biochim. Biophys. Acta* **1018**, 151–154.

44. Skulachev, V. P. (1991) Fatty acid circuit as a physiological mechanism of uncoupling of oxidative phosphorylation. *FEBS Lett.* **294**, 158–162.

45. Christiansen, E. N., Pedersen, J. I., and Grav, H. J. (1969) Uncoupling and recoupling of oxidative phosphorylation in brown adipose tissue mitochondria. *Nature* **222**, 857–860.

46. Pedersen, J. I. (1970) Coupled endogenous respiration in brown adipose tissue mitochondria. *Eur. J. Biochem.* **16**, 12–18.

47. Rafael, J., Klaas, D., and Hohorst, H. W. (1968) Mitochondria from brown fat: enzymes and respiratory chain phosphorylation during the pre- and postnatal development of the intrascapular fat body of the guinea pig. *Hoppe-Seyler's Z. Physiol. Chem.* **349**, 1711–1724.

48. Christiansen, E. N. (1971) Calcium uptake and its effect on respiration and phosphorylation in mitochondria from brown adipose tissue. *Eur. J. Biochem.* **19**, 276–282.

49. Lin, C., and Klingenberg, M. (1982) Characteristics of the isolated purine nucleotide binding protein from brown fat mitochondria. *Biochemistry* **21**, 2950–2956.

50. Nicholls, D. G. (1976) Hamster brown-adipose tissue mitochondria: purine nucleotide control of the ion conductance of the inner membrane, the nature of the nucleotide binding site. *Eur. J. Biochem.* **62**, 223–228.

51. Rafael, J., Pampel, I., and Wang, X. (1994) Effect of pH and $MgCl_2$ on the binding of purine nucleotides to the uncoupling protein in membrane particles from brown fat mitochondria. *Eur. J. Biochem.* **223**, 971–980.

52. Jezek, P., Houstek, J., and Drahota, Z. (1988) Alkaline pH, membrane potential, and magnesium cations are negative modulators of purine nucleotide inhibition of H^+ and Cl^- transport through the uncoupling protein of brown adipose tissue mitochondria. *J. Bioenerg. Biomembr.* **20**, 603–622.

53. Jezek, P., and Garlid, K. D. (1990) New substrates and competitive inhibitors of the Cl^- translocating pathway of the uncoupling protein of brown adipose tissue mitochondria. *J. Biol. Chem.* **265**, 19303–19311.

54. Nedergaard, J., and Cannon, B. (1994) Sulfonates are low-affinity ligands for the GDP-binding site of brown-fat mitochondria. *Biochim. Biophys. Acta* **1185**, 311–317.

55. Cannon, B., Sundin, V., and Romert, L. (1977) Palmitoyl coenzyme A: a possible physiological regulator of nucleotide binding to BAT mitochondria. *FEBS Lett.* **74**, 43–46.

56. Katiyar, S. S., and Shrago, E. (1991) Differential interaction of fatty acids and fatty acyl CoA esters with the purified/reconstituted brown adipose tissue mitochondrial uncoupling protein. *Biochem. Biophys. Res. Commun.* **175**, 1104–1111.

57. Woldegiorgis, G., Lawrence, J., Ruoho, A., Duff, T., and Shrago, E. (1995) Photoaffinity labeling of mitochondrial proteins with 2-azido [^{32}P] palmitoyl CoA. *FEBS Lett.* **364**, 143–146.

58. Woldegiorgis, G., Duff, T., Contreras, L., Shrago, E., and Ruoho, A. E. (1989) Photoaffinity labeling of hamster brown adipose tissue mitochondria by an [^{125}I] coenzyme A derivative: differential interaction with the uncoupling protein and the ADP/ATP carrier. *Biochem. Biophys. Res. Commun.* **161**, 502–507.

59. Nicholls, D. G., and Lindberg, O. (1973) Brown adipose tissue mitochondria. The influence of albumin and nucleotides on passive ion permeabilities. *Eur. J. Biochem.* **37**, 523–530.

60. Garlid, K. D., and Beavis, A. D. (1986) Evidence for the existence of an inner membrane anion channel in mitochondria. *Biochim. Biophys. Acta* **853**, 187–204.

61. Beavis, A. D. (1992) Properties of the inner membrane anion channel in intact mitochondria. *J. Bioenerg. Biomembr.* **24**, 77–90.

62. Jezek, P., Beavis, A. D., DiResta, D. J., Cousino, R. N., and Garlid, K. D. (1989) Evidence for two distinct chloride uniport pathways in brown adipose tissue mitochndria. *Am. J. Physiol.* **257**, C1142–C1148.

63. Rial, E., and Nicholls, D. G. (1989) On the mechanism of transport by the uncoupling protein from brown adipose tissue mitochondria. In *Anion Carriers of Mitochondrial Membranes* (Azzi, A., Nalecz, K. A., Nalecz, M. J., and Wojtczak, L., Eds.) pp. 261–268, Springer Verlag, Berlin.

64. Rial, E., and Nicholls, D.G. (1986) Chemical modification of the brown-fat-mitochondrial uncoupling protein with tetranitromethane and N-ethylmaleimide. *Eur. J. Biochem.* **161**, 689–694.

65. Jezek, P. (1987) Sulfhydryl groups are involved in H^+ translocation via the uncoupling protein of brown adipose tissue mitochondria. *FEBS Lett.* **211**, 89–93.

66. Rial, E., Arechaga, I., Sainz-de-la-Maza, E., and Nicholls, D. G. (1989) Effect of hydrophobic sulphydryl reagents on the uncoupling protein and inner-membrane anion channel of brown-adipose-tissue mitochondria. *Eur. J. Biochem.* **182**, 187–193.

67. Jezek, P., and Drahota, Z. (1989) Sulfhydryl groups of the uncoupling protein of brown adipose tissue mitochondria. *Eur. J. Biochem.* **183**, 89–95.

68. Kopecky, J., Jezek, P., Drahota, Z., and Houstek, J. (1987) Control of uncoupling protein in brown-fat mitochondria by purine nucleotides. Chemical modification by diazobenzenesulfonate. *Eur. J. Biochem.* **164**, 687–694.

69. Winkler, E., and Klingenberg, M. (1992) Photoaffinity labeling of the nucleotide-binding site of the uncoupling protein from hamster brown adipose tissue. *Eur. J. Biochem.* **203**, 295–304.

70. Mayinger, P., and Klingenberg, M. (1992) Labeling of two different regions of the nucleotide binding site of the uncoupling protein from brown adipose tissue mitochondria with two ATP analogs. *Biochemistry* **31**, 10536–10543.

71. Fernandez, M., Nicholls, D. G., and Rial, E. (1987) The uncoupling protein from brown-adipose-tissue mitochondria. Chymotrypsin-induced structural and functional modifications. *Eur. J. Biochem.* **164**, 675–680.

72. Eckerskorn, C., and Klingenberg, M. (1987) In the uncoupling protein from brown adipose tissue the C-terminus protrudes to the C-side of the membrane as shown by triptic cleavage. *FEBS Lett.* **226**, 166–170.

73. Klingenberg, M., and Appel, K. (1989) The uncoupling protein dimer can form a disulfide cross-link between the mobile C-terminal SH groups. *Eur. J. Biochem.* **180**, 123–131.

74. Gonzalez-Barroso, M. M., Fleury, C., Arechaga, I., Zaragoza, P., Levi-Meyrueis, C., Raimbault, S., Ricquier, D., Bouillaud, F., and Rial, E. (1996) Activation of the uncoupling protein by fatty acids is modulated by mutations in the C-terminal region of the protein. *Eur. J. Biochem.* **239**, 445–450.

75. Pedersen, P. L. (1993) An introduction to the mitochondrial anion carrier family. *J. Bioenerg. Biomembr.* **25**, 431–434.

76. Andreyev, A. Y., Bondareva, T. O., Dedukhova, V. I., Mokhova, E. N., Skulachev, V. P., Tsofina, L. M., Volkov, N. I., and Vygodina, T. V. (1989) The ATP/ADP-antiporter is involved in the uncoupling effects of fatty acids on mitochondria. *Eur. J. Biochem.* **182**, 585–592.

77. Brustovetsky, N. N., Dedukhova, V. I., Egorova, M. V., Mokhova, E. N., and Skulachev, V. P. (1990) Inhibitors of the ATP/ADP antiporter suppress stimulation of mitochndrial respiration and H^+ permeability by palmitate and anionic detergents. *FEBS Lett.* **272**, 187–189.

78. Nelson, D. R., Lawson, J. E., Klingenberg, M., and Douglas, M. G. (1993) Site-directed mutagenesis of the yeast mitochndrial ADP/ATP translocator. Six arginines and one lysine are essential. *J. Mol. Biol.* **230**, 1159–1170.

79. Murdza-Inglis, D. L., Modriansky, M., Patel, H. V., Woldegiorgis, G., Freeman, K. B., and Garlid, K. D. (1994) A single mutation in uncoupling protein of rat brown adipose tissue mitochondria abolishes GDP sensitivity of H^+ transport. *J. Biol. Chem.* **269**, 7435–7438.

80. Kaplan, R. S., Mayor, J. A., and Wood, D. O. (1993) The mitochondrial tricarboxylate transport protein. cDNA cloning, primary structure, and comparison with other mitochondrial transport proteins. *J. Biol. Chem.* **268**, 13682–13690.

81. Xu, Y., Mayor, J. A., Kakhniashvili, D., Gremse, D. A., Wood, D. O., and Kaplan, R. S. (1997) Construction and functional characterization of cysteine-less yeast mitochondrial citrate transport protein variants. *Biophys. J.* **72**, A407.

82. Ridley, R. G., Patel, H. V., Gerber, G. E., Morton, R. C., and Freeman, K. B. (1986) Complete nucleotide sequence and derived amino acid sequence of cDNA encoding the mitochondrial uncoupling protein of rat brown adipose tissue: lack of mitochondrial targeting presequence. *Nucleic Acids Res.* **14**, 4025–4035.

83. Jacobsson, A., Stadler, U., Glotzer, M., and Kozak, L. (1985) Mitochondrial uncoupling protein from mouse brown fat. Molecular cloning, genetic mapping, and mRNA expression. *J. Biol. Chem.* **260**, 16250–16254.

84. Aquila, H., Link, T. A., and Klingenberg, M. (1985) The uncoupling protein from brown fat mitochondria is related to the mitochondrial ADP/ATP carrier.

Analysis of sequence homologies and of folding of the protein in the membrane. *EMBO J.* **4**, 2369–2376.

85. Balogh, A. G., Ridley, R. G., Patel, H. V., and Freeman, K. B. (1989) Rabbit brown adipose tissue uncoupling protein mRNA: use of only one of two polyadenylation signals in its processing. *Biochem. Biophys. Res. Commun.* **161**, 156–161.

86. Casteilla, L., Bouillaud, F., Forest, C., and Ricquier, D. (1989) Nucleotide sequence of a cDNA encoding bovine brown fat uncoupling protein. Homology with ADP binding site of ADP/ATP carrier. *Nucleic Acids Res.* **17**, 2131.

87. Cassard, A. M., Bouillaud, F., Mattei, M. G., Hentz, E., Raimbault, S., Thomas, M., and Ricquier, D. (1990) Human uncoupling protein gene: structure, comparison with rat gene, and assignment to the long arm of chromosome 4. *J. Cell. Biochem.* **43**, 255–264.

88. Fiermonte, G., Walker, J. E., and Palmieri, F. (1993) Abundant bacterial expression and reconstitution of an intrinsic membrane-transport protein from bovine mitochondria. *Biochem. J.* **294**, 293–299.

89. Xu, Y., Mayor, J. A., Gremse, D. A., and Kaplan, R. S. (1995) Overexpression and functional reconstitution of the tricarboxylate transport protein from rat liver mitochondria. *Biophys. J.* **68**, A437.

90. Ferreira, G. C., and Pedersen, P. L. (1992) Overexpression of higher eukaryotic membrane proteins in bacteria. *J. Biol. Chem.* **267**, 5460–5466.

91. Miroux, B., Casteilla, L., Klaus, S., Raimbault, S., Grandin, S., Clement, J. M., Ricquier, D., and Bouillaud, F. (1992) Antibodies selected from whole antiserum by fusion proteins as tools for the study of the topology of mitochondrial membrane proteins. *J. Biol. Chem.* **267**, 13603–13609.

92. Klaus, S., Casteilla, L., Bouillaud, F., Raimbault, S., and Ricquier, D. (1990) Expression of the brown fat mitochondria uncoupling protein in *Xenopus* oocytes and import into mitochondrial membrane. *Biochem. Biophys. Res. Commun.* **167**, 784–789.

93. Casteilla, L., Blondel, O., Klaus, S., Raimbault, S., Diolez, P., Moreau, F., Bouillaud, F., and Ricquier, D. (1990) Stable expression of functional mitochondrial uncoupling protein in Chinese hamster ovary cells. *Biochemistry* **87**, 5124–5128.

94. Romanos, M. A., Scorer, C. A., and Clare, J. J. (1992) Foreign gene expression in yeast: a review. *Yeast* **8**, 423–488.

95. Murdza-Inglis, D. L., Patel, H. V., Freeman, K. B., Jezek, P., Orosz, D. E., and Garlid, K. D. (1991) Functional reconstitution of rat uncoupling protein following its high level expression in yeast. *J. Biol. Chem.* **266**, 11871–11875.

96. Murdza-Inglis, D. L., Patel, H. V., Freeman, K. B., Orosz, D. E., Modriansky, M., and Garlid, K. D. (1993) Functional analysis of rat uncoupling protein site directed mutants. *FASEB J.* A1108.

97. Arechaga, I., Raimbault, S., Prieto, S., Levi-Meyrueis, C., Zaragoza, P., Miroux, B., Ricquier, D., Bouillaud, F., and Rial, E. (1993) Cysteine residues are not essential for uncoupling protein function. *Biochem. J.* **296**, 693–700.

98. Ricquier, D., Casteilla, L., and Bouillaud, F. (1991) Molecular studies of the uncoupling protein. *FASEB J.* **5**, 2237–2242.

99. Nicholls, D. G., Snelling, R., and Rial, E. (1984) Proton and calcium circuits across the mitochondrial inner membrane. *Biochem. Soc. Trans.* **12**, 388–390.

100. Rial, E., Poustie, A., and Nicholls, D. G. (1983) Brown-adipose-tissue mitochondria: the regulation of the 32000-M_r uncoupling protein by fatty acids and purine nucleotides. *Eur. J. Biochem.* **137**, 197–203.

101. Beavis, A. D., Brannan, R. D., and Garlid, K. D. (1985) A structural interpretation of the relationship between light scattering and matrix volume. *J. Biol. Chem.* **260**, 13424–13433.

102. Garlid, K. D., and Beavis, A. D. (1985) Swelling and contraction of the mitochondrial matrix. II. Quantitative application of the light scattering technique to solute transport across the inner membrane. *J. Biol. Chem.* **260**, 13434–13441.

103. Kaplan, R. S., and Pedersen, P. L. (1985) Determination of microgram quantities of protein in the presence of milligram levels of lipid with Amido Black 10B. *Anal. Biochem.* **150**, 97–104.

104. Orosz, D. E., and Garlid, K. D. (1993) A sensitive new fluorescence assay for measuring proton transport across liposomal membranes. *Anal. Biochem.* **210**, 7–15.

105. Nicholls, D. G. (1977) The effective proton conductance of the inner membrane of mitochondria from brown adipose tissue. Dependency on proton electrochemical potential gradient. *Eur. J. Biochem.* **77**, 349–356.

106. Jezek, P., Drahota, Z., and Ring, K. (1989) The activating effects of fatty acids on the mitochondrial uncoupling protein reconstituted in liposomes. *J. Lipid Mediators* **2**, 85–94.

107. Locke, R. M., Rial, E., Scott, I. D., and Nicholls, D. G. (1982) Fatty acids as acute regulators of the proton conductance of hamster brown-fat mitochondria. *Eur. J. Biochem.* **129**, 373–380.

108. Garlid, K. D., Beavis, A. D., and Ratkje, S. K. (1989) On the nature of ion leaks in energy-transducing membranes. *Biochim. Biophys. Acta* **976**, 109–120.

109. LaNoue, K. F., Strzelecki, T., Strzelecka, D., and Koch, C. (1986) Regulation of the uncoupling protein in brown adipose tissue. *J. Biol. Chem.* **261**, 298–305.

110. Strieleman, P. J., and Shrago, E. (1985) Specific interactions of fatty Acyl-CoA esters with brown adipose tissue mitochondria. *Am. J. Physiol.* **248**, E699–E705.

111. Chinet, A., Friedli, C., Seydoux, J., and Girardier, L. (1978) Does cytoplasmic alkalinization trigger mitochondrial energy dissipation in the brown adipocyte? *Experientia* **32**, 25–32.

112. Cannon, B., and Nedergaard, J. (1985) The biochemistry of an inefficient tissue: brown adipose tissue. *Essays Biochem.* **20**, 110–164.

113. Schaffer, J. E., and Lodish, H. F. (1994) Expression cloning and characterization of a novel adipocyte long chain fatty acid transport protein. *Cell* **79**, 427–436.

114. Klingenberg, M. (1993) Dialectics in carrier research: the ADP/ATP carrier and the uncoupling protein. *J. Bioenerg. Biomembr.* **25**, 447–457.

115. Jezek, P., Orosz, D. E., Modriansky, M., and Garlid, K. D. (1994) Transport of anions and protons by the mitochondrial uncoupling protein and its regulation by nucleotides and fatty acids. *J. Biol. Chem.* **269**, 26184–26190.

116. Bieber, L. L., Pettersson, B., and Lindberg, O. (1975) Studies on norepinephrine-induced efflux of free fatty acid from hamster brown-adipose-tissue cells. *Eur. J. Biochem.* **58**, 375–381.

117. Lee, S. C., Hamilton, J. S., Trammell, T., Horwitz, B., and Pappone, P. A. (1994) Adrenergic modulation of intracellular pH in isolated brown fat cells from hamster and rat. *Am. J. Physiol.* **267**, C349–C356.

118. LaNoue, K. F., Koch, C. D., and Meditz, R. B. (1982) Mechanism of action of norepinephrine in hamster brown adipocytes. *J. Biol. Chem.* **257**, 13740–13748.

119. Prusiner, S. B., Cannon, B., Ching, T. M., and Lindberg, O. (1968) Oxidative metabolism in cells isolated from brown adipose tissue. 2. Catecholamine regulated respiratory control. *Eur. J. Biochem.* **7**, 51–57.

120. Stryer, L. (1988) *Biochemistry*, 3rd Edn., p. 473, W. H. Freeman and Co., New York.

121. Nicholls, D. G., Grav, H. J., and Lindberg, O. (1972) Mitochondria from hamster brown-adipose tissue. Regulation of respiration *in vitro* by variations in volume of the matrix compartment. *Eur. J. Biochem.* **31**, 526–533.

122. Vallin, I. (1970) Norepinephrine response in brown adipose tissue from newborn rats. *Acta Zool.* **51**, 129–139.

123. Halestrap, A. P. (1989) The regulation of the matrix volume of mammalian mitochondria *in vivo* and *in vitro* and its role in the control of mitochondrial metabolism. *Biochim. Biophys. Acta* **973**, 355–382.

124. Garlid, K. D., Paucek, P., Yarov-Yarovoy, V., Sun, X., and Schindler, P. A. (1995) The mitochondrial K_{ATP} channel as a receptor for potassium channel openers. *J. Biol. Chem.* **271**, 8796–8799.

125. Grinstein, S., Rotin, D., and Mason, M. J. (1989) Na^+/H^+ exchange and growth factor-induced cytosolic pH changes. Role in cellular proliferation. *Biochim. Biophys. Acta* **988**, 73–97.

126. Modrianský, M., Orosz, D. E., Jezek, P., and Garlid, K. D. (1994) The uncoupling protein is an anion channel whose physiological role is to enable fatty acids to act as protonophores in brown adipose tissue mitochondria. *Biophys. J.* **66**, A333.

127. Garlid, K. D., Paucek, P., Sun, X., and Woldegiorgis, G. (1995) Mitochondrial cation transport systems. *Methods Enzymol.* **260**, 331–348.

128. Sun, X., and Garlid, K. D. (1992) On the mechanism by which bupivacaine conducts protons across the membranes of mitochondria and liposomes. *J. Biol. Chem.*, **267**, 19147–19154.

129. Garlid, K. D., and Nakashima, R.A. (1983) Studies on the mechanism of uncoupling by amine local anesthetics. Evidence for mitochondrial proton transport mediated by lipophilic ion pairs. *J. Biol. Chem.* **258**, 7974–7980.

130. Bell, R. P. (1973) *The Proton in Chemistry*, p. 98, Cornell University Press, Ithaca, NY.

131. Doyle, A. C. (1893) *The Memoirs of Sherlock Holmes*, George Neunes, London.

132. Hamilton, J. A., and Cistola, D. P. (1986) Transfer of oleic acid between albumin and phospholipid vesicles. *Proc. Natl. Acad. Sci. U.S.A.* **83**, 82–86.

133. Kamp, F., and Hamilton, J. A. (1992) pH gradients across phospholipid membranes caused by fast flip-flop of un-ionized fatty acids. *Proc. Natl. Acad. Sci. U.S.A.* **89**, 11367–11370.

134. Pedersen, J. I., Slinde, E., Grynne, B., and Aas, M. (1975) The intracellular localization of long-chain acyl-CoA synthetase in brown adipose tissue. *Biochim. Biophys. Acta* **398**, 191–203.

135. Ruzicka, M., Borecký, J., Hanu, J. and Jezek, P. (1996) Photoaffinity labelling of the mitochondrial uncoupling protein by [^{3}H] azido fatty acid affects the anion channel. *FEBS Lett.* **382**, 239–243.

136. Kamp, F., and Hamilton, J. A. (1993) Movement of fatty acids, fatty acid analogues, and bile acids across phospholipid bilayers. *Biochemistry* **32**, 11074–11086.

137. Hani, T., Smrz, M., Klír, P., Macek, K. Klíma J., Base J., and Deyl, Z. (1988) Determination of fatty acids as phenacyl esters in rat adipose tissue and blood vessel walls by high-performance liquid chromatography. *J. Chromatogr.* **452**, 443–457.

138. Langner M., Isac, T. Hui, S. W. (1995) Interaction of free fatty acids with phospholipid bilayers. *Biochim. Biophys. Acta* **1236**, 73–80.

139. Anel, A., Richieri, G. V., and Kleinfeld, A. M. (1993) Membrane partition of fatty acids and inhibition of T cell function. *Biochemistry* **32**, 530–536.

140. Richieri, G. V., Ogata, R. T., and Kleinfeld, A. M. (1992) A fluorescently labeled intestinal fatty acid binding protein. Interactions with fatty acids and its use in monitoring free fatty acids. *J. Biol. Chem.* **267**, 23495–23501.

141. Stryer, L. (1988) *Biochemistry*, 3rd Edn., p. 19, W. H. Freeman and Co., New York.

142. Kunkel, T. A., Roberts, J. D., and Zakour, R. A. (1987) Rapid and efficient site-specific mutagenesis without phenotypic selection. *Methods Enzymol.* **154**, 367–382.

143. Gasser, S. M. (1983) Import of polypeptides into isolated yeast mitochondria. *Methods Enzymol.* **97**, 329–336.

144. Murdza-Inglis, D. L. (1995) Ph.D. Thesis: *Structure/Function Studies of Rat UCP in Yeast Mitochondria*. McMaster University, Hamilton, Canada.

145. Runswick, M. J., Walker, J. E., Bisaccia, F., Iacobazzi, V., and Palmieri, F. (1990) Sequence of the bovine 2-oxoglutarate/malate carrier protein: structural relationship to other mitochondrial transport proteins. *Biochemistry* **29**, 11033–11040.

146. Kunkel, T. A. (1985) Rapid and efficient site-specific mutagenesis without phenotypic selection. *Proc. Natl. Acad. Sci. U.S.A.* **89**, 11367–11370.

147. Himms-Hagen, J. (1990) Brown adipose tissue thermogenesis: interdisciplinary studies. *FASEB J.* **4**, 2890–2898.

148. Klingenberg, M., Herlt, M., and Winkler, E. (1986) Nucleotide binding assay for uncoupling protein from brown fat mitochondria. *Methods Enzymol.* **126**, 498–504.

149. Huang, S.-G., and Klingenberg, M. (1996) Two-stage nucleotide binding mechanism and its implications to H^+ transport inhibition of the uncoupling protein from brown adipose tissue mitochondria. *Biochemistry* **35**, 7846–7854.

150. Huang, S.-G., and Klingenberg, M. (1995) Fluorescent nucleotide derivatives as specific probes for the uncoupling protein: thermodynamics and kinetics of binding and the control by pH. *Biochemistry* **34**, 349–360.

151. Gimeno, R. E., Dembski, M., Weng, X., Deng, N., Shyjan, A. W., Gimeno, C. J., Iris, F., Ellis, S. J., Woolf, E. A., and Tartaglia, L. A. (1997) Cloning and characterization of an uncoupling protein homolog. A potential molecular mediator of human thermogenesis. *Diabetes* **46**, 900–906.

152. Winkler, E., Wachter, E., and Klingenberg, M. (1997) Identification of the pH sensor for nucleotide binding in the uncoupling protein from brown adipose tissue. *Biochemistry* **36**, 148–155.

153. Nicholls, D. G., Cannon, B., Grav, H. J., and Lindberg, O. (1974) Energy dissipation in non-shivering thermogenesis. In *Dynamics of Energy-transducing Membranes* (Ernster, L., Ed.) pp. 529–537, Elsevier, Amsterdam.

154. Klingenberg, M. (1988) Nucleotide binding to ucoupling protein. Mechanism of control by protonation. *Biochemistry* **27**, 781–791.

155. Miroux, B., Frossard, V., Raimbault, S., Ricquier, D., and Bouillaud, F. (1993) The topology of the brown adipose tissue mitochondrial uncoupling protein determined with antibodies against its antigenic sites revealed by a library of fusion proteins. *EMBO J.* **12**, 3739–3745.

BIOGRAPHICAL SKETCH

Martin Modriansky was born in Karvina, Czech Republic, on November 11, 1966. He attended Palacky University in Olomouc, Czech Republic, and in 1992 earned a Bachelor of Science in Biophysics. In 1992, Martin joined the laboratory of Dr. Keith D. Garlid in the Department of Pharmacology at the Medical College of Ohio, Toledo, OH. In 1993, Martin continued his work in the laboratory after its move to the Department of Biochemistry and Molecular Biology at the Oregon Graduate Institute of Science and Technology from which he received his Ph.D. in Biochemistry and Molecular Biology.

List of Publications

Murdza-Inglis, D. L., Modriansky, M., Patel, H. V., Woldegiorgis, G., Freeman, K. B., and Garlid, K. D. (1994) A single mutation in uncoupling protein of rat brown adipose tissue mitochondria abolishes GDP sensitivity of H^+ transport. *J. Biol. Chem.* **269**, 7435-7438.

Jezek, P., Orosz, D. E., Modriansky, M., and Garlid, K. D. (1994) Transport of anions and protons by the mitochondrial uncoupling protein and its regulation by nucleotides and fatty acids. *J. Biol. Chem.* **269**, 26184-26190.

Garlid, K. D., Orosz, D. E., Modriansky, M., Vassanelli, S., and Jezek, P. (1996) On the mechanism of fatty acid-induced proton transport by mitochondrial uncoupling protein. *J. Biol. Chem.* **271**, 2615-2620.

Jezek, P., Modriansky, M., and Garlid, K. D. (1997) Inactive fatty acids are unable to flip-flop across the lipid bilayer. *FEBS Lett.* **408**, 161–165.

Jezek, P., Modriansky, M., and Garlid, K. D. (1997) A structure-activity study of fatty acid interaction with mitochondrial uncoupling protein. *FEBS Lett.* **408**, 166–170.

Modriansky, M., Patel, H. V., Murdza-Inglis, D. L., Freeman, K. B., and Garlid, K. D. (1997) Identification by site-directed mutagenesis of three arginines in uncoupling protein that are essential for nucleotide binding and inhibition. Submitted to *J. Biol. Chem.*